Heart Failure rapidly induces Wasting-related Program in Skeletal Muscle

Inaugural dissertation

for the attainment of the title of doctor
in the Faculty of Mathematics and Natural Sciences
at the Heinrich Heine University Düsseldorf

presented by

Lucia Maria Leitner
from Linz, Austria

Düsseldorf, March 2017

from the institute for "Herz- und Kreislaufphysiologie"
at the Heinrich Heine University Düsseldorf

Published by permission of the
Faculty of Mathematics and Natural Sciences at
Heinrich Heine University Düsseldorf

Supervisor: Prof. Dr. Axel Gödecke
Co-supervisor: Prof. Dr. Ulrich Rüther

Date of the oral examination: 06.04.2017

Contents

Abstract

Skeletal muscle wasting is highly associated with chronic disease such as heart failure (HF) or cancer, where the condition is also referred to as cachexia. Although the pathways involved in muscle wasting are well described, the molecular triggers in contrast remain to be identified. This is especially of importance as cachexia, once manifested, is hardly treatable. Until now there are only some factors identified which are released from the failing heart and are supposed to initiate muscle wasting, including Il-6 and Myostatin (Mstn).

To study the cross talk between the failing heart and skeletal muscle, novel heart failure models were used in this work. In cardiomyocyte KO models of p38 mitogen-activated protein kinase alpha (p38MAPKα), heart failure was induced within two days by Angiotensin II (ANGII), applied via osmotic mini pumps (1.5 mg/kg/day). Cardiac function was assessed by high resolution ultrasound, characterizing heart failure by reduced ejection fraction with an extensive left ventricular dilatation. Additionally, a massive cardiac neutrophil infiltration was found.

The cardiac depression was associated with a severe weight loss (Control 95.39%$\pm$2.10; KO 86.27%$\pm$3.18). Additionally, more than 4000 differentially expressed transcripts (>2-fold) were uncovered in ANGII treated KO hearts when compared to ANGII treated controls using microarray analysis (Agilent 8x60K Mouse Array). Interestingly, in the skeletal muscle (SkM) *Musculus plantaris* (*M. plantaris*) of these KO mice more than 3000 altered transcripts were identified. Both, *M. plantaris* and heart showed increased levels of cytokine expression (e.g. *Il-6, Il-1b, Il-6ra, Il-1r2*). Furthermore several deregulated transcripts found in *M. plantaris* were involved in SkM protein degradation (e.g. atrogenes as *Foxo1, Foxo3, Murf1, Atrogin1* and autophagy associated genes such as *Bnip3*, *Gabarapl1* and *Catepsin L*) indicating the start of a SkM wasting related gene program, triggered by heart failure. Cardiac upregulation of *Mstn* could not be detected. To further elucidate a possible heart-skeletal muscle crosstalk the time course (before and after 12, 24 and 48h of ANGII treatment) of transcript expression was analyzed by quantitative PCR. This revealed that cytokines in the heart were upregulated already after 24h followed by cytokine and atrogene deregulation 24h later in *M. plantaris*.

The transcript expression analysis of the slow oxidative *Musculus soleus* revealed no significant induction of atrogenes after heart failure compared to fast glycolytic *M. plantaris*, which mainly consists of fast type 2 fibers. This finding suggests a fiber type specific atrophy of fast muscles after HF, which was further supported by histological investigations, which revealed a decrease in glycolytic fiber size, as well as morphological alterations exclusively found in native tissue section of type 2 fibers.

Neutrophil depletion as a potential intervention to counteract the initial inflammatory response significantly improved the cardiac and SkM phenotype. Surprisingly cardiac *Il-6* expression was not altered after neutrophil depletion, whereas an attenuated upregulation of other cytokines and most atrogenes was found.

In these novel heart failure models, neither cardiac *Il-6* was sufficient to induce muscle wasting nor was cardiac *Mstn* required to initiate skeletal muscle wasting.

The cardiomyocyte p38MAPKα KO models are a promising model to investigate early triggers of HF-induced muscle wasting.

Zusammenfassung

Skelettmuskelatrophie tritt oft in Zusammenhang mit chronischen Erkrankungen auf. Im Rahmen einer Herzinsuffizienz (HI) oder Tumorerkrankung ist dieser Zustand auch als Kachexie bekannt. Obwohl bei Muskelatrophie ablaufende Prozesse umfassend beschrieben wurden, sind die molekularen Auslöser derselben weitestgehend unbekannt. Dies ist insofern von Bedeutung, da manifestierte Kachexie kaum behandelbar ist. Bislang wurden nur wenige vom Herzen ausgeschüttete Faktoren identifiziert, welche Muskelatrophie induzieren können sollen, wie Il-6 und Myostatin (Mstn).

Um das Zusammenspiel des versagenden Herzens und des Skelettmuskels (SkM) zu untersuchen, wurden in dieser Arbeit neue HI Modelle verwendet. In diesen Modellen, wo die p38 Mitogen-aktivierten Protein Kinase alpha (p38MAPKα) in Kardiomyozyten inaktiviert (KO) wurde, wurde HI innerhalb von zwei Tagen durch Angiotensin II (ANGII) induziert, welches über eine osmotische Minipumpe appliziert wurde (1,5 mg/kg/Tag). Die Herzfunktion wurde mittels Echokardiographie bestimmt, wodurch eine HI anhand erniedrigter Ejektionsfraktion sowie einer umfangreichen linksventrikulären Dilatation charakterisiert wurde. Ebenso wurde eine massive kardiale Infilatration von Neutrophilen festgestellt.

Diese kardiale Einschränkung ging mit einem deutlichen Gewichtsverlust einher (Kontrolle 95,39%±2,10; KO 86,27%±3,18). Zusätzlich wurden mittels *Microarray* Analysen (Agilent 8x60K Mouse Array) mehr als 4000 veränderte Transkripte (<2-fach) in ANGII behandelten KO Herzen im Vergleich zu ANGII behandelten Kontrollherzen gefunden. Interessanterweise wurden im Skelettmuskel *Musculus plantaris* (*M. plantaris*) dieser KO Mäuse mehr als 3000 veränderte Transkripte (<2-fach) identifiziert. Im Herzen und *M. plantaris* wurde eine erhöhte Expression von Zytokinen gefunden (z.B. *Il-6, Il-1b, Il-6ra, Il-1r2*). Des Weiteren waren einige der im *M. plantaris* gefundenen veränderten Transkripte in SkM Proteinabbau involviert (z.B. Atrogene wie *Foxo1, Foxo3, Murf1, Atrogin1* und Autophagie assoziierte Gene wie *Bnip3*, *Gabarapl1* und *Catepsin L*), welche auf eine HI gesteuerte Induktion eines atrophie-ähnlichen Programmes im SkM hindeuten. Eine kardiale Hochregulation von *Mstn* wurde nicht gefunden. Um das mögliche Zusammenspiel zwischen Herz und SkM genauer aufzuklären, wurde der Zeitverlauf (vor und nach 12, 24 und 48 Stunden ANGII Behandlung) transkriptionaler Expression mittels quantitativer PCR analysiert. Dadurch konnte gezeigt werden, dass Zytokine im Herzen bereits nach 24 Stunden hochreguliert wurden, gefolgt von einer Hochregulation von Zytokinen und Atrogenen weitere 24 Stunden später im *M. plantaris*.

Die Transkriptexpressionsanalyse des langsam oxidativen *Musculus soleus* zeigte keine signifikanten Veränderungen nach HI, verglichen mit dem schnell glykolytischen *M. plantaris*, welcher hauptsächlich aus schnellen Typ 2 Muskelfasern besteht. Dieses Ergebnis deutete auf eine fasertypspezifische Atrophie von schnellen Muskeln nach HI hin, unterstützt durch histologische Untersuchungen, welche eine Größenabnahme von glykolytischen Fasern aufzeigten, sowie morphologische Veränderungen, welche ausschließlich in Typ 2 Muskelfasern in nativen Gewebeschnitten zu finden waren.

Neutrophildepletion, als mögliche Intervention um der initialen Immunantwort entgegenzuwirken, konnte den kardialen und SkM Phänotyp deutlich verbessern. Überraschenderweise wurde die kardiale *Il-6* Expression durch Neutrophildepletion nicht verändert, obwohl weitere Zytokine und ein Großteil der Atrogene kaum hochgeruliert wurden.

In diesen neuartigen HI Modellen war weder kardiales *Il-6* ausreichend um eine SkM Atrophie auszulösen, noch war kardiales *Mstn* notwendig, um SkM Atrophie zu initiieren.

Diese p38MAPKα KO Modelle sind vielversprechendes Modelle um frühe Auslöser HI-induzierter Muskelatrophie zu untersuchen.

1 Introduction

1.1 Cachexia

The term cachexia (chronic disease-associated weight loss) is often mistaken for anorexia (weight loss due to insufficient food intake) or sarcopenia (age-associated weight loss), although it is highly distinct from these conditions. In 2006, scientists and clinicians met to reach a consensus on the definition of cachexia, defining it as a "complex metabolic syndrome associated with underlying illness and characterized by loss of muscle with or without loss of fat mass" (Evans et al. 2008). Cachexia is the consequence of an underlying chronic illness such as cancer, chronic heart failure, chronic kidney disease, chronic infection and sepsis or AIDS. Clinical features of cachexia include weight loss, anorexia, inflammation, insulin resistance, hypogonadism and anemia. Especially muscle wasting plays an important role in cachectic patients, as it is mainly responsible for the weight loss, weakness and fatigue of patients. Per definition a patient is diagnosed cachectic if he lost at least 5% of his body weight (non edematous) in the last 12 month including three out of five of the following parameters (also see figure 1.1):

1. decreased muscle strength,
2. fatigue,
3. anorexia,
4. low fat-free mass index and
5. abnormal biochemistry (Evans et al. 2008).

Treatment of cachexia is mainly limited to treat the underlying chronic disease. Even parenteral nutrition does not prevent the ongoing loss of muscle mass, hence once wasting is diagnosed it has a very poor prognosis (Anker et al. 1997). Currently approximately nine million patients suffer from cachexia originating from various chronic diseases, meaning 0.15% of world's population is affected. The mortality rate increases from 17% to 50% in cachectic patients in a 18 month follow up (Haehling and Anker 2010). Different chronic diseases can ultimately lead to cachexia, but there seem to be some general pathomechanisms involved in the induction of cachexia (Morley et al. 2006).

1. Inflammation - several pro-inflammatory cytokines, including interleukin (IL) 1, IL-2, IL-6, interferon γ, and tumor necrosis factor alpha (TNF-α) are often found to be upregulated in patients suffering from cachexia. They affect muscle protein synthesis

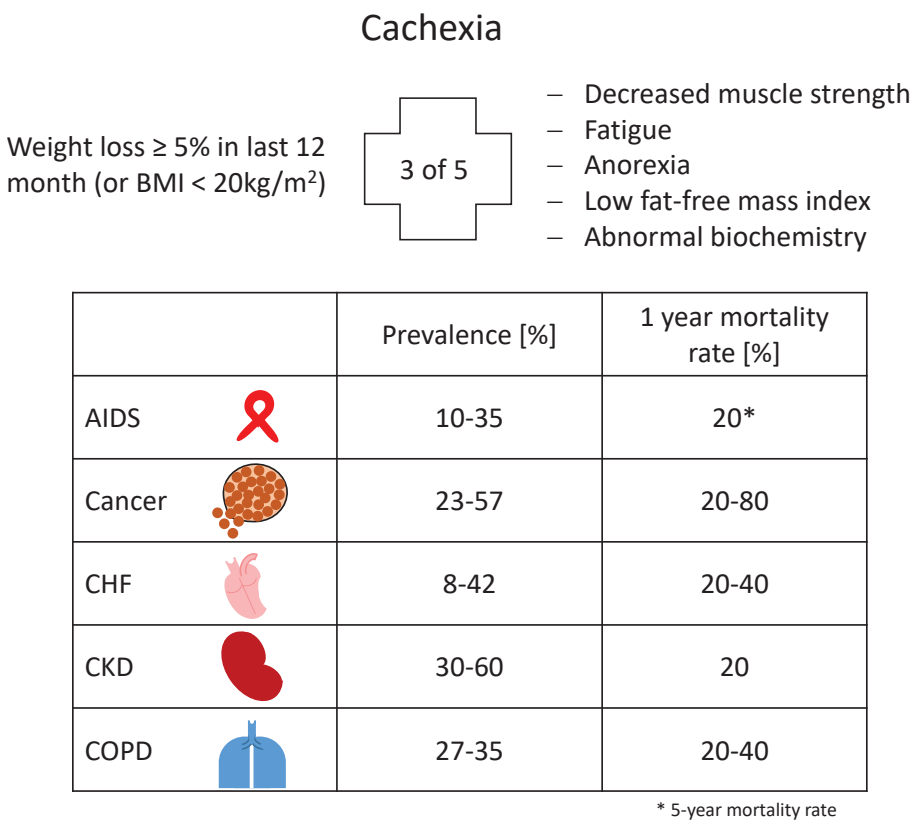

Figure 1.1: Definition, Prevalence and Mortality Rate of Cachexia
General parameters to diagnose cachexia and the variability in prevalence and 1-year mortality of cachexia associated chronic diseases (acquired immunodeficiency syndrome (AIDS)*, cancer, chronic heart failure (CHF), chronic kidney disease (CKD) and chronic obstructive pulmonary disease (COPD)). * 5-year mortality rate (Leitner et al. 2017)

(Guttridge et al. 2000), the release of cortisol and catecholamines from the adrenal gland (Pende et al. 1990, Shintani et al. 1995), lipolysis and -oxidation (Rydén et al. 2004) - all leading to loss of body weight and negative energy balance.

2. Circulating factors - besides cytokines there are several circulating factors which seem to play an important role in cachectic conditions:

   - Adrenal hormones
     Especially glucocorticoids play an important role in glucose and amino acid utilization in muscle by inhibiting their transporters (Dimitriadis et al. 1997). They are involved in the elevated transcription of ubiquitin-proteasome related genes in muscle (Wing and Goldberg 1993), inhibition of protein synthesis and induction of gluconeogenesis. Taken together increased glucocorticoids levels likely lead to impaired protein synthesis.
   - Insulin-like growth factor 1 (IGF-1)
     Besides its distinct correlation with food consumption, IGF-1 has a long known positive effect on muscle protein synthesis (Monier et al. 1983). Muscle bulk and

strength is – among others – regulated by growth hormones and testosterone, which also lead to increased IGF-1 concentrations (Barton et al. 2002). Hence a decrease of IGF-1 levels could be an indicator of malnutrition as well as cachexia (Caregaro et al. 2001).

- Myostatin
  The hormone Myostatin is mainly produced in muscle and is a major suppressor of muscle growth (Roth and Walsh 2004) and increased Myostatin levels are often seen in cachectic patients (Dschietzig 2014).
- Testosterone
  Testosterone is associated with muscle growth and repair (Bhasin et al. 2003), as well as its anti-inflammatory effect (D'Agostino et al. 1999). Additionally declined levels of testosterone are related to increasing leptin concentration, which is known to induce anorexia and lipolysis (Baumgartner et al. 1999).

1.1.1 Cardiac Cachexia

Cardiac cachexia is found in 8-42% of patients suffering from chronic heart failure (CHF) with a mortality rate of 20-40% per year in these patients (Haehling and Anker 2010). Besides the initial burden of heart failure, these patients also develop cachexia associated maladies including skeletal muscle atrophy. The CHF induced muscle wasting is most likely triggered by factors, released by the failing heart. Until now it remains uncertain, whether these factors, directly or indirectly, induce the loss of skeletal muscle. Cytokines as Il-6 and growth factors like Myostatin seems to be involved in the induction of muscle wasting (Carson and Baltgalvis 2010, Breitbart et al. 2011).

Cachexia - Mouse Models

There are no "exclusive" models of cachexia, as cachexia always is the consequence of a chronic disease. Nevertheless to investigate cachexia, mouse models associated with an underlying chronic disease can be used. In particular cancer mouse models, either generated by genetic predisposition, or by the transplantation of cancer cells, are often used. Especially Lewis Lung Carcinoma, colorectal tumors (commonly used model for cancer cachexia is the $Apc^{Min/+}$ mouse) or syngenic sarcomas are associated with high cachectogenic potential (Mehl et al. 2005, DeBoer 2009).

Additionally animals models, which suffer from a specific (chronic) illness (such as kidney failure, heart failure, sepsis ...) are used, which ultimately might lead to cachexia (DeBoer 2009, Romanick et al. 2013).

To investigate cardiac cachexia, genetic calsequestrin (transgenic mice overexpressing cardiac calsequestrin) and Dahl salt-sensitive models, the monocrotaline model and the surgical models (left anterior descending (LAD) ligation, transverse aortic constriction (TAC) or ascending aortic banding) can be used (summarized by Molinari et al. 2016). Nonetheless the occurrence, onset and severity of cardiac cachexia is not predictable in these models, making it rather challenging to quantify these experiments. Once established, cachexia is hardly treatable, hence the initiation phase of cachexia seems to be of great importance.

It is known that weight loss (including muscle wasting and loss of fat mass) is one of the earliest signs of cachexia, providing the opportunity of intervention. Therefore a mouse model, where heart failure can be precisely and reproducibly induced, is very useful to investigate the early time points of HF-induced weight loss.

Cardiac and Vascular Smooth Muscle Cell-specific p38 MAP-alpha Kinase KO Mouse

p38 mitogen-activated protein kinases (MAPK) are involved in pressure overload induced cardiac remodeling (Bao et al. 2007). This and other stress stimuli lead to the phosphorylation of p38 MAP kinase, but whether its activation is beneficial or detrimental in the process of cardiac remodeling is still controversially discussed. The use of p38 MAPK inhibitors after myocardial infarction and pressure overload decreased the severity of cardiac impairment (See et al. 2004, Liu et al. 2005, Behr et al. 2001), whereas p38 MAPK knock-out revealed both - protective (Braz et al. 2003, Kaiser et al. 2004, Nishida et al. 2004) and negative (Otsu et al. 2003, Zhang et al. 2003, Kaiser et al. 2004, Ren et al. 2005) effects in pressure overload and cardiac ischemic animal models.

In our laboratory the characterization of cardiac and vascular smooth muscle cell (VSMC)-specific KO mice, hereafter referred to as SM22p38MAPKα KO mice (see section 3.1), after Angiotensin II (ANGII) induced pressure overload, uncovered the considerable involvement of p38MAPKα in the early phase of cardiac adaptation to pathological stimuli (Bottermann, Leitner et al, in preparation). Within 2 days SM22p38MAPKα KO mice developed drastically impaired cardiac function marked by reduced ejection fractions (EF) and increased end systolic and end diastolic volumes (ESV and EDV) (see figure 1.2 A+B). This effect persisted for 14 days and led to a higher mortality of the affected mice. Additionally to this functional impairment, histological investigations of the hearts revealed a significant accumulation of lipid droplets in KO hearts after 48 hours of ANGII treatment (figure 1.2 C). These severe functional and morphological alterations were accompanied by a drastic change at transcript expression levels analyzed by microarray (figure 4.9) and quantitative real-time PCR (Bottermann, Leitner et al, in preparation).

As the severe heart failure is reproducibly induced within two days and persisted over 14 days in SM22p38MAPKα KO mice, these mice might serve as a promising model to investigate heart failure induced muscle wasting.

1.2 Skeletal Muscle

A mammalian body consists of about 600 different skeletal muscles, necessary for specific functions (locomotor activity, postural behavior and breathing). Some properties of skeletal muscles are already determined during embryogenesis (muscle shape, orientation and connection with other body parts), whereas properties such as muscle mass are likely to change throughout life in health and disease.

This muscle plasticity includes alterations in the structure and function of muscle fibers according to variations of living conditions. The dynamic state of a skeletal muscle is defined

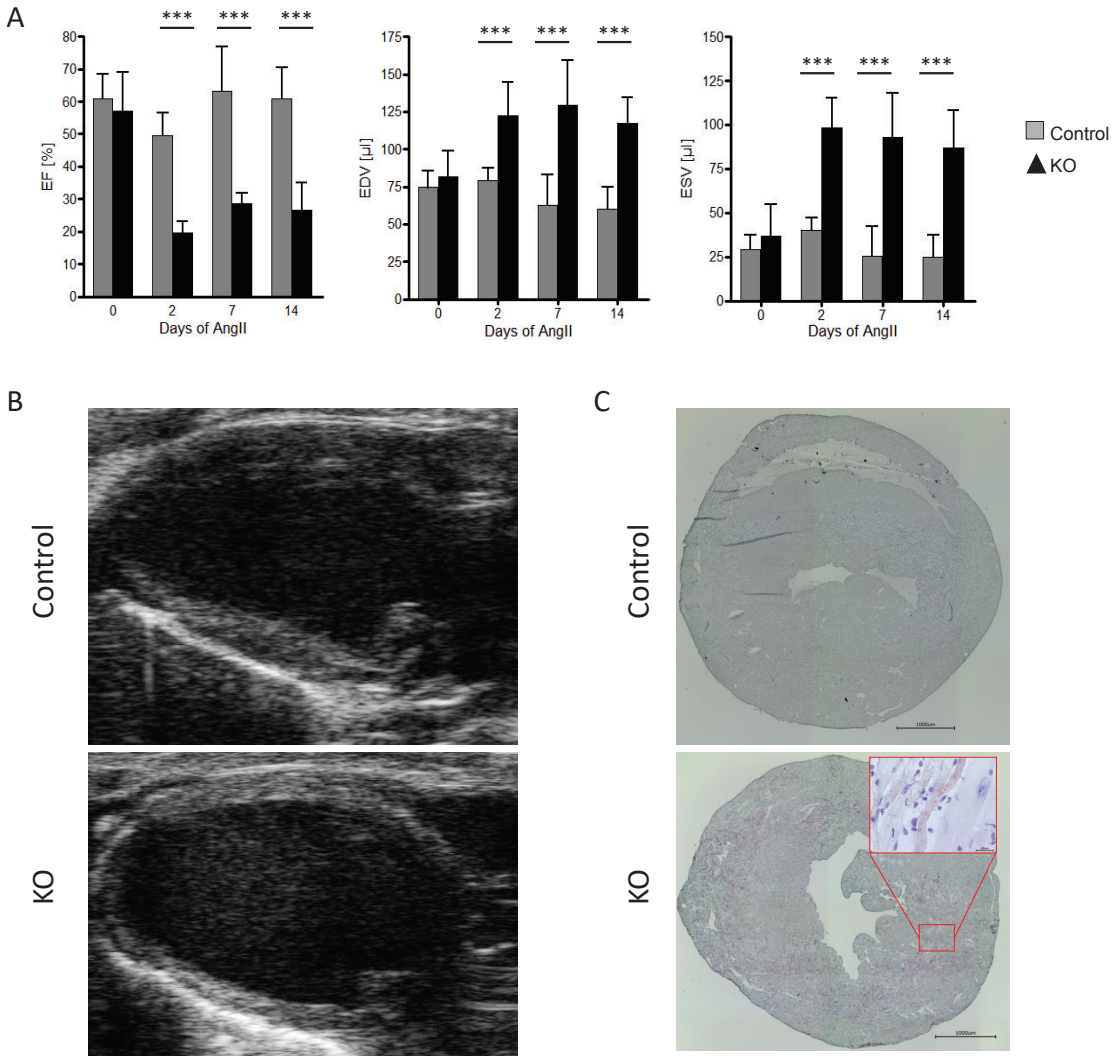

Figure 1.2: Characterization of Heart Failure in SM22p38MAPKα KO Mice
The development of cardiac dysfunction in the time course of A) ejection fraction (EF), end diastolic volume (EDV) and end systolic volume (ESV) of SM22 p38MAPKα control (grey) and KO (black) hearts at baseline and after 2, 7 and 14 days of ANGII treatment. Data represent mean±SD; ***: $p<0.001$; n=5-9. B) High resolution ultrasound images of control (upper pannel) and KO (lower pannel) hearts at day 14 after ANGII treatment. C) Histological sections of SM22p38MAPKα control and KO heart after 48 hours of ANGII treatment showing lipid accumulation in KO hearts (fat red staining). Scale bar = 1000μm

by its plasticity and specialization which is responsive to environmental cues (Blaauw et al. 2011).

1.2.1 Structure and Function of Skeletal Muscle

As depicted in figure 1.3 skeletal muscles are generally composed of fused mononucleated myocytes forming the multinucleated syncytium (myoblasts). These cells mainly mature into contracting muscle fibers, with some remaining undifferentiated precursor cells - the muscle specific stem cells or satellite cells (Chargé and Rudnicki 2004; Ciciliot and Schiaffino 2010).

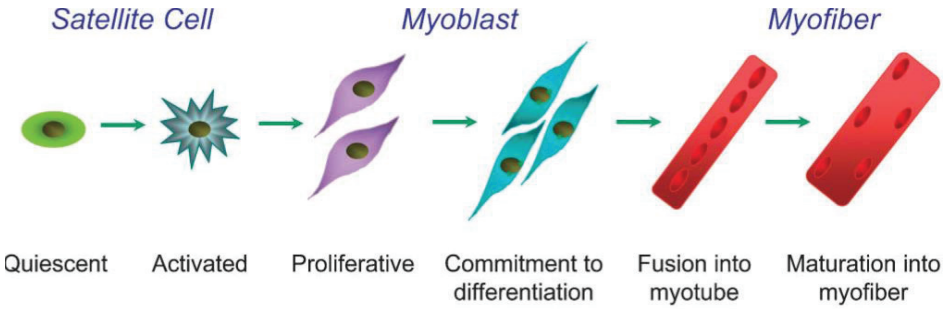

Figure 1.3: Schematic of Skeletal Muscle Differentiation Quiescent satellite cells (muscle stem cells) can be activated by external cues, like muscle damage. Thereby they start to proliferate and differentiate into myoblasts, which ultimately fuse and form myotubes. These multinucleated myotubes further mature into functional myofibers. (Schematic adapted from Zammit et al. 2006).

As seen in figure 1.4, there are three different layers of connective tissue – the epimysium, the perimysium and the endomysium. The endomysium encases the contracting muscle fibers which are then grouped into fascicles (perimysium) to form a skeletal muscle (surrounded by epimysium).

A single skeletal muscle fiber is about 50 μm in diameter and can be several centimeters in length (in humans). In the cytoplasm primarily myofibrils are found - these are cylindrical bundles of thick (myosin) and thin filaments (actin). A myofibril is a concatenation of contractile units (sarcomeres) leading to the skeletal muscle's eponymous striated appearance.

As seen in figure 1.4 (e) a sarcomeric unit spans from one Z disc to another, with M line in the middle. One contractile unit is divided into I and A bands and H zone. In I band and H zone either actin or myosin is found, respectively, whereas A bands, mainly containing myosins, shows overlaps with actin filaments in peripheral regions. Actin filaments are attached to Z discs, myosin filaments to the M line. The proteins Titin and nebulin stabilize the sarcomere structure. Muscle contraction implies the shortening of sarcomeres, the Z discs getting closer, I band and H zone nearly disappear, whereas the A band width remains unchanged. During contraction myosin and actin filaments interact, generating a movement relative to one another, also known as the sliding filament model, where myosin functions as a motor of this motion.

Skeletal muscle myosin protein (about 500 kD) consists of two heavy and two light chains. The long α-helical tail of the two identical heavy chains form a coiled-coil dimer with the light chains associated to the neck of the heavy chain head region (figure 1.5).

Hundreds of myosin molecules are arranged in parallel in the thick filaments with their heads sticking out and binding actin filaments. Thereby they form cross-bridges between the thick and thin filaments. Their orientation is mirrored at the M disc, allowing to shorten the sarcomere from both sides, which results in muscle contraction.

Additionally to the actin binding property, myosin heads also bind and hydrolyze ATP. The thereby originated conformational change of myosin leads to repeated cycles of interaction between myosin heads and actin and drives the filament sliding.

To trigger contraction of skeletal muscle a nerve impulse stimulates the release of Ca^{2+} from the sarcoplasmic reticulum. This release increases the cytosolic Ca^{2+} from 10^{-7} to

10^{-5} M. Two Ca^{2+} sensitive proteins, tropomyosin and troponin, signal muscle contraction. The tropomysin protein binds actin filaments as well as troponin. Troponin is a complex of three polypeptides: troponin C (Ca^{2+}-binding), troponin I (inhibitory), and troponin T (tropomyosin-binding). Under low Ca^{2+} concentration, the tropomyosin/troponin complex inhibits the actin/myosin interaction, whereas at high concentration, Ca^{2+} binds to troponin C, and inducing thereby the conformational switch in myosin filament, resulting in muscle contraction (Cooper 2000).

In rodents there are four different Myosin heavy chains (MyHC) in skeletal muscles, which can be distinguished by

1. their appearance
2. their velocity of twitching
3. their metabolic profile

MyHC type 1 (MyHC1) fibers appear red, they are rich in mitochondria (oxidative profile) and they also are known as endurance fibers (slow twitch). The MyHC type 2 fibers are subdivided into **MyHC type 2a** (MyHC2a), an intermediate oxidative-glycolytic fiber type which is red in color and is considered as a fast twitch fiber. **MyHC type 2d/x** (MyHC2d/x) fibers as well as **MyHC type 2b** (MyHC2b - this fiber type is not seen in humans) fibers appear white (pale) in color, they mainly run on a glycolytic profile and are used for fast force

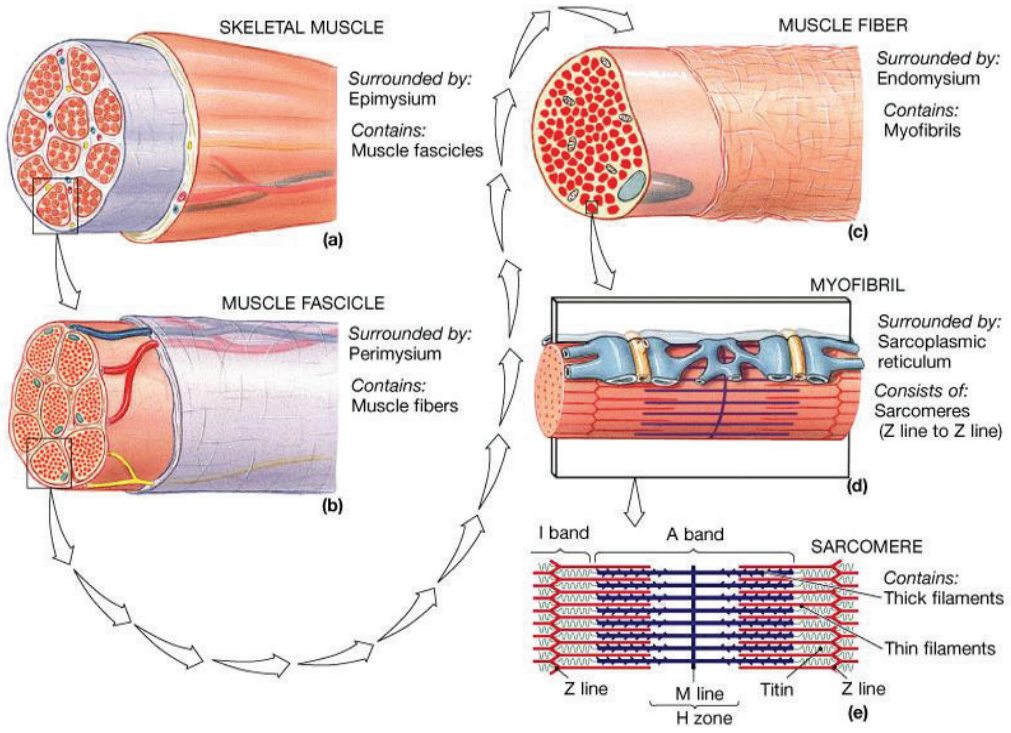

Figure 1.4: Structure of Skeletal Muscles
The skeletal muscles is coated with the Epimysium and contains several muscle fascicles (a). These fascicle is surrounded by the Perimysium and is made of single muscle fibers (b). Each muscle fiber, which is coated with the Endomysium, consists of myofibrils (c), which are embedded in the sarcoplasmic reticulum (d). The myofibrils are made of sarcomeres (ranging from Z line to Z line), which consists of thick and thin filaments (e).

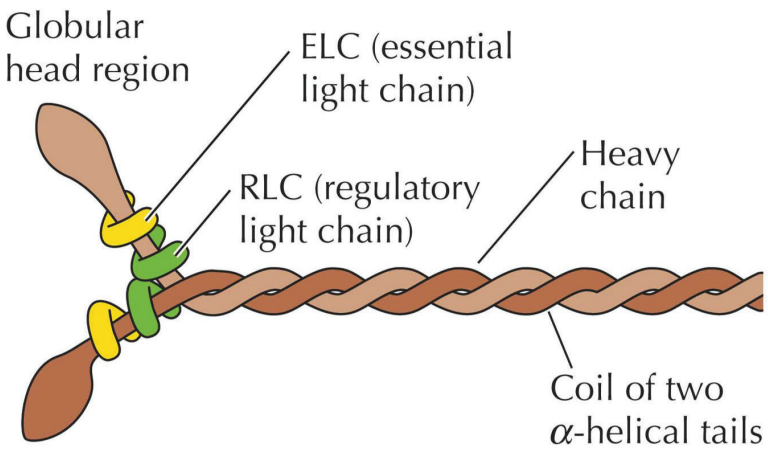

Figure 1.5: Structure of Myosin
Myosin consists of two alpha helical tails, which make up the heavy chains, and two light chains, the essential (ELC) and regulatory light chain (RLC). (Copyright © 2003 THE CELL, Third Edition, Figure 11.23 ASM Press and Sinauer Associates, Inc.)

Table 1.1: Properties of Skeletal Muscle Fiber Types

Properties	**Type I Slow oxidative fibers**	**Type 2a Fast oxidative fibers**	**Type 2 b and d/x Fast glycolytic fibers**
Colour	Red (due to myoglobin)	Red (due to myoglobin)	White (absence of myoglobin)
Contraction time	Slow	Fast	Very fast
Oxidative capacity	High	High	Low
Resistance to fatigue	High	Medium (intermediate)	Low
Cross sectional area	Small	Medium (intermediate)	Large
Capillary density	High	Medium (intermediate)	Low
Mitochondrial density	High	High	Low
Glycogen reserves	Low	Intermediate	High
Main (metabolic) pathway for production of ATP	Aerobic metabolism	Aerobic and anaerobic metabolism	Anaerobic metabolism
Force production	Low	Medium-high	Very High

generation (fast twitch) (Schiaffino and Reggiani 2011). The different properties of skeletal muscle fibers are summarized in table 1.1.

Due to their metabolic properties their responsiveness to external factors varies. In hypertrophic conditions, were an increase in muscle mass is seen, like during exercise, there is a shift either to oxidative fibers (endurance training) or glycolytic fibers (strength training). In contrast to hypotrophic conditions, where muscle mass is lost, either oxidative fibers are more susceptible to degeneration (e.g. denervation) or glycolytic fibers (cancer cachexia) (Ciciliot et al. 2013), which will be described in more detail in section 1.3.4.

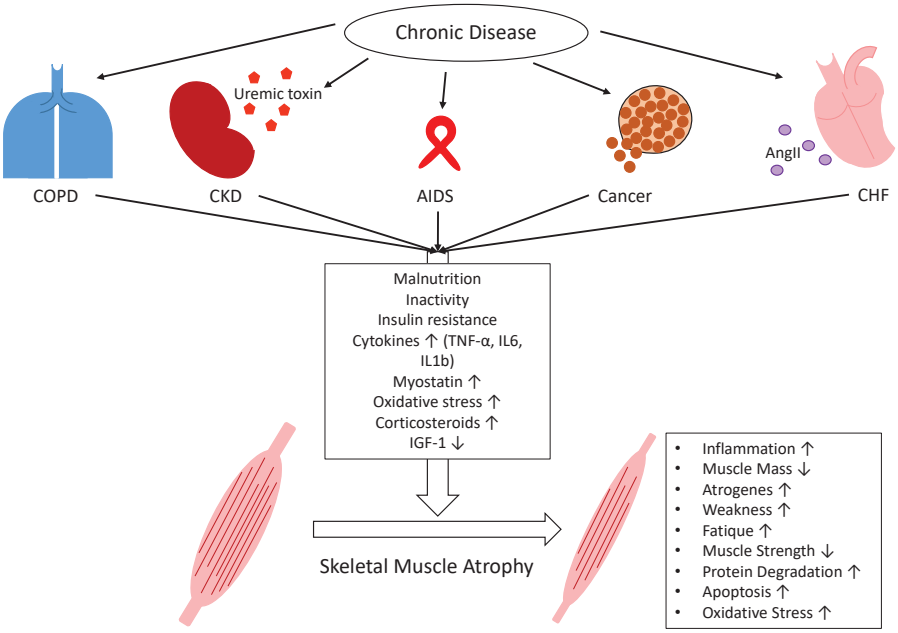

Figure 1.6: Skeletal Muscle Wasting Induced by Chronic Diseases
Chronic diseases, such as chronic obstructive pulmonary disease (COPD), chronic kidney disease (CKD), acquired immunodeficiency syndrome (AIDS), Cancer and chronic heart failure (CHF) share common metabolic changes (malnutrition; inactivity; insulin resistance; increased levels of cytokines (TNF-α, IL-6, IL-1b), Myostatin and corticosteroids, increased oxidative stress and decreased levels of insulin-like growth factor 1 (IGF-1)) which lead to skeletal muscle atrophy. Beside these common features, some disease-specific factors further contribute to muscle wasting, e.g. uremic toxins in CKD or Angiotensin II (ANGII) in CHF. All these metabolic changes induce a catabolic program in skeletal muscles indicated by increased inflammation, weakness, fatigue, protein degradation, atrogene expression, apoptosis and oxidative stress as well as decreased muscle mass and muscle strength (Leitner et al. 2017).

1.3 Skeletal Muscle Atrophy

The underlying trigger of skeletal muscle atrophy can vary, including age-associated weight loss (sarcopenia), acute injury, chronic diseases as well as disuse/denervation of the skeletal muscle. Generally speaking the loss of muscle mass is due to an imbalance of anabolic and catabolic states including protein synthesis/degradation and altered substrate utilization. Especially chronic diseases have a major impact on skeletal muscle wasting (figure 1.6), although it remains unclear whether muscle atrophy is solely initiated by the primary diseased organ, or whether other, peripheral organs, are involved in this inter-organ communication as well.

Nonetheless there seem some general pathways included in skeletal muscle wasting as depicted in figure 1.7, including circulating factors such as Angiotensin II (ANGII), cytokines (e.g., Interleukin 6 (IL-6)), and growth factors of the tumor growth factor beta (TGFβ) family (e.g. Myostatin).

In 2004 Lecker et al. defined a common set of skeletal muscle atrophy related genes, so-called 'atrogenes'. These genes are mainly involved in protein degradation, transcription, translation, energy production or extracellular matrix degradation (Lecker et al. 2004).

Two distinct pathways, the ubiquitin-proteasome pathway and the autophagy/lysosomal

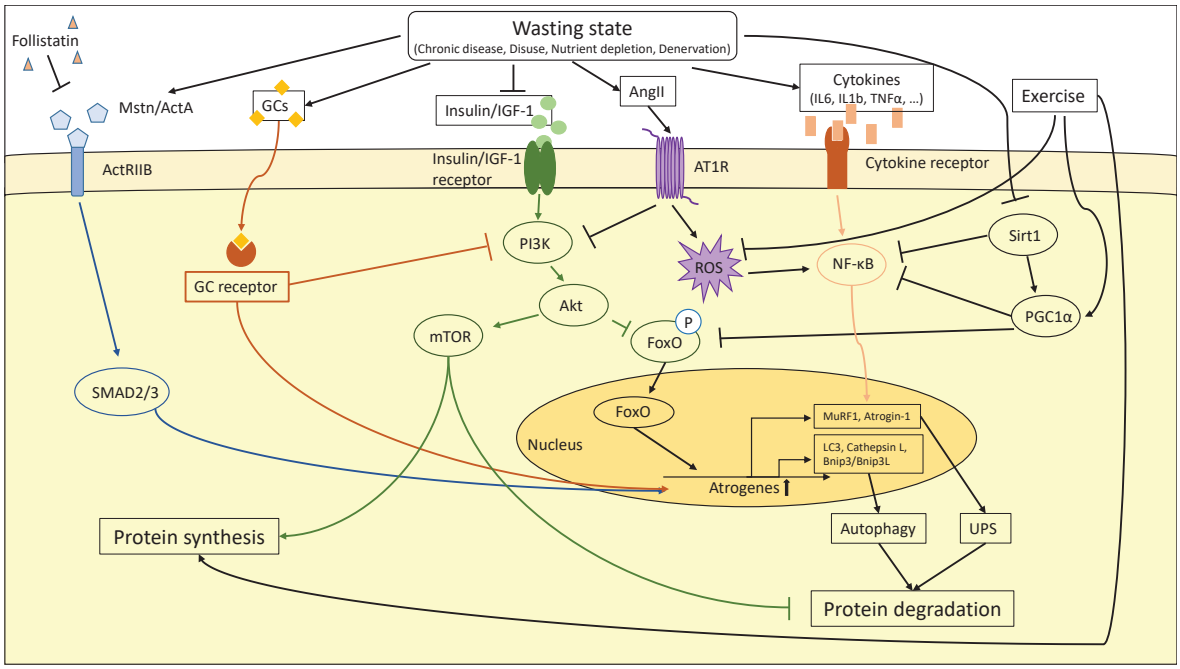

Figure 1.7: Molecular Pathways involved in Skeletal Muscle Protein Degradation The induction of atrogenes in catabolic muscle is driven by various molecular pathways. Upregulation of atrogenes leads to skeletal muscle protein degradation via the ubiquitin-proteasome system (UPS) and autophagy. Specific transcription factors such as forkhead box O (Foxo) proteins, nuclear factor-κB (NF-κB) and SMAD2/3, as well as glucocorticoids (GCs) activate the transcription of atrogenes. The transcription factors themselves are activated by external stimuli – Myostatin (Mstn), Activin A (ActA), GCs, insulin, insulin-like growth factor 1 (IGF-1) and cytokines. In addition, the anabolic PI3K-AKT-mTOR activity is suppressed, which decreases skeletal muscle protein synthesis and leads to accelerated skeletal muscle protein degradation. Exercise on the other hand promotes protein synthesis, blocks ROS production and enhances peroxisome proliferator-activated receptor-γ coactivator 1 α (PGC1α) gene expression. Phosphoinositide 3-kinase (PI3K); V-Akt Murine Thymoma Viral Oncogene Homolog 1 (AKT); mammalian target of rapamycin (mTOR); activin A receptor, type IIB (ActRIIB); muscle-specific RING-finger 1 (MURF1); NAD-dependent protein deacetylase sirtuin 1 (SIRT1); Dystrophinglycoprotein complex (DGC); Interleukin 1/6 (IL-1, IL-6); Tumor necrosis factor alpha (TNFα); Microtubule-associated protein 1 light chain 3 (LC3); BCL2/Adenovirus E1B 19kDa interacting protein 3/ligand (Bnip3/Bnip3l); Angiotensin II (ANGII) receptor (AT1R); Reactive oxygen species (ROS) (Leitner et al. 2017)

proteolytic pathway, are highly associated with skeletal muscle wasting. Both contribute to the degradation of skeletal muscle protein and are mainly induced by Forkhead box O (Foxo) transcription factors. Nonetheless the causal role of autophagy in development of muscle wasting remains controversial.

1.3.1 Foxo Transcription Factors and their Role in Skeletal Muscle Wasting

Foxo transcription factors (TFs) are highly conserved through evolution and are involved in apoptosis, cell cycle regulation, DNA damage repair, energy metabolism and oxidative stress handling. The structure of Foxos consists of the forkhead motif, a special DNA binding motif and a nuclear localization sequence, a nuclear export sequence and a c-terminal transactivation domain, necessary for transcriptional activity.

Foxo activity is mainly regulated by the IGF-1/PI3K/Akt signaling pathway, which is

activated in skeletal muscle hypertrophy. There are four Foxo transcription factors – Foxo1, Foxo3, Foxo4 and Foxo6, all of them are expressed in skeletal muscle, but only Foxo1 and Foxo3 play a central role in skeletal muscle atrophy (Sanchez et al. 2014) and will thereby explained in more detail.

Foxo1

Whereas Foxo3 and Foxo4 KO mice are viable, Foxo1 KO mice die during embryogenesis due to incomplete vasculogenesis (Hosaka et al. 2004). Despite its important role as a transcription factor in vaculogenesis, it regulates energy homeostasis in skeletal muscle, having a major impact on glucose metabolism (just as in adipose tissue (Nakae et al. 2002), bone (Rached et al. 2010), liver (Schmoll et al. 2000) and pancreas (Nakae et al. 2002)). It directly binds to the promotor of the pyruvate dehydrogenase kinase 4 (Pdk4) gene, a well known factor regulating blood glucose levels. In times of reduced carbohydrate catabolism (eg. during fasting), it promotes the expression of Pdk4, which subsequently leads to decreased activity of pyruvate dehydrogenase (Pdh) known to catalyze the reaction of pyruvate to acetyl-CoA. By decreasing Phds activity, less carbohydrates will be used as energy substrates (Bowker-Kinley et al. 1998). In addition to that it was shown that Foxo1 also regulates muscle fat oxidation, indicated by its correlation with increased lipoprotein lipase (Lpl) expression levels. Lpl provides the muscle with fatty acids and glycerol by hydrolysing plasma triglycerides under fasting or exercise conditions (Rauramaa et al. 1980). Furthermore Foxo1 facilitates fatty acid uptake into muscle cells by altering the subcellular localization of the membrane fatty acid translocase/cluster of differentiation 36 (FAT/CD36) (Bastie et al. 2005). Both findings demonstrate that Foxo1 most likely is a switch towards lipid utilization instead of glucose as substrates under different stress conditions (Sanchez et al. 2014). Foxo1 together with Foxo3 is playing an important role in skeletal muscle protein breakdown via the ubiquitin-proteasome pathway. Both Foxos are required for the transcription of the main E3 ubiquitin ligases - *Muscle atrophy Fbox* (*Mafbx*)/*Atrogin-1* and *Muscle-Specific RING Finger Protein 1* (*Murf1*), which target specific skeletal muscle proteins for degradation. This pathway will be described in more detail in section 1.3.2. In the promoter region of *Atrogin1*, Foxo1 binding sites are found, inducing its transcription, when Foxo1 gets activated (Sandri et al. 2004).

Foxo transcription factors themselves are regulated by different external stimuli (including insulin, insulin-like growth factor 1 (IGF-1), nutrients, cytokines, and oxidative stress), which either induce post-translational modifications (such as phosphorylation, acetylation, ubiquitination, and methylation) or change their transcriptional activity (Daitoku et al. 2011).

Foxo1 has different acetylation sites, but in contrast to many other proteins, which get activated by acetylation, Foxo1-dependent transcription gets attenuated when acetylated due to its reduced affinity to its DNA binding sites (Daitoku et al. 2004, Hatta et al. 2009). Furthermore Foxo1 acetylation increases Akt-mediated phosphorylation of Foxo1 and thereby translocating Foxo1 from the nucleus to the cytoplasm (Matsuzaki et al. 2005).

In response to insulin and serum growth factors, Foxos can be degraded via ubiquitin-proteasome pathway. In this context it is noteworthy that acetylation prevents ubiquitin-induced degradation, as both, ubiquitination and acetylation, occur on lysine residues, espe-

cially under oxidative stress (Kitamura et al. 2005).

As summarized by Daitoku et al there are many different tissue specific protein-protein interactions, which regulate the stability of Foxo1 (Daitoku et al. 2011).

Foxo3

Foxo3 KO mice, although viable, get infertile with age (Hosaka et al. 2004) and show an impaired muscle regeneration ability, mainly due to reduced MyoD transcription levels, a key regulator of myogenesis (Hu et al. 2008). Hearts of Foxo3 KO mice show a hypertrophic phenotype as possible contribution to growth of striated muscle cells (Ni et al. 2006). The activity of Foxo3 in skeletal muscle is reduced by acetylation and ubiquitination (Bertaggia et al. 2012). When p300, a histone acetyltransferase, is overexpressed in skeletal muscle, Foxo3's nuclear localization and activity is altered, whereas Foxo1-dependent gene expression gets induced, indicating a possible regulatory role of acetylation on Foxo homologues. Foxo3 gets inhibited via the IGF-1/PI3K/Akt pathway, where Akt phorsphorylates specific threonin and serin sites of Foxo3 and thereby inhibits Foxo3 (Stitt et al. 2004).

Together with Foxo1, Foxo3 is required for the transcription of two major players of the ubiquitin-proteasome pathway – *MAFbx/Atrogin-1* and *MuRF1*, responsible for skeletal muscle protein degradation (Sandri et al. 2004).

Additionally Foxo3 plays an important role in autophagy-lysosomal pathway, as it regulates the transcription of several autophagy-specific genes (Atgs), including *Beclin*, *Microtubule-associated protein 1 light chain 3* (*Lc3*); *BCL2/Adenovirus E1B 19kDa interacting protein 3* (*Bnip3*), *GABA Type A Receptor Associated Protein Like 1* (*Gabarapl1*) and others. The regulatory function of Foxo3 on these two pathways seems to be independently controlled (Sanchez et al. 2014).

In general Foxo1, 3 and 4 inhibit skeletal muscle protein proliferation. Overexpression of Foxo3 negatively influences muscle precursor cell proliferation, as it induces the expression of the kinase inhibitor p27KIP1 (Rathbone et al. 2008).

1.3.2 Ubiquitin-Proteasome Pathway

The ubiquitin-proteasome system is needed for protein degradation. Briefly, as depicted in figure 1.8, the protein is bound by either a single ubiquitin or a polyubiquitin chain. The ubiquitination takes place at substrate lysines, catalyzed by a cascade of three enzymes - E1, E2 and E3. E1 activates ubiquitin in an ATP-dependent fashion, where a thioester is formed with the ubiquitin C terminus. This thioester is transferred to the active site cysteine of the E2 and forms an E2-Ub thioester intermediate. The intermediate is recognized by E3 ligases, which, additionally to the intermediate, also binds the substrate and transfers the ubiquitin from E2 to substrate lysine or N terminus, thereby marking the protein for proteosomal degradation by the 26S proteasome consisting of a 19S regulatory and a 20S core subunit. The velocity of this degradation process is dependent on E3 ligases (Berndsen and Wolberger 2014). Additionally to the classical ubiquitin-proteasome pathway via the 26S proteasome, in cachexia, the 20S proteasome is also upregulated. In contrast to the 26S proteasome, it degrades oxidized protein directly, without prior modification by ubiquitination. It is most

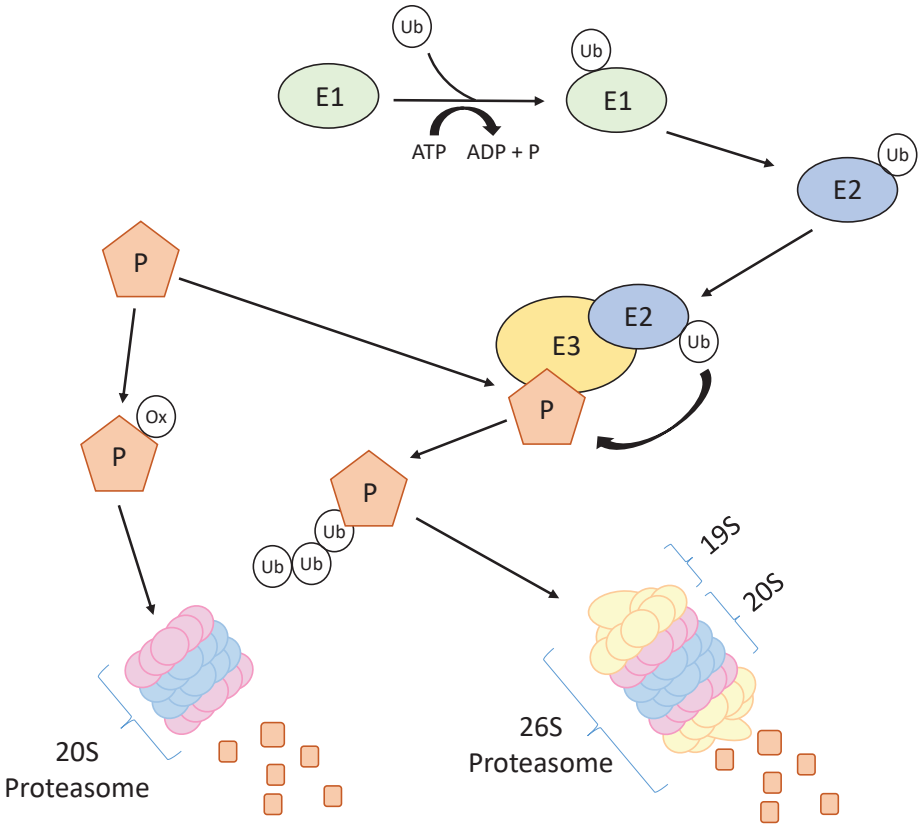

Figure 1.8: Schematic Overview of Ubiquitin-proteasome Pathway
A protein can be marked for degradation either by ubiquitination or oxidation. Activated ubiquitin binds to E1 and is then transferred to E2, the ubiquitin-conjugating enzyme. The loaded E2 delivers the ubiquitin to ubiquitin ligases (E3), which covalently attach ubiquitin to a lysine residues of target proteins (P). Poly-ubiquitinated proteins are then degraded by the 26S proteasome consisting of a 19S regulatory and a 20S core subunit. If a protein gets oxidized (ox) it will be directly degraded via the 20S proteasome (Leitner et al. 2017).

likely that ROS, which is elevated in cachectic muscle, further contributes to protesomal degradation of skeletal muscle protein (Shringarpure et al. 2003, Nakayama et al. 2016, Leitner et al. 2017).

The main substrate of proteosomal degradation in skeletal muscle are sarcomeric proteins. There are only few skeletal muscle specific E3 ligases which get upregulated during muscle loss. The most prominent ones, which are found to be upregulated in nearly every model of muscle atrophy, are Atrogin-1/MAFbx (muscle atrophy Fbox) also called F-Box Protein 32 (Fbxo32) and Muscle Ring Finger 1 (Murf1) also named Tripartite Motif Containing 63 (Trim63) (Bodine et al. 2001). Until now there are not many known substrates for Atrogin-1, mostly proteins involved in muscle growth and survival, such as MyoD (a key muscle transcription factor) (Tintignac et al. 2005) or Eukaryotic translation initiation factor 3 subunit F (Eif3-f) (an inducer of muscle protein synthesis)(Csibi et al. 2010). Additionally cell culture experiments suggest an interaction of Atrogin-1 with sarcomeric proteins, transcription and translational factors, enzymes involved in glycolysis and gluconeogenesis, and mitochondrial proteins (Lokireddy et al. 2012).

MuRF1 interacts with structural muscle proteins, like troponin I (Kedar et al. 2004), myosin heavy chains (Clarke et al. 2007), actin (Polge et al. 2011), myosin binding protein C and myosin light chains 1 and 2 (Cohen et al. 2009; Schiaffino et al. 2013).

There is rather limited knowledge about other E3 ligases (such as Trim32 and TRAF6), which also seems to be involved in skeletal muscle degradation (Cohen et al. 2012; Paul et al. 2010) and some of those might be found only in a specific condition or at a specific timepoint during muscle wasting (Schiaffino et al. 2013).

The ubiquitin-proteosomal degradation is found in every setting of skeletal muscle wasting.

1.3.3 Autophagy/Lysosomal Proteolytic Pathway

Autophagy is the second important pathway besides the ubiquitin-proteasome system, which is also regulated by Foxos and is induced during muscle atrophy. Despite the fact that autophagy is strongly associated with skeletal muscle atrophy, it might be induced by cell damage occurring in wasting states. In this context the autophagy pathway is probably important to clear cells from damaged complexes or organelles and thereby mitigating additional damage. It is likely that autophagosomes act as a protective mechanism rather than causing muscle wasting (Nichenko et al. 2016). This is supported by several groups, who show an augmented cell damage if components of the autophagic machinery are inactivated (Halling et al. 2016, Masiero et al. 2009, Masiero and Sandri 2010, Nascimbeni et al. 2012, Raben et al. 2008).

In contrast to the ubiquitin-proteasome pathway, which is responsible for clearing short-lived protein, the autophagy/lysosomal proteolytic pathway removes long-living proteins, protein aggregates, and organelles, including mitochondria (Ju et al. 2016, Milan et al. 2015, Nichenko et al. 2016).

In general, there are three types of autophagy in mammals: macroautophagy, chaperone-mediated autophagy (CMA) and microautophagy, but macroautphagy (hereafter referred to as autophagy) plays the greatest role in skeletal muscle autophagy. Autophagy starts with an isolated membrane, the so called phagophore, which expands to envelope intra-cellular subjects (protein aggregates, organelles and ribosomes) in a double-membraned autophagosome. This newly formed autophagosome fuses with a lysosome (autolysosome) and thereby promotes the degradation of autophagosomal contents via lysosomal acid proteases as seen in figure 1.9 (Glick et al. 2010).

The first involvements of autophagy in muscle atrophy was detected in models of denervation and fasting – in fact, it was shown that fast-twitch muscles have more autophagosomes than slow-twitch muscles (Furuno et al. 1990; Mizushima et al. 2004). One of the first lysosomal proteases found in atrophying muscle was Cathepsin L (Deval et al. 2001). *Cathepsin L* as well as many other skeletal muscle autophagy related genes are mainly regulated by Foxo3, including *Lc3 (microtubule-associated protein 1 light chain 3 alpha)*, the Lc3 homologue *Gabarapl1 (GABA(A) receptor-associated protein like 1)* as well as *Bnip3* and *Bnip3l (BCL2/adenovirus E1B 19 kDa protein-interacting protein 3 (ligand))*, all contributing to autophagosome formation (Lecker et al. 2004; Mammucari et al. 2007).

Although autophagy is noted as a non-selective degradation pathway, it is very likely that there are more selective forms of autophagy under various conditions. In skeletal muscle

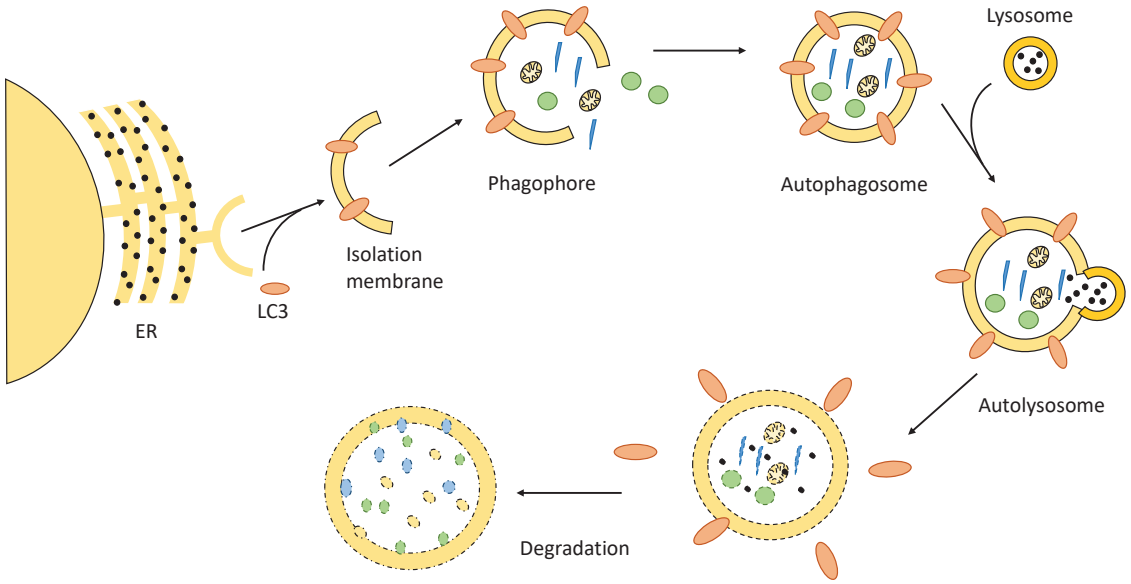

Figure 1.9: Schematic Overview of Autophagy
Autophagy is initiated by Microtubule-associated protein 1A/1B-light chain 3 (LC3) conjugation to the nascent phagophore, called isolation membrane – a membrane part derived from the endoplasmic reticulum (ER). While the phagophore expands, it engulfs degradable substrates and finally forms the autophagosome. The autophagosome fuses with a lysosome, which releases its hydrolytic enzymes into the newly formed autolysosome. The content thereby gets degraded and can be recycled by the cell (Leitner et al. 2017).

selective forms of autophagy are found, specifically to mention mitophagy, which describes the clearance of (defective) mitochondria. Parkin, PINK1 (phosphatase and tensin homolog-induced putative kinase 1), Bnip3 and Bnip3l are regulators of mitophagy and are found to be upregulated in many conditions of skeletal muscle wasting (Narendra and Youle 2011; Mammucari et al. 2007).

PINK1 is usually constitutively degraded by mitochondrial proteases in healthy mitochondria. In damaged mitochondria, PINK1 accumulates and induces parkin recruitment to mitochondria. Parkin in turn ubiquitinates mitochondrial membrane proteins, a signal for autophagic vesicles (Narendra and Youle 2011). Bnip3 and Bnip3l are localized at the outer membrane of the mitochondria after cellular stress. There they bind directly to Lc3, which attracts the autophagosome to damaged mitochondria (Hanna et al. 2012; Schiaffino et al. 2013).

1.3.4 Fibertype-Specific Effects in Muscle Wasting

As mentioned earlier there are two different types of fibers in skeletal muscles - slow-twitch, oxidative type 1 fibers and fast-twitch, mainly glycolytic type 2 fibers. During wasting conditions, these fiber types are affected differentially. In diseases including cancer, sepsis, and elevated glucocorticoids, type 2 fibers seem to be more prone to muscle atrophy, suggesting a higher resistance of the oxidative fibers (Mendell and Engel 1971, Tiao et al. 1997, Acharyya et al. 2005).

In 2007 Li et al described the fiber type specific atrophy in glycolytic, but not oxidative muscles in a chronic heart failure mouse model. Whereas the oxidative *Musculus soleus* sustained its muscle mass, the glycolytic *Musculus plantaris* showed fiber type specific atrophy as the cross sectional areas of type 2d/x and 2b fibers were significantly decreased. Additionally they could demonstrate a significant induction of *Mafbx/Atrogin-1* mRNA in fast glycolytic *Musculus vastus lateralis* (Li et al. 2007).

On the other hand human data of patients with chronic heart failure in contrast showed a shift from oxidative to glycolytic fibers (healthy subjects: type 1 fibers 54.5±14% (type 2, 45.5%); chronic heart failure patients: type 1 fibers 40.5±12% (type 2, 59.5%) in patients with chronic heart failure) (Drexler et al. 1992).

Additionally physical inactivity, malnutrition, hypoxia, oxidative stress as well as increased circulating inflammatory cytokines contribute to the fiber type susceptibility (Ciciliot et al. 2013, Piepoli and Crisafulli 2014).

Nonetheless the molecular basis for the higher resistance of oxidative fibers in different wasting conditions needs to be further investigated.

An important factor to mention is the co-activator Peroxisome proliferator-activated receptor gamma coactivator 1-alpha (Pgc1α). Pgc1α plays an important role in the regulation of oxidative metabolism and mitochondrial biogenesis. When it is transgenically expressed in muscle, it induced a shift from glycolytic to oxidative type 1 fibers, indicated by a switch in myosin isoform toward type I, elevated mitochondrial density, and enhanced myoglobin expression (Lin et al. 2002). During denervation or chronic disease, such as cancer cachexia, diabetes, and renal failure, *Pgc1α* mRNA levels were largely decreased in rodents. In transgenic mice, overexpressing *Pgc1α*, the decrease in muscle fiber diameter, caused by denervation and fasting, was significantly smaller compared to controls. Additionally the transcript expression of *Atrogin-1* and *Murf-1* was reduced in these mice. It was demonstrated that Pgc1α reduced the binding capacity of Foxo3 to *Atrogin-1* promoter and thereby increased the resistance to atrophy in this mice (Sandri et al. 2006).

This effect was also shown in a mouse model of cardiac cachexia (transgenic mice with cardiac-specific calsequestrin overexpression, which leads to heart failure and cachexia in this mice), where overexpression of PGC1α in glycolytic muscles attenuated the muscle wasting induced by CHF (Geng et al. 2011). In oxidative fibers, which show higher levels of PGC1α than gylcolytic fibers, inducible nitric oxide synthase (iNOS) and endothelial NOS (eNOS) were upregulated as well. Additionally superoxide dismutases (SOD1, SOD2, and SOD3) were also elevated, all leading to lower levels of reactive oxygen species (ROS), hence reduced oxidative stress in type 1 fibers compared to type 2 fibers, most likely accounting for their fiber type specific resistance to atrophy (Okutsu et al. 2014).

1.4 Aim of the Project

Pathways, involved in heart-failure induced muscle wasting are well described, nonetheless how the cross talk between heart and skeletal muscle is orchestrated remains unclear. The involvement of different humoral and neuronal factors, released from the failing heart, is highly suggested, but whether and which factors are required or even sufficient to induce

muscle wasting has to be elucidated. One mayor challenge to investigate this cross talk in more detail was the unpredictability of the onset of muscle wasting in existing models.

The novel cardiomyocyte specific p38 KO model, as described earlier, provides promising evidence of a fast, reliable and especially reproducible heart failure model to investigate the interorgan communication between heart and skeletal muscle. First an effect of the failing heart on skeletal muscle has to be demonstrated. Thereafter precise analysis of skeletal muscles on histological as well as transcriptional levels has to be performed, which contributes to a better understanding of the onset of cross talk between heart and skeletal muscle.

Once established the model could serve as a valuable tool to not only elucidate early biomakers of heart failure-induced skeletal muscle wasting, but also enabled to investigate the early pathomechanisms leading to the wasting state, and possibly intervene with or even reverse the progression of the disease.

2 Materials

2.1 Laboratory Equipment

Device	Manufacturer (Product name)
Analysis scales	Kern (PCB), Mettler-Toledo (PE 3600), Sartorius (BP1215)
Autoclave machine	Systec (Vx-100)
Centrifuge	Eppendorf (5417R), VWR (Mega Star 1.6R), Hettich (Rotofix 32)
Cryostat	Leica (CM1850)
Fluorescence microscope	Keyence (Keyence BZ 9000)
Freezer (-20°C)	Privileg (*Super Energiesparer*, Senator), Liebherr (Comfort)
Freezer (-80°C)	Revco/Thermo Fischer (UltimaII)
Fridge	Liebherr (Comfort)
Ice Machine	Ziegra
Incubator	Heraeus
Light microscope	Zeiss (ID 03), Leica
Liquid N_2 tanks	Air Liquide (Arpege 110)
Magnetic stirrer	Heidolph (MR3001)
Microwave	AEG (Micromat)
Minicentrifuge	Technico (Mini), Roth (Rotilabo)
Nitrocellulose Blotter	Thermo Fisher (Pierce^{TM} G2 Fast Blotter)
Photometer	Eppendorf (BioPhotometer plus)
Pipettes	Gilson (Pipetman 10-1000μl)
Real Time PCR System	Applied Biosystems (StepOnePlus)
Spectrophotometer	Peqlab (Nanodrop, ND-1000 Spectrometer)
Sterile bench	Antair (BSK), Heraeus (LaminAir)
Shaker	Edmund Bühler (KL-2)
Test tube shaker	Heidolph (Reax top)
Thermomixer	Eppendorf (Thermomixer comfort)
Tissue Ruptor	Qiagen

Ultrasound device	Visualsonics (Vevo 2100)
Water purification system	Miipore (Milli-Q plus)
Water bath (37°C)	GLF (GFL 1083)

2.2 General Chemicals and Materials

2,4,6-trinitrophenol (TNP)	VWR, Germany
4OH-Tamoxifen (OHTX)	Sigma, USA
Angiotensin II, human	Sigma, USA
Aquatex	Merck, Germany
β-Mercaptoethanol	Sigma, USA
Disposable Base Molds (15x15x5mm)	Ted Pella Inc., USA
Formaldehyde	VWR, Germany
NBT	Sigma, USA
Normal goat serum	Vector Laboratories, USA
Oil-Red-O	Sigma, USA
Paraformaldehyde	Sigma, USA
Peanutoil	Sigma, USA
Potassiumcyanide (KCN)	Sigma, USA
ProLong Gold Antifade (+/- DAPI)	Invitrogen, USA
Saponin	Roth, Germany
Succinat	Merck, Germany
Super PAP Pen Liquid Blocker	Science Services, Germany
Tissue Tek O.C.T. Compound	Sakura, Germany
Triton X-100	Sigma, USA
Tween-20	Merck, Germany

2.3 Chemicals for Cell Culture

DMEM (high glucose 4500mg/L)	Sigma, USA
DMSO (Dimethylsulfoxide)	Sigma, USA
Fetal Bovine Serum (FBS)	Biochrom, Germany
Horse Serum (HS)	Sigma, USA
Trypsin-EDTA	Invitrogen, USA
Penicillin / Streptomycin (P/S)	Invitrogen, USA
Glutamax (L-gluatamine 200mM)	Invitrogen, USA
Trypan blue 0.4%	Invitrogen, USA

2.4 Enzymes

Collagenase	Worthington, USA
DNAse I RNase free	Fermentas, Lithuania
Pancreatin	Sigma, USA
Proteinase K	Fluka, Switzerland
Restriction Enzymes	New England Biolabs, USA
Taq DNA Polymerase	Fermentas, Lithuania
Trypsin	LifeTechnologies, USA

2.5 Antibodies

2.5.1 Primary Antibodies

Rat anti-CD31 (553370)	BD Pharmingen, USA
Rat anti-Ly6G (551461)	BD Pharmingen, USA
Mouse anti-MyHC1 (BA-F8)	DSMZ, Germany
Mouse anti-MyHC2a (SC-71)	DSMZ, Germany
Mouse anti-MyHC2b (BF-F3)	DSMZ, Germany
Mouse anti-p38α (2793)	Cell Signaling, USA
Rabbit anti-panAKT (4691)	Cell Signaling, USA

2.5.2 Secondary Antibodies

AffiniPure Fab fragments goat anti-rabbit IgG (115-007-003)	Jackson IR, USA
Alexa Wheat Germ Agglutinin (WGA) (W11261)	Molecular Probes, USA
AMCA goat anti-mouse IgM (155-155-075)	Jackson IR, USA
Cy3 goat anti-rabbit IgG (111-165-144)	Jackson IR, USA
Fluorescein (FITC) goat anti-mouse IgG (155-095-062)	Jackson IR, USA
Fluorescein (FITC) goat anti-mouse IgG1 (155-095-205)	Jackson IR, USA
Rhodamine red goat anti-rat IgG (122-295-167)	Jackson IR, USA
Rhodamine red goat anti-mouse IgG2b (155-295-207)	Jackson IR, USA
IRDye 800CW Goat Anti-Mouse IgG (925-32210)	LI-COR, USA

IRDye 800CW Goat Anti-Rabbit IgG (925-32211)	LI-COR, USA
IRDye 680RD Goat Anti-Mouse IgG (925-68070)	LI-COR, USA
IRDye 680 Goat Anti-Rabbit IgG (925-68071)	LI-COR, USA

WGA, a lectin, binds to glycoproteins of the cell membrane, and is routinely used to stain for skeletal sarcolemma to determine cross sectional area. CD31 is a widely used marker for endothelial cells in histological tissues, which allows conclusions about capillary density. DAPI is a fluorescent stain that binds strongly to A-T rich regions in DNA and is used as marker of cell nuclei.

2.6 Kits and Master Mixes

RNeasy Fibrous Tissue Kit	Qiagen, Germany
RNeasy Kit	Qiagen, Germany
QuantiTect Reverse Transcription Kit	Qiagen, Germany
Maxima SYBR Green/ROX pPCR Master Mix (2x)	Thermo Scientific, USA

2.7 PCR Primers

Primers		Sequence 5' - 3'
Bnip3	Fwd	ACCACAAGATACCAACAGAG
	Rev	AATCTTCCTCAGACAGAGT
Csnk2b	Fwd	GATCTTAGACCTGGAACCTG
	Rev	CAACCCATAAAGCATCTCAG
Ctsl	Fwd	GTTCTATAGTTCAGGCATCTAC
	Rev	GAATCTGTTCCTTCATAGC
Cxcl5	Fwd	TGTTTGCTTAACCGTAACTC
	Rev	CAGTTTAGCTATGACTTCCAC
Cxcr2	Fwd	CTACTGCAGGATTAAGTTTACC
	Rev	GACGTATATTACAACCACAGC
Fbxo32	Fwd	CTGAAAGTTCTTGAAGACCAG
	Rev	GTGTGCATAAGGATGTGTAG
Foxo1	Fwd	AAACACATATTGAGCCACTG
	Rev	TCTACTCTGTTTGAAGGAGG
Foxo3	Fwd	CTCCGTCGTGTTTTACTATC
	Rev	GAAAACTCAGAGGGTCAAAG
Gabarapl1	Fwd	CCAGTTCTACTTCTTAATCCG
	Rev	CTGCCTCATTTTCCATAGA
Il-1b	Fwd	GGATGATGATAACCTGC
	Rev	CATGGAGAATATCACTTGTTGG
Il-1r2	Fwd	AAAACTATGTGGAAGTGTCG
	Rev	GAAGAGACTTCTTTGACTGTG
Il-6	Fwd	AAGAAATGATGGATGCTACC
	Rev	GAGTTTCTGTATCTCTCTGAAG
Il-6ra	Fwd	AAAGTTCTACAGAAGCAACG
	Rev	TTGAGTCTCAGGATGATGAAG
Mstn	Fwd	CTATAAGACAACTTCTGCCAAG
	Rev	AGAAAGTCAGACTCTGTAG
Trim63	Fwd	ACATGGACTACTTTACTCTGG
	Rev	CATTGGTGTTCTTCTTTACCC

2.8 Hybridoma Cell Lines

Hybridoma cell lines are established by fusion of immortalized cancer cells (used here: NSO myeloma cells) with antibody producing cells (used here: spleen cells from a BALB/c mouse). These cells then are cultivated according to the distributors recommendations. The secreted antibodies can be harvested from the supernatant and used directly as primary antibodies in immunohistochemical stainings or are purified used in Western blotting.

All three hybridoma cell lines used in this work were deposited by Prof. S. Schiaffino,

University of Padova, Padova, Italy.

2.8.1 BA-F8

These hybridoma cells were derived from mice that had been immunized with purified myosin from bovine atrium and secretes a murine monoclonal antibody (IgG2b) that reacts with rat type 1 (slow-twitch, oxidative) fibers (Borrione et al. 1988).

2.8.2 BF-F3

These hybridoma cells were derived from mice that had been immunized with purified myosin from fetal bovine muscles and secretes a murine monoclonal antibody (IgM) that reacts with rat type 2B (fast-twitch, glycolytic) fibers (Schiaffino et al. 1989).

2.8.3 SC-71

These hybridoma cells were derived from mice that had been immunized with purified myosin from bovine subcutaneous muscle and secretes a murine monoclonal antibody (IgG1) that reacts with rat type 2A (fast-twitch, oxidative) fibers (Schiaffino et al. 1989).

3 Methods

3.1 KO Mouse Models

All described animal experiments were in accordance with the national guidelines and approved by the local animal care and use committee (LANUV, Recklinghausen, Licence no. AZ: 84-02.04.2014.A220). The animals were housed at 20-22°C room temperature and a 12h-light-dark-cycle with water and standard diet chow ad libitum.

3.1.1 SM22p38MAPKα Mice

SM22p38MAPKα KO mice were generated by crossing an inbred C57Bl/6 mouse line expressing Cre recombinase specifically in vascular smooth muscle cells and cardiomyocytes under the control of the sm22α promoter (KIsm22α-Cre, Strain Name B6.129S6-Taglntm2(cre)Yec/J, Stock Number 006878, The Jackson Laboratory, Bar Harbor, ME) (Lepore et al. 2005; Zhang et al. 2006) with C57Bl/6 mice homozygously expressing floxed p38MAPKα (p38$^{flox/flox}$, Exon 2 and 3) (Ventura et al. 2007). The p38MAPKαflox/flox mice were kindly provided by M. Pasperakis, Institute for Genetics, University of Cologne, Germany. 12 week old male mice were used for experiments. As controls, p38MAPK$\alpha^{flox/flox}$ litter mates were used.

3.1.2 iCMp38MAPKα Mice

iCMp38MAPKα KO mice were generated by crossing p38MAPK$\alpha^{flox/flox}$ mice with mice hemizygously expressing the tamoxifen-inducible Cre-recombinase merCremer (Verrou et al. 1999; Sohal et al. 2001) under control of an α-MHC promotor (a cardiac-specific promoter of murine alpha myosin-heavy chain (α-MHC)). For KO induction mice were injected with 500μg 4OH-Tamoxifen (5mg/ml in peanut oil) i.p. for 10 days, starting at 6 weeks of age, following a 4 week recovery period before experiments.

12 week old male mice were used for experiments. As controls, p38MAPK$\alpha^{flox/flox}$ litter mates were used, which were also injected with 500μg 4OH-Tamoxifen i.p. for 10 days.

3.1.3 cCMp38MAPKα Mice

cCMp38MAPKα KO mice were generated by crossing p38MAPK$\alpha^{flox/flox}$ mice with mice hemizygously expressing the Cre-recombinase (Agah et al. 1997) under control of an α-MHC promotor.

12 week old male mice were used for experiments. As controls, p38MAPK$\alpha^{flox/flox}$ litter mates were used.

3.2 Echocardiography

Echocardiographic investigations were performed using Vevo 2100 High Frequency Ultrasound System (Visualsonics, Toronto, Canada). Anaesthetic induction was done with 4% isoflurane in a closed chamber. Thereafter the mice were placed on a moveable heating plate and were kept anesthetized with 2-2.5% isoflurane via a nose cone, to obtain a regular heart beat of about 500 beats per minute (bpm). Their paws were fixed onto electrodes to monitor heart rate (via electrocardiogram (ECG)) and breathing frequency. Their body temperature was anally observed with a temperature probe, if the temperature dropped, they could be warmed with infrared lamp. The breast of the mice was first shaved, then hair removal cream was applied to depilate the breast completely for best ultrasound results. Before imaging the breast was covered with pre-warmed sonication gel. The echocardiographic measurements were done with transducer MS400 (18-38 MHz) for up to 30 minutes. B-mode and M-mode measurements of the parasternal long and short axis were performed.

To estimate ejection fraction (EF), end diastolic- and end systolic volume (EDV and ESV) the biplane Simpson's protocol was used. For that parasternal short (apical, mid and basal sections) and long axis B-Mode images of systole and diastole were measured using the Vevo LAB 1.7.1 software. The Simpson method is the most accurate way to estimate ejection fraction (EF), end diastolic- and end systolic volume (EDV and ESV) based on 2D images.

3.3 Cell Cuture of Hybridoma Cells

Three different hybridoma (BA-F8, BF-F3 and SC-71) cell lines were used in this work - see section 2.8.

3.3.1 Culture Media

Freezing Medium

- 60% DMEM
- 20% Fetal Bovine Serum
- 20% DMSO (Dimethylsulfoxid)

Growth Medium

- 89% Dulbecco's MEM (4.5 g/L glucose)
- 10% Fetal bovine serum (SC-71 and BF-F3)/Horse serum (BA-F8)
- 1% Penicillin/Streptomycin
- 2 mM L-glutamine

3.3.2 Thawing of Hybridoma Cells

The cells were stored in 2 ml cryotubes in liquid nitrogen at -196°C. After removal from the liquid nitrogen, the cells were thawed as fast as possible in a 37°C water bath and transferred to a 15 ml Falcon tube. Growth medium (approx. 8 ml) was slowly added, whereby the tube was continuously gently shaken. The cells were then centrifuged for 7 minutes, at 1000 rpm at room temperature. The supernatant was aspirated and the cell pellet was resuspended in 5 ml fresh growth medium. Afterwards the cells were plated onto either a 6-well plate or a 10 cm cell culture dish. Thereafter they were incubated at 37°C and 5% CO_2.

3.3.3 Cultivation of Hybridoma Cells

Cells were maintained at 0.1-0.5 x 10^6 cells/ml at 37°C and 5% CO_2. The growth medium was changed every 1-2 days.

3.3.4 Splitting of Hybridoma Cells

Usually hybridoma cells were split every 2-4 days, when they reached a confluence of about 80% (or 1 x 10^6 cells/ml).

Before splitting, the number of living cells had to be calculated. As hybridoma cells are hardly adherent, dead cells were identified using trypan blue (0.4%). Trypan blue is used to mark dead cells, as it can not enter cells with an intact membrane. An aliquot of cell suspension was incubated with trypan blue (1:1) for 5 minutes, thereafter the amount of living cells (unstained) was calculated using a Neubauer chamber cell counter.

The cells were then pelleted at 1000 rpm at room temperature for 7 minutes. Thereafter they were resuspended in an appropriate amount of fresh growth medium to reach a cell number of 0.1-0.5 x 10^6 cells/ml.

3.3.5 Increasing the Antibody Production

Hybridoma cells were starved (no change of growth media) for 2-3 days before antibodies were harvested. This was done to maximize the antibody secretion, as stress boosts the antibody production in hybridoma cells. The harvest of antibodies is described later in section 3.3.7.

3.3.6 Freezing of Hybridoma Cells

Before freezing, the amount of living cells was counted (using a Neubauer chamber) and adjusted to 1-2 x 10^6 cells/ml. Freshly prepared freezing medium was slowly added to the cell suspension, until a final concentration of 0.5-1 x 10^6 cells/ml was reached (500 μl cell suspension + 500 μl freezing medium). The cells were then portioned into 1 ml cryotubes. These tubes were placed in a thick-walled Styrofoam container and were put in a -80°C freezer for at least 48 hours, to reassure the slow freezing of the cells of maximally -1°C/min. Thereafter they were transferred into liquid nitrogen tanks for long time storage.

3.3.7 Antibody Production From Hybridoma Cell Lines

To maximize the number of antibodies in the supernatant, the media was not changed 2-3 days before harvesting. This nutrient depletion causes stress to the hybridoma cells, which consequently produce more antibodies. As the supernatant turned yellow (which indicates acidification and consequently depletion of nutrients) and cells starting to die, the cell suspension was centrifuged at full speed for 10 minutes. Thereafter the supernatant was transferred into a new falcon tube and centrifuged once again. The supernatant, containing the antibodies, was aliquoted in 1.5 ml tubes and stored at -80°C until usage.

To determine the best efficiency of these antibodies, serial experiments were performed, to test whether the antibodies had to be serially applied, or whether they can be used as an antibody cocktail. To uncover the ideal concentration, varying amounts of antibody were used. Those test-experiments revealed, that the antibodies were specific enough to be used as a cocktail. The concentration of antibodies depended on the batch used, as the amount of antibodies differed at the time of harvest. Therefore this had to be tested after every harvest of new antibodies. Nonetheless the range, which worked best for these antibodies, was 1:10 to 1:50 dilutions. Of notice, that the IgM antibody (BF-F3, anti-MyHC type 2B) had to be used more concentrated (1:10) than the others. For SC-71 (anti-MyHC type 2A) and BA-F8 (anti-MyHC type 1) it was best to start with an 1:25 dilution.

3.4 Histological Analysis

Muscles from the murine hind limb (*Musculus gastrocnemius*, *Musculus plantaris* and *Musculus soleus*) were harvested immediately after sacrificing the mice. The muscles were specifically oriented (the Achilles tendon pointed at a pre-marked side of the mold with the *M. soleus* on the upside) and immersed in an O.C.T. compound filled mold. These molds were plunged in pre-chilled isopentane (-90 – -100°C), until the block was completely frozen (about one minute). Nonetheless the block should not be simply dropped into the isopentane, as this might crack the block, due to uneven freezing. In contrast to other organs, like heart, which are frozen at about - 35°C, in skeletal muscle this low temperature is of great importance to avoid freezing artifacts. In general skeletal muscle are very prone to tissue damage while freezing, hence a fast procedure at the right temperature is important. It is an absolute necessity to avoid (partly) thawing of the tissue thereafter, as the tissue gets irreparable damaged which makes histological investigations impossible. Therefore one has to make sure to keep the tissue block always on dry ice after freezing, especially if more than one animal is harvested. For long time storage, the tissue block can be kept at -80°C until usage.

3.4.1 Cryosectioning

For cutting skeletal muscles the cryostat has to be pre-cooled at -22°C. The tissue blocks were also put to -22°C at least 1 hour before cutting (or o/n) to equilibrate temperature. 8 μm thick skeletal muscle sections were made. Two sequential sections were put on one object slide, dried for 5 minutes with a hairdryer (not heated), marked with a pencil and stored in a microscope slide box containing dry beads to avoid humidity. Additionally the slide boxes are

sealed with adhesive tape to keep them dry as long as possible. For long term storage the boxes can be stored at either -20°C or -80°C. Before opening the box, it has to be slowly warmed to room temperature, by putting them at 4°C over night followed by 30 minutes equilibration to room temperature using a hairdryer. Dry beads should be changed if necessary (indicated by a change of color from blue to pink) after opening the box. It always has to be kept in mind that some stainings, which are based on enzymatic reactions, might get impaired by multiple freeze-thaw cycles.

3.4.2 Succinate Dehydrogenase (SDH) Staining

The sections were stained according to a modified protocol from Lojda et al (Lojda et al. 1976).

SDH, also known as respiratory complex II, is located in the inner mitochondrial membrane. This assay is based on the enzymatic reactivity of SDH, which oxidizes succinate to fumarate in the citric acid cycle. The following transfer of electrons to ubiquinone is mimicked by an artificial electron acceptor - Nitroblue tetrazolium (NBT) - which enables visualization (by its intensity of purple stain) of mitochondrial density and the SDH activity. Therefore slow-twitch, mitochondria rich (oxidative) muscle fibers display a relatively dense, purple speckled pattern, can be easily distinguished from fast-twitch, mitochondria poor (nonoxidative) fibers, which have a smaller amount of purple staining (also see figure 4.4).

The substrate solution contains 0.5mg/ml Nitroblue tetrazolium (NBT), 50mM succinat and 0.8% potassium cyanide (KCN) dissolved in 0.1M phosphate buffered saline (PBS). For one batch of 20 object slides 150ml of the solution is needed, therefore 150ml of PBS is mixed with following amounts of chemicals:

Chemical	**Molecular Weight [g/Mol]**	**Amount [mg]**
NBT	817.6	75
Succinat	118.1	885
KCN	65.1	1200

The substrate solution is pre-warmed to 37°C (for about 30 minutes). Thereafter fresh or thawed (at 4°C o/n) unfixed skeletal muscle sections are incubated in the solution for about 50 minutes. The actual time depends on enzyme reactivity indicated by a distinct blue staining, which has to be visually observed. After the incubation time the slides were rinsed with Aqua destillata to stop the enzymatic reaction, then they are placed in PBS (200ml) for 5 minutes. For fixation the slides were immersed in buffered formalin for 10 minutes. Then the slides were rinsed 3 times with Aqua destillata (1x short, 2x 5'), and finally the sections were embedded with aqua mount (to protect the tissue from drying out) and covered with a cover glass. After drying, the slides can be investigated using bright light microscopes. These sections be kept for long term as the SDH stain will not fade over time.

3.4.3 Fat-Red Staining

The Fat-Red staining of lipids is based on the better solubility of Sudan-dyes in lipids compared to the solvent. Sections used for staining are not to be treated with any fat-soluble solutions (xylol, high-proof alkohol) at any time.

Cryosections were fixed with Formol-Calcium for 10 minutes and washed for 3x10 minutes with aqua bidest. After the washing steps the sections were put in 60% isopropanol for 5 minutes, then they were stained with the freshly filtered staining solution for 10 minutes. Excessive dye was washed out by putting the section for 4-6 seconds in 60% isopropanol, thereafter the sections were again washed for 3x10 minutes with aqua bidest. The nuclei were stained with Mayers hematoxylin (Merck) for 2 minutes, which is blued under tap water. Finally the sections were washed once more with aqua bidest and mounted with a water soluble solution (such as Aquatex, Merck or Aqua mount, Plano).

Fixation solution (Formol-Calcium):
1g $CaCl_2$ dissolved in 80ml aqua bidest; 10ml formalin (37%) is added and neutralized with Ca_2HCO_3.
Staining solution (Fat Red):
0.5g of Oil-Red-O (also called Fatred 7B) is dissolved in 100ml 99% isopropanol (stock solution). 6 parts of the stock solution are mixed with 4 parts of aqua bidest and left for 24 hours before usage. Then the solution is filtered and ready to use.

3.4.4 Immunofluorescence

Immunofluorescence staining was performed as described by Emde et al (Emde et al. 2014). Briefly, 8 μm thick skeletal muscle sections were fixed with either 4% paraformaldehyde (PFA) or 4% Zambonis fixative in 0.1M phosphate buffered saline (PBS; pH 7.4) for 10 min. The sections got permeabilized with 0.2% saponin in PBS and then blocked by 10% normal goat serum (NGS) in 0.2% saponin in PBS for 60 minutes. Primary antibody (in 2% NGS) was incubated at 4°C over night, secondary antibody for 3 hours at room temperature in the dark. Mounting was performed with Pro long gold antifade reagent with or without DAPI. Mouse on mouse protocol included an additional cleaning step after fixation with 1% Triton X-100 in PBS for 60 minutes at room temperature (RT). For the NGS blocking step, 1% Triton X-100 in PBS was used instead of saponin + PBS. After blocking with NGS an endogenous IgG block was performed using anti-mouse-Fab-fragments from goat (1:10) in PBS + Tween20 (0.2%) for 3 hours at RT. Tween20 in PBS was used for the rest of the protocol, instead of 0.2% saponin in PBS, despite the final washing step, where only 0.1M PBS was used. A list of used primary and secondary antibodies can be found in section 2.5.

Microscopical images were taken with fluorescence microscope Keyence BZ 9000 (Keyence). Overview images were made by using the 'multiimage-function', where several, overlapping pictures (4-fold magnification) were automatically merged into one image. To compare images the intensities of different fluorescence channels should be kept the same throughout one experiment.

3.5 Protein Analysis

3.5.1 Protein Isolation from Tissue

After the animals were sacrificed, tissues for protein analysis were harvested and snap-frozen in liquid nitrogen. The tissue were homogenized (using tissue rupture) in lysis buffer (10 mM Tris-Cl, 150 mM NaCl, 0.1% IGEPAL, pH 7.4), which was supplemented with protease- and phosphatase inhibitors. The homogenization step was followed by a 5-10 minutes centrifugation step at full speed at 4°C.

3.5.2 BCA Assay

To determine the concentration of proteins the bicinchoninic acid (BCA) assay was used. The standard series was made using ascending concentration of BSA in lysis buffer (25-2000 μg/ml). Samples (25 μl of (un)diluted samples mixed with 200 μl of BCA reagent) were pipetted as doublets onto a 96-well plate. This plate was then incubated for 30 minutes at 37°C. The absorption of the samples at 577 nm was measured with Elisa-Reader SpectraCount (Packard) and analyzed with the computer program PlateReader V3.0. The protein concentration was determined based on the standard curve. Thereafter a specific protein concentration could be prepared (usually 1 μg/μl).

3.5.3 Polyacryamidgelelectrophoresis with SDS

Before proteins could be separated, they had to be denatured. Therefore the samples were mixed with Laemmli-buffer and heated at 95°C for 5 minutes.

There are two different gels needed for a SDS-polyacrylamidgel - a stacking gel and a separation gel. The stacking gel enables the uniform transition of protein into the separation gel, where the proteins get separated according to their molecular size. The electrophorectical separation was done using Hoefer-electrophoresis tanks filled with SDS-running buffer at 50-200 V. To estimate the size of proteins the PageRuler Prestained Protein Ladder (Fermentas) (10-170 kDa) was used.

Laemmli-buffer:

0.25 M	Tris (pH 6.8)
8% (w/v)	SDS
100 mM	DTT
20% (v/v)	Glycerol
0.02% (w/v)	Bromphenol blue

Stacking gel (2.5%):

2.5 ml	40% Acrylamid
2.5 ml	1M Tris (pH 6.8)
200 μl	10% SDS
30 μl	TEMED
60 μl	10% APS
ad 14.8 ml	H_2O

Separation gel (10%)

10 ml	40% Acrylamid
10 ml	1M Tris (pH 8.8)
400 μl	10% SDS
80 μl	TEMED
100 μl	10% APS
ad 20 ml	H_2O

SDS running buffer:

25 mM	Tris
250 mM	Glycin (pH 8.3)
0.1% (w/v)	SDS
ad 2 l	H_2O

3.5.4 Western Blot Analysis

The proteins from the SDS-polyacrylamidgel were transferred to a nitrocellulose membrane using Pierce^{TM} G2 Fast Blotter with pre-programmed method for mixed molecular weight (25V, 1.3mA, 7 minutes). After the transfer the membrane was blocked in a blocking solution (TBS 1:1 LI-COR Odyssey solution) for 30-60 minutes to avoid unspecific binding of antibodies.

Thereafter the membrane was wrapped in a plastic foil and incubated with the primary antibody (concentration according to distributor; diluted in 5% BSA and TBS-T) at 4°C over night. The membrane was washed three times with TBS-T for 10 minutes, then the secondary fluorescent antibodies (LI-COR antibodies, 1:15000 in LI-COR Odyssey solution) were incubated for 45 minutes at room temperature in the dark. After another 5 washings steps using TBS-T and TBS, the fluorescence of the secondary antibodies could be detected using the LI-COR Odyssey imaging systems. The analysis were done using the computer program LI-COR Image Studio.

3.6 Real-time Quantitative Polymerase Chain Reaction (qPCR)

Polymerase chain reaction (PCR) is an often used tool to detect and quantify DNA by amplification, as, in an optimized reaction, the amount of DNA will double during each cycle. In real-time quantitative PCR (qPCR) this amplification is linked to fluorescence intensity

which is assessed after each amplification cycle. This allows to quantify the initial amount of DNA based on the fluorescence signal during the exponential phase of amplification as the fluorescence intensity correlates with the amount of synthesized DNA. Fluorescent reporter molecules are either double-stranded DNA binding probes (e.g. SybrGreen) or fluorescent labeled gene-specific primers (e.g. TaqMan). The fluorescence readout can be processed by specific qPCR machines, which blot fluorescence vs. cycle number for each sample. Thereafter a threshold level has to be set, which is above the background and within the linear phase of all samples. The value, where a sample hit this threshold is called threshold cycle (Ct). The Ct value enables the calculation back to starting amount of each target. With this method the amount of genomic DNA (gDNA) can be assessed as well as the amount of complementary DNA (cDNA), transcribed from mRNA as the readout of transcript expression.

3.6.1 Isolation of messenger RNA (mRNA)

Hearts, *M. gastrocnemius*, *M. plantaris* and *M. soleus* were harvested and weighted individually immediately after sacrificing the mice. They were snap-frozen in liquid nitrogen and stored at -80°C until usage. Whole *M. plantaris* (about 18mg), whole *M. soleus* (about 10mg) and 30mg of *M. gastrocnemius* or heart (maximum amount of tissue per isolation) were used. The Fibrous Tissue RNeasy Minikit, Qiagen (#74704) was used to isolate mRNA according to manufacturer's recommendation.

Briefly, up to 30mg of tissue was homogenized in a specific amount of lysis buffer, containing β-mercaptoethanol. After treatment with proteinase K, the homogenate was centrifuged. The supernatant was mixed with 98% ethanol and transferred on a RNA specific column. Several washing steps with or without on column genomic DNA digestion (Microarray analysis only), were followed by the elution of mRNA with 30-50μl RNase free water. The concentration of mRNA was determined using Nanodrop ND-1000. The 280/260 ratio of the samples indicates the purity of the RNA relative to proteins and should be above 1.9.

3.6.2 cDNA Transcription

Up to 1μg mRNA was transcribed into complementary DNA (cDNA) using QuantiTect Reverse Transcription Kit, Qiagen (#205313) according to manufacturer's protocol.

Briefly, mRNA was diluted with RNase free water to a final concentration of 500ng-1μg per 20μl reaction volume. First genomic DNA was eliminated, then mRNA was reverse transcribed at 42°C for 15 minutes. The reverse transcriptase got inactivated at 95°C for 3 minutes. The newly synthesized cDNA could be immediately used for PCR or stored at -20°C.

3.6.3 SybrGreen

For detection of transcript expression (cDNA), the 'Maxima SYRB Green/ROX qPCR Master Mix' of Thermo Scientific (#K0223) was used. The master mix (MM) contains Maxima Hot Start Taq DNA Polymerase and dNTPs in an optimized PCR buffer. Additionally cDNA and primers were utilized as indicated below:

SybrGreen MM [2x]	10.0μl
ddH_2O	7.2μl
cDNA [20-40ng/μl]	1.0μl
Fwd Primer [450nM]	0.9μl
Rev Primer [450nM]	0.9μl
Total	20.0μl

cDNA of skeletal muscles was used at a final concentration of 20ng/well (40ng/well for heart). Pre-designed primers (listed in section 2.7) were used, which were specifically designed for cDNA based qPCR, as at least one primer (forward or reverse) was exon spanning. Hence genomic DNA (gDNA), which in contrast to cDNA still consists of exons and introns, could not get amplified. The primer specificity was also validated using the melting curve analysis at the end of each qPCR run. The melting point of each amplicon is defined by its length and nucleotide composition. Once its specific melting temperature is reached, the double strands will open, the intercalated fluorophores are released and the fluorescent signal is lost. If all amplicons are of same size, there is only one peak, indicating that only the correct transcript was amplified. To illustrate the transcript specificity, figure 3.1 shows the melting curves of *Csnk2b, Foxo1* and *Foxo3*.

Each gene was measured in technical duplicates and compared to Csnk2b, which was used as a reference gene in skeletal muscles. A calibrator was included on every plate (also see section 4.5.2) , to enable the comparison of different plates. Additionally a negative control for each primer was included on every plate (MM without cDNA).

3.6.4 Settings

All experiments were performed with the 'StepOne Plus Real-Time PCR Detection System' (Applied Biosystems). Following setting for gene amplification was used: First cycle at 95°C for 10 minutes (activation of Taq-polymerase) followed by 40 cycles at 95°C for 15 seconds and 60°C for 60 seconds. The specificity of amplicons was verified by melting curve analysis starting with 95°C for 15 seconds, then 60°C for 60 seconds. Thereafter the temperature was increased 0.3°C every 15 seconds, until the final temperature of 90°C was reached.

3.6.5 Analysis

In qPCR to quantitatively analyze genes of interest (GOIs) the comparative Ct or X_0 method can be used. Both methods require an endogenous reference gene (RG) to compare different experimental/genotypical conditions or different timepoints.

Comparative Ct Method

The comparative Ct Method, also known as $2^{-\Delta\Delta Ct}$ method, is used to analyze the relative changes in gene expression from qPCR experiments. This method compares gene expression of a gene of interest (GOI), normalized to an endogenous reference gene (RG), under specified conditions to control conditions and is represented as fold-change (Livak and Schmittgen 2001). Briefly, first ΔCt is calculated, where the Ct value of the RG gets subtracted from the

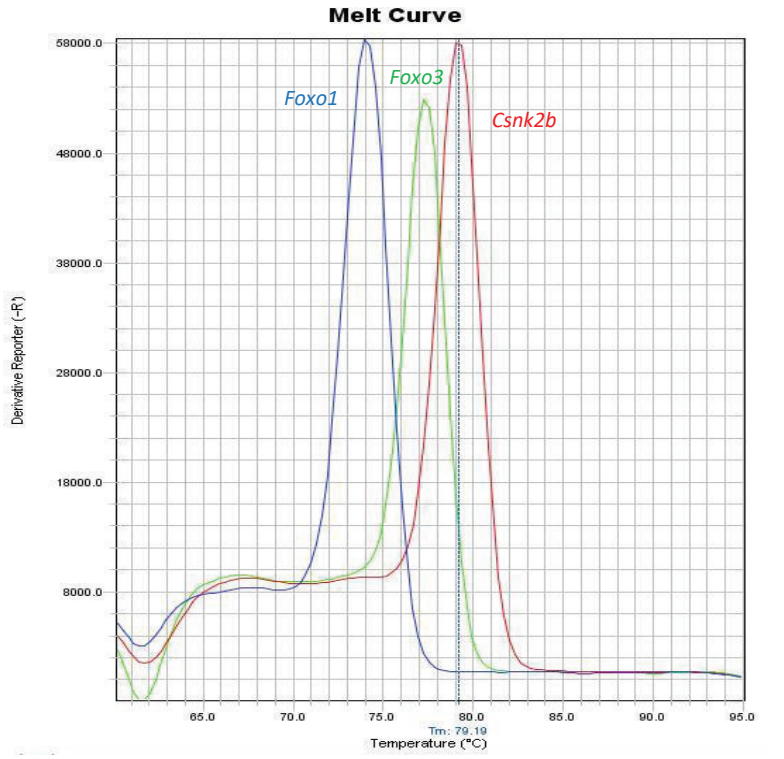

Figure 3.1: Melt Curve Analysis
The specificity of *Csnk2b* (red) , *Foxo1* (blue) and *Foxo3* (green) amplicons was verified by melting curve analysis starting with 95°C for 15 seconds, then 60°C for 60 seconds. Thereafter the temperature was increased 0.3°C every 15 seconds, until the final temperature of 90°C was reached. At a specific melting temperature, dependent on the length and nucleotide composition of each transcript, the double stranded amplicon denatured, releasing the intercalated SybrGreen fluorophores.

Ct value of the GOI. Thereafter the mean value of ΔCt from different conditions get calculated (eg. KO and control). The ΔΔCt step compares different conditions, hence the mean ΔCt value of condition 1 (eg. control) gets subtracted from the mean ΔCt value of condition 2 (eg. KO). Last the fold-change (FC) is calculated by the eponymous formula $FC=2^{-\Delta\Delta Ct}$, indicating an up- or downregulation of the GOI by values >1 or <1, respectively. As transcript expression slightly fluctuates between plates, only transcripts with more than 2-fold expression change were considered to be significant.

X_0 Method

In contrast to the comparative Ct Method, where only the fold-change is calculated, the X_0 method provides additional information about transcript expression levels as well as it is possible to calculate standard deviations.

The X_0 method is based on the equation (Thomsen et al. 2010):

$$X_n = X_0 \times (1+E_{amp})^n.$$

In this equation it is assumed that E_{amp} equals 1 ($\widehat{=}$ 100% efficiency of the qPCR), 'n'

equals a manually set threshold within the linear phase of transcript expression; X_n (also known as Ct) equals the value at this specific threshold; and X_0 equals the initial amount of cDNA in a sample. If values of 'n' and X_n are known, the equation can be solved after X_0:

$$X_0 = \frac{X_n}{2^n}.$$

To identify differences between two conditions, the X_0 value of a gene of interest was divided by the reference gene of the same sample. Thereafter it is possible to statistically compare different conditions (e.g. transcript expression changes over time or transcript expression changes at a given timepoint between groups).

3.7 Microarray Transcript Expression Analysis

To identify the transcript profile of heart and skeletal muscles (*M. plantaris*), mRNA of SM22p38MAPKα control and KO animals was isolated under baseline condition and after 48 hours of ANGII treatment. Four animals were used for each group (Control baseline, Control ANGII, KO baseline, KO ANGII).

The mRNA was isolated as described in section 3.6.1. Important to notice is the on-column digestion with DNase, to eliminate genomic DNA contamination of the isolates. The mRNA concentration was estimated using Nanodrop ND-1000. If applicable the mRNA was diluted to a final concentration of 100ng/μl. The mRNA was first analyzed by Dr. René Deenen of the 'Biologisch-Medizinisches Forschungszentrum (BMFZ)' of the Heinrich Heine University Düsseldorf for quality by determining the RNA integrity number (RIN), which indicates the integrity of RNA, by classifying RNA based on their 18S to 28S ribosomal subunits ratio (as degradation of RNA can be seen by a decrease in the 18S to 28S ribosomal band ratio and an increase in the baseline signal between the two ribosomal peaks and the lower marker). It ranks from 1 to 10, with 1 being the most degraded profile and 10 being the most intact (Schroeder et al. 2006). For microarray analysis a high quality mRNA (RIN of 8-10) is preferable. The high quality of the RNA samples generated are illustratively shown in figure 3.2, where mRNA isolates of heart (Hrt), *M. gastrocnemius* (G), *M. plantaris* (P) and *M. soleus* (S) are depicted, all showing a RIN above 8.

Passing the quality control, the mRNA could be used for microarray transcript analysis, which also were performed and analyzed by Dr. René Deenen (Bottermann, Leitner et al, in preparation), as described in supplemental section 9.2.

3.7.1 Ingenuity Pathway Analysis (IPA) of Microarray Data

Lists of significantly altered transcripts (fold-change >1.5) of *M. plantaris* of SM22p38MAPKα control and KO mice 48 hours after ANGII treatment by microarray analysis were uploaded and analyzed using the IPA software (Qiagen). Core analysis of microarray data was done to identify significantly altered canonical pathways as well as associated diseases and functions listed by their p-value.

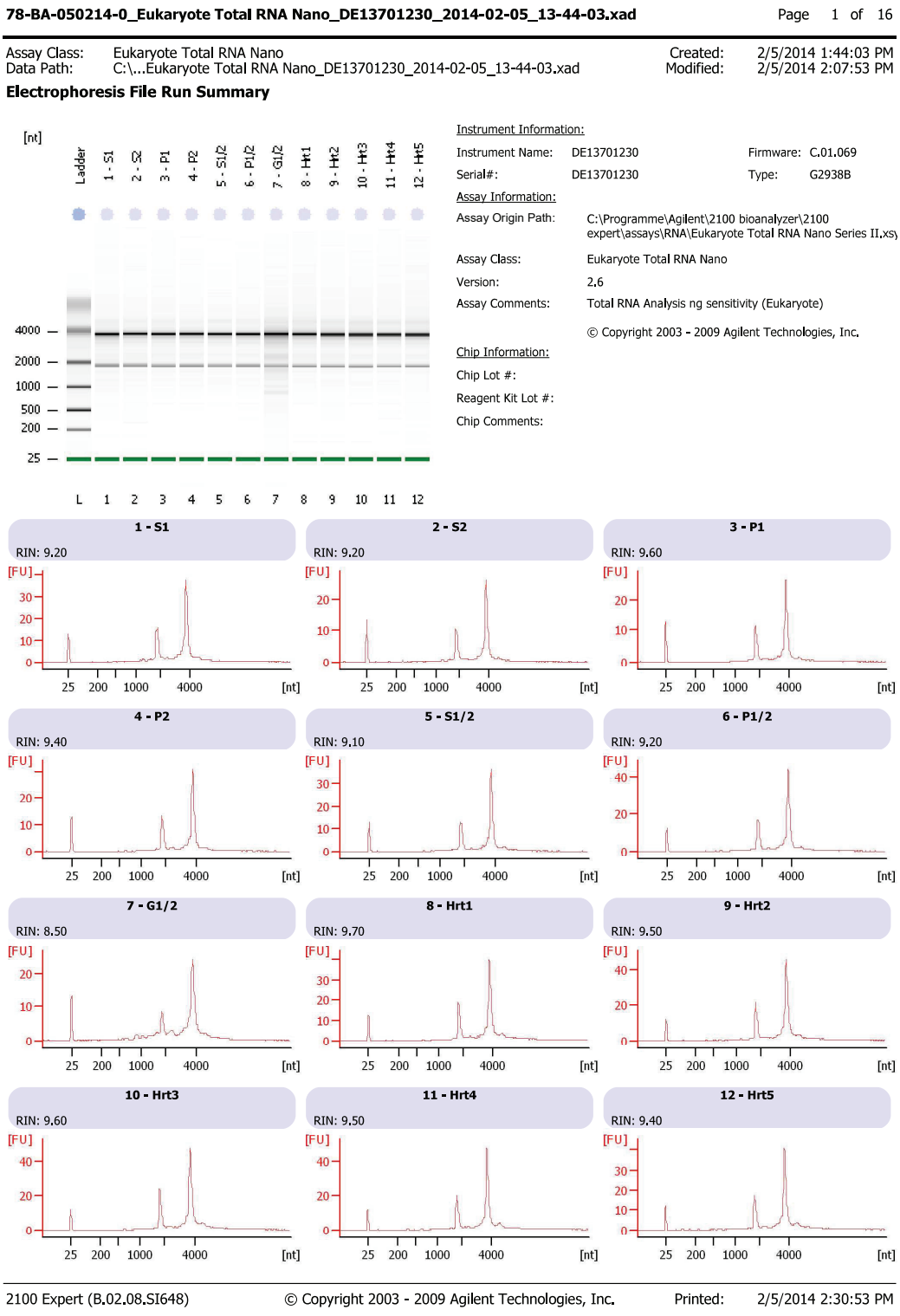

Figure 3.2: Quality Control of mRNA Isolates
The quality of mRNA isolated from heart (Hrt), *M. gastrocnemius* (G), *M. plantaris* (P) and *M. soleus* (S). The length of 18S and 28S mRNA is depicted in nucleotides [nt], where 18S is about 2000nt in size and 28S about 4000nt. The amount of both ribosomes is calculated based on their fluorescence [FU].

3.8 Angiotensin II Treatment

Angiotensin II (ANGII) modulates many cardiac functions including cardiac contractility, remodeling, growth and apoptosis. Long term, systematically applied ANGII in hyperphysiological conditions (1.5μg/g/day) leads to vasoconstriction, subsequently to blood pressure overload and ultimately resulting in heart failure (Crowley et al. 2006).

3.8.1 Osmotic Minipump Implantation

Mice received 1μg/kg/min Angiotensin II (ANGII; Sigma, #A9525) via Alzet osmotic mini pumps (model 1003D) for 2 and 14 days, respectively. The function of the pumps is based on the osmotic principle between a compartment within the pump and the tissue environment. As fluids of the tissue environment enter the mini pump, the substance gets released into the body.

Each pump model has its specified pumping rate. The pump rate of the 1003D model (3d pump) is 1μl/hr with a final filling volume of 100μl. As the function is based on an osmotic principle it is of great importance, that the pumps are filled completely (minimum 90%), even if the time of infusion is below maximal duration. The complete filling had to be validated by weighting the pumps before and after filling. If the filling did not exceed 90% ($\cong$ 90μl $\cong$ 90mg), the pump was emptied and refilled before implantation.

To get the substrate administration started, the pumps had to be incubated for at least 4-6 hours (preferentially o/n) at 37°C before implantation to guarantee immediate ANGII administration once implanted. To implant the pumps the mice were anesthetized with 2.5 % isoflurane and kept anesthetized throughout the intervention. The neck got locally shaved followed by a small incision, where the pumps were subcutaneously (by carefully forming a subcutaneous pocket using a surgical clamp) implanted on the back of the mice. Thereafter the wound is sutured with 4-5 stitches.

3.9 Neutrophil Depletion

For the depletion of neutrophil anti-Ly6G-antibody, clone 1A8 (BioXCell, #BE0075-1) was used. To rule out non-specific effects of the antibody, a control group was treated with an isotype control antibody (InVivoMab Rat IgG2a, clone 2A3, BioXCell, #BE0089). 500μg of the anti-Ly6G antibody and the corresponding isotype control were injected i.p. 12-16 hours before osmotic mini pump implantation. Four different groups were defined - isotype treated controls (Ctrl+IT) and KOs (KO+IT) and anti-Ly6G antibody treated controls (Ctrl+AB) and KOs (KO+AB). The animal number investigated as listed:

	Ctrl+IT	KO+IT	Ctrl+AB	KO+AB
Number of Animals	6	6	8	8

The flow cytometric analysis of circulating neutrophils in blood serum was performed by Dr. Maria Grandoch as described in Grandoch et al. 2015. 48 hours after pump implantation the successful depletion of neutrophils could be validated, as demonstrated in supplemental figure 9.4.

Cardiac parameter of mice were echocardiographically assessed by Dr. Bottermann at baseline and after 48 hours of ANGII treatment.

12-16 hours after the injection of the antibodies (anti-Ly6G and IT), ANGII filled osmotic minipumps were implanted. After 48 hours of treatment, the tissues were harvested and used for histological investigations, as well as mRNA analyses as described earlier.

3.10 Statistics

All data are depicted as mean ± standard deviation, statistical analysis were performed using Microsoft Excel Professional Plus 2013 and Graph Pad Prism 5. For time line analysis two way ANOVA followed by Bonferoni post test was used. Two groups were compared using student's t-test. For comparison of multiple groups one way ANOVA followed by Tukey post test was performed. Differences of $p<0.05$ were considered statistically significant (* $p<0.05$, ** $p<0.01$, *** $p<0.001$).

4 Results

4.1 Heart Failure Model – SM22p38MAPKα KO Mouse

To better understand early triggers of heart-skeletal muscle cross talk the SM22p38MAPKα KO mouse model, as described in the introduction (see section 1.1.1 and method section 3.1.1) was used. The SM22p38MAPKα mouse develops a dilative phenotype with severe cardiac dysfunction over 14 days after ANGII treatment (see figure 1.2). 12 week old male mice were used for the experiments. As controls p38MAPK$\alpha^{flox/flox}$ litter mates were used, without expressing the Cre recombinase.

Under baseline conditions functional heart parameters of SM22p38MAPKα KO mice were indistinguishable from controls, as seen in figure 1.2. After induction of heart failure, using ANGII applied via osmotic mini pumps, the echocardiographical analysis of SM22p38MAPKα mice unraveled the full establishment of cardiac dysfunction in KO hearts already 2 days after ANGII treatment, which did not improve over time. Control animals, which also showed a small decrease of ejection fraction (EF) after 2 days, fully recovered, as seen at day 7 and day 14.

Besides the heart failure, a severe loss of body mass over time of SM22p38MAPKα KO mice was observed, as shown in figure 4.1. The body weight of SM22p38MAPKα control and KO animals drops in the first two days, but in contrast to control mice, which recover over time, KO animals stayed below initial body weight throughout the time of investigation.

This observation lead to the assumption that SM22p38MAPKα KO mice could serve as a model to investigate muscle wasting, likely induced by heart failure.

As heart failure in these mice was already fully established after 2 days of treatment, this time point was chosen as the starting point to investigate influences of cardiac impairment on skeletal muscles. To test for early signs of skeletal muscle wasting, histological sections could provide valuable first insights, as atrophy could affect cross sectional areas of single fibers. Therefore following muscles from the hind limb were harvested and analyzed: *M. gastrocnemius*, *M. plantaris* and *M. soleus*. These muscles are often chosen for analysis, as they are definite, easily accessible and due to their different metabolic properties: fast-twitch, glycolytic or slow twitch, oxidative muscle fibers (also see table 1.1). Especially *M. plantaris* and *M. soleus* are often analyzed, as they exhibit a homogenous distribution of mainly glycolytic or oxidative fibers, respectively.

To get a better impression of their actual size, a photograph of the muscles is shown in

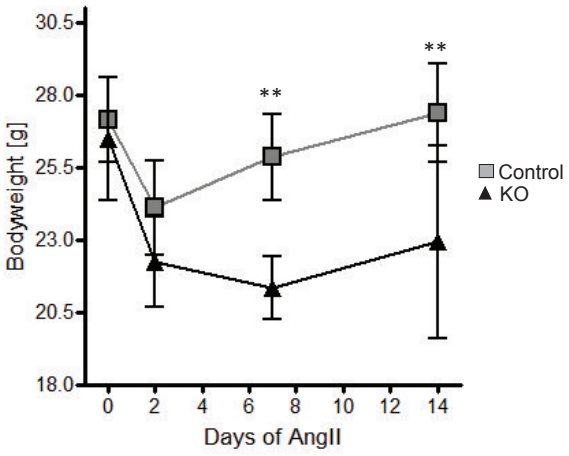

Figure 4.1: Body Weight Progression of SM22p38MAPKα Mice
Body weight progression of SM22p38MAPKα control (grey) and KO (black) mice over 14 days of ANGII treatment. Data represent mean±SD; **: $p<0.01$; n=4-9.

figure 4.2. From left to right *M. gastrocnemius* (about 150mg), *M. plantaris* (about 18mg) and *M. soleus* (about 10mg) from the same animal are depicted. Due to the high amount of myoglobin of slow oxidative fibers, the color of *M. soleus* appears dark red. In contrast *M. plantaris* consists mainly of type 2 fibers, which contain less myoglobin and therefore appears paler in color. Areas of rather oxidative or glycolytic fibers in *M. gastrocnemius* can also be estimated by their different shades of red (myoglobin content) in this photograph.

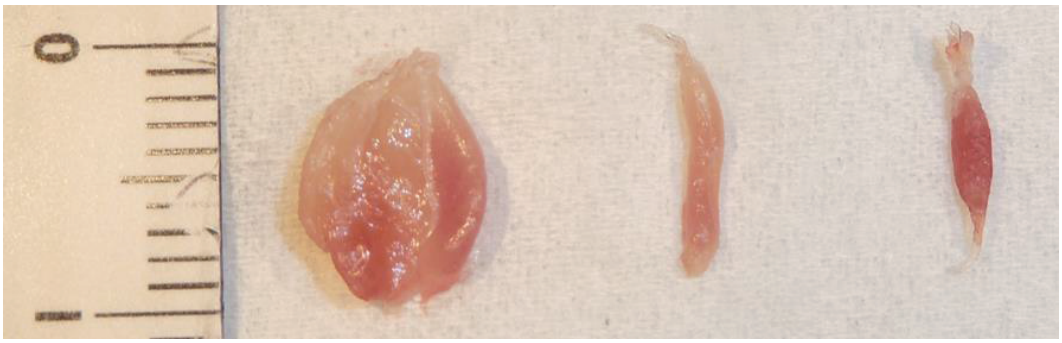

Figure 4.2: Image of *M. gastrocnemius*, *M. plantaris* and *M. soleus*
Photographic image of (from left to right) *M. gastrocnemius*, *M. plantaris* and *M. soleus*. The intensity of red color is due to different myoglobin contents (dark red - oxidative fibers, pale color - glycolytic fibers). Scale = 1cm

4.2 Histological Analysis of Skeletal Muscles

To investigate possible morphological alterations in skeletal muscles, they were harvested, frozen and sectioned as described in section 3.4. Serial 8 μm cross sections were made of murine calf muscles (including *M. gastrocnemius*, *M. plantaris* and *M. soleus*) of control and p38MAPKα KO mice. Two consecutive cross sections were placed on one microscope slide

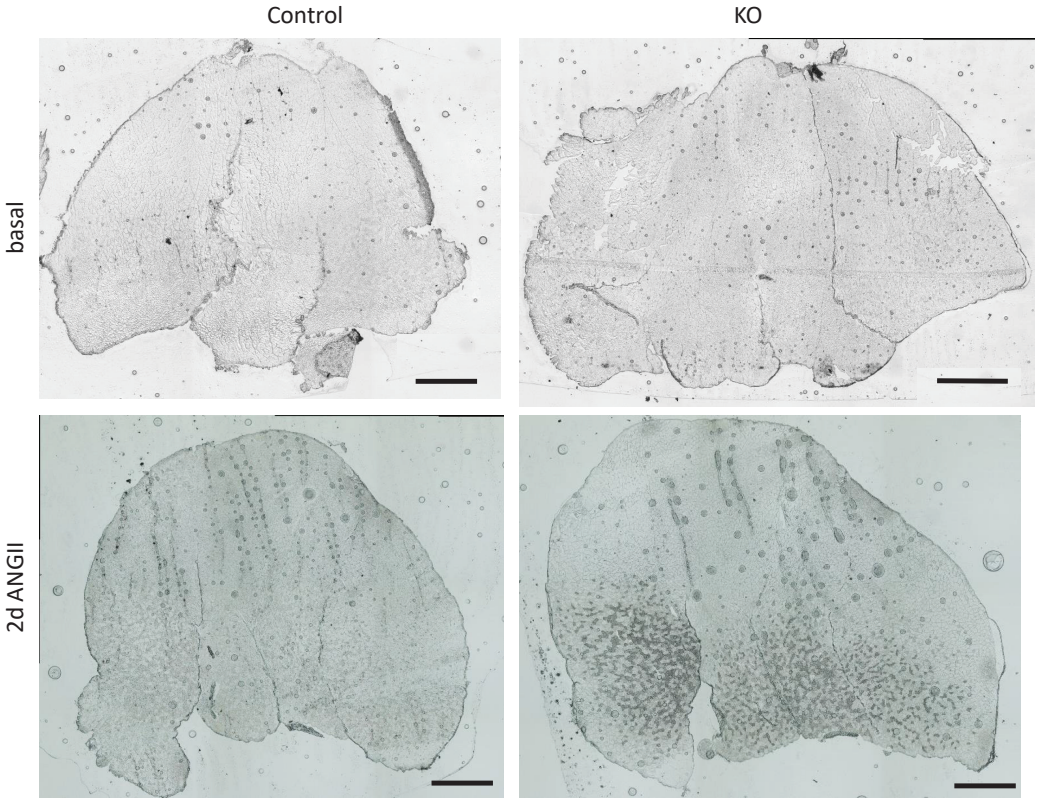

Figure 4.3: Morphological Alterations in Skeletal Muscles after Heart Failure
Native cross sections of murine hind limb of SM22p38MAPKα control (A+C) and KO (B+D) animals under baseline conditions (A+B) and 2 days after ANGII treatment. Scale bars 1000 μm

and 6 slides were made of each sample.

Skeletal muscle sections were analyzed under baseline condition and 48 hours after ANGII treatment in SM22p38MAPKα mice. Surprisingly native cross sections of ANGII-treated SM22p38MAPKα KO mice exhibited darker appearing fibers in a spotted pattern in skeletal muscle sections, in contrast to native cross sections of untreated SM22p38MAPKα control and KO mice, which did not show any abnormalities, as seen in figure 4.3. This was the first indication of ongoing alterations in skeletal muscles shortly after induction of heart failure. To identify a possible fiber-type specificity of these alterations, which were solely found in ANGII treated SM22p38MAPKα KO mice, several enzymatic and immunological stainings were performed.

4.2.1 Identifying Oxidative Fibers within Skeletal Muscle

To get a better understanding of fiber type distribution within the skeletal muscles of interest the oxidative potential of muscles fibers was identified with the succinate dehydrogenase (SDH) assay, an assay based on the oxidative capacity of mitochondrial complex II (see section 3.4.2). This enables to distinguish between oxidative (rich in mitochondria) and glycolytic fibers. In figure 4.4 the usual distribution of oxidative (dark) and glycolytic fibers (bright) of *M. gastrocnemius*, *M. plantaris* and *M. soleus* is depicted. Whereas *M. plantaris* and *M. soleus* show a rather homogenous distribution of muscle fibers, *M. gastrocnemius* has different

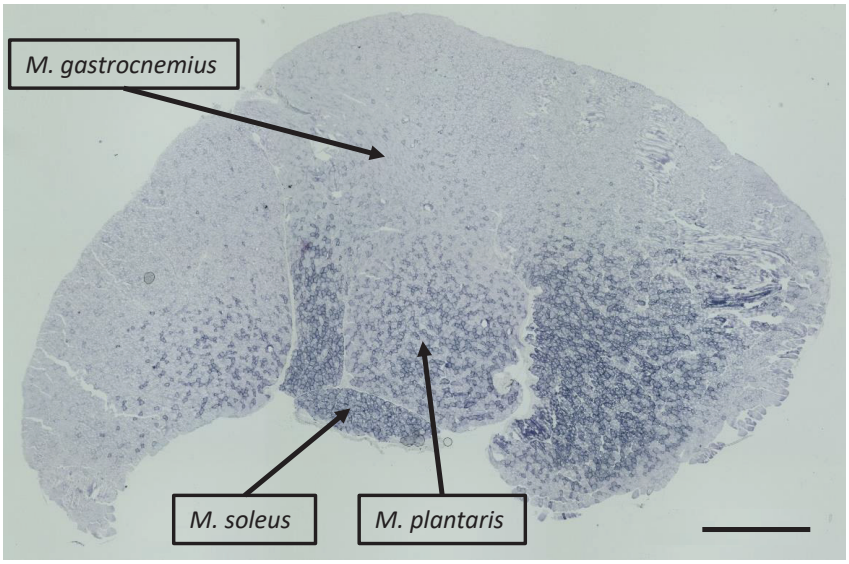

Figure 4.4: Oxidative Potential of Skeletal Muscles
Succinat dehydrogenase (SDH) stained 8μm thick cross section of oxidative (dark) and glycolytic (light) skeletal muscle fibers. *M. gastrocnemius*, *M. plantaris* and *M. soleus* are marked within the section. Scale bar = 1000μm.

areas of mainly glycolytic or oxidative fibers.

4.2.2 Fiber-type specific Staining

Interestingly the pattern of the morphologically altered fibers of SM22p38MAPKα KO mice after heart failure was similar to SHD stained sections. Hence the next logical step was to decipher a possible fiber type specificity. For that reason the sections were stained with fiber-type specific antibodies. Three fiber type specific antibodies, which identify the different myosin heavy chains (MyHCs) of skeletal muscle fibers (anti-MyHC1, anti-MyHC2a and anti-MyHC2b) were harvested from hybridoma cell lines, as described in section 3.3.7 and 2.8. Briefly the slow, oxidative type 1 fiber, was identified by MyHC1 and labeled with a red fluorescent (Rhodamine red) secondary antibody. The intermediate type 2a fiber, marked by MyHC2a, was labeled with a green fluorescent (FITC) secondary antibody, whereas the fast glycolytic type 2b fiber (MyHC2b) was labeled with a blue fluorescent (AMCA) secondary antibody. The fourth, glycolytic type 2d/x fiber (MyHC2d/x) remained unstained and appeared therefore dark in fluorescent images.

The staining revealed that the morphologically differently appearing fibers are type 2a (all) and type 2d/x (some) specific as illustrated in figure 4.5.

4.2.3 Testing for Lipid Droplet Accumulation and Immune Cell Infiltration

In hearts of p38MAPKα KO mice a massive lipid droplet accumulation as well as an infiltration of neutrophils after 2d of ANGII treatment was found (see figure 4.15 C). This rose the question, whether one of these processes also accounts for the different appearance of type 2a

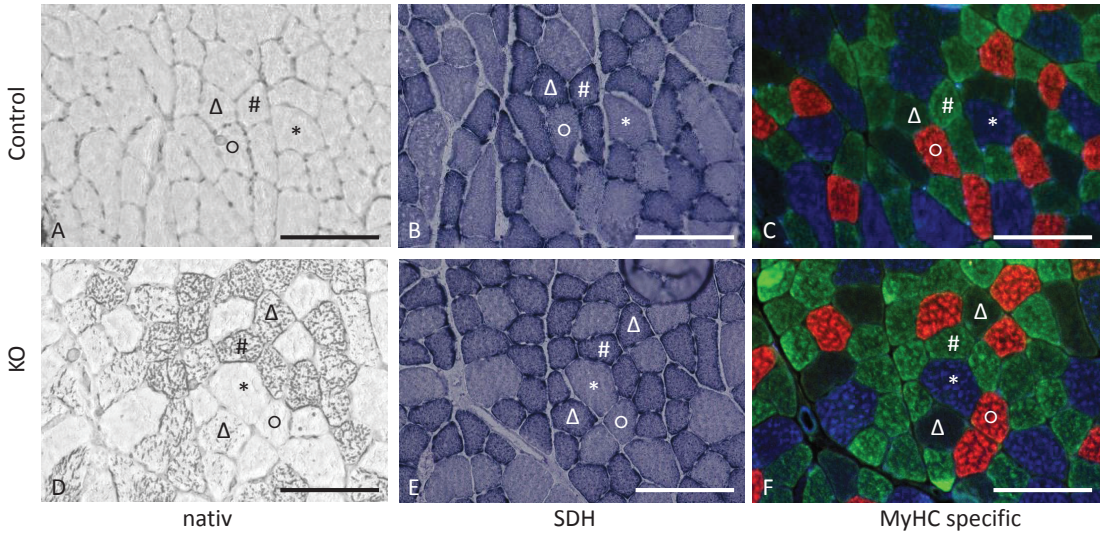

Figure 4.5: Native and Stained Cryosections of Control and KO Mice treated with Angiotensin II for two Days
Three consecutive cross sections of SM22p38MAPKα control (A-C) and KO (D-F) mice are depicted. In A and D a closeup of native sections show morphological changes of single fibers in KO mice (D); the sections in B and E are stained with succinat dehydrogenase (SDH) to distinguish oxidative (dark) from glycolytic (light) fibers. C and F are immunostained with Myosin heavy chain (MyHC) specific antibodies (○: MyHC 1; #: MyHC 2a; △: MyHC 2d/x; *: MyHC 2b). Scale bars = 100μm.

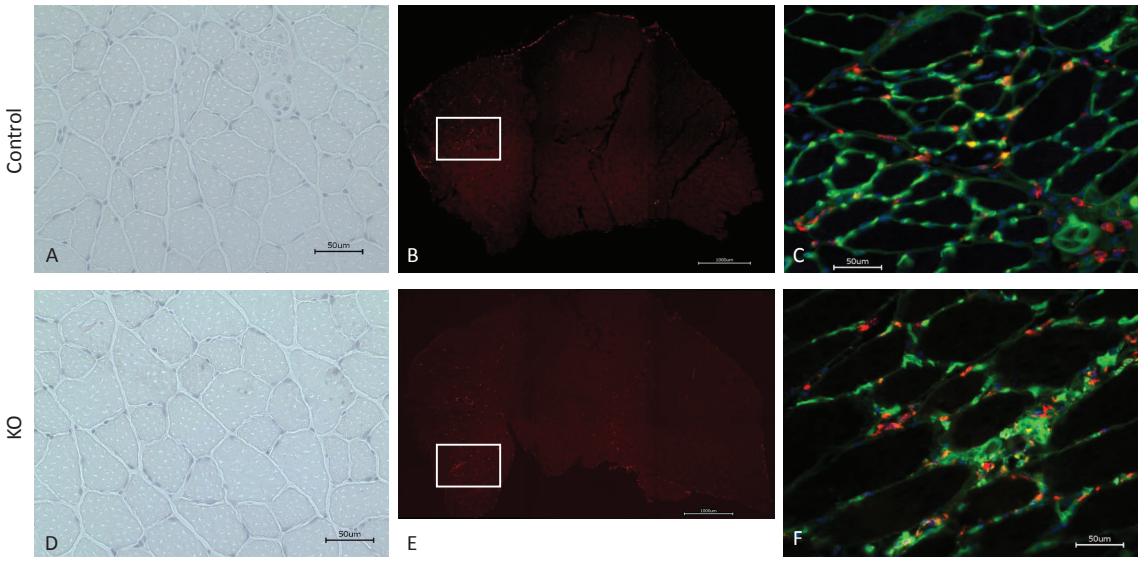

Figure 4.6: No Detection of Lipid Accumulation or Inflammation in Skeletal Muscles after Heart Failure
Cross sections of SM22p38MAPKα control (A-C) and KO (D-F) mice are depicted. No lipids were detectable in A and D with 40-fold magnification (fat-red staining). Only some areas of infiltrating neutrophils (anti-Ly6G) are detected in B and D overview sections (Immunofluorescence staining with anti-Ly6G, red), of which higher magnifications (areas marked as white boxes) are seen in C and F (Immunofluorescence staining with anti-Ly6G red, cell membranes (WGA) green, nuclei (DAPI) blue). Scale bars = 50μm (A, C, D, F); 1000μm (B, E).

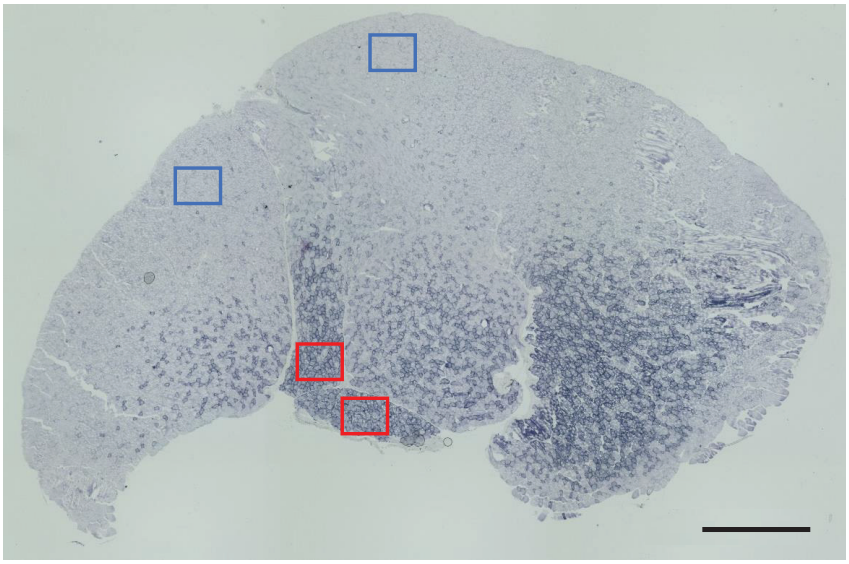

Figure 4.7: Areas of Oxidative and Glycolytic Fibers
Representative areas selected for fiber characterization of mainly glycolytic (blue box) or oxidative (red box) fibers, based on SDH-stained sections. Scale bar = 1000 μm

and type 2d/x fibers. Therefore consecutive muscle sections were stained with anti-Ly6G (an antigen, which detects a surface marker of neutrophils) as well as with fat-red, a dye used to detect lipids (section 3.4.3). There were no lipids detectable in ANGII treated muscles (figure 4.6 A and D) and only some neutrophils were detected in ANGII treated skeletal muscles, but these rare appearance of neutrophils was neither muscle region nor genotype (control or KO) nor treatment (w or w/o ANGII) specific. Representative fluorescent images of muscles harboring some neutrophils are depicted in figure 4.6 B-F (anti-Ly6G).

Neither lipids nor infiltrating immune cells account for the morphologically differently appearing fibers.

4.2.4 Characterization of Cell Size, Cell Number and Capillary Density

To test for additional morphological alterations in these muscles, consecutive sections of the muscle were stained with Wheat Germ Agglutinin (WGA) (cell membranes), anti-CD31 antibodies (capillaries) and DAPI (nuclei) according to the protocol described in section 3.4.4.

Two 500x400nm areas were defined within oxidative and glycolytic regions of the muscle, respectively. This selection, as marked in figure 4.7, was based on the fiber type distribution seen by SDH staining. The number of cells, their cross sectional area (CSA) as well as the capillary density was counted and analyzed using the computer program "ImageJ". 4-6 control and KO animals were used for these analyses (baseline, 2d ANGII). The quantitative data are summarized in figure 4.8. In general oxidative fibers are smaller in size with a higher capillary density compared to glycolytic fibers (Schiaffino and Reggiani 2011). First these parameter were also analyzed in the SM22p38MAPKα model under baseline conditions in both, control and KO mice. The cell size of oxidative fibers at baseline was smaller than that

of glycolytic fibers (oxidative: 1422.75μm^2±276.09 (control); 1325.53μm^2±327.94 (KO) vs glycolytic: 2035.58μm^2±260.25 (control); 2131.81μm^2±337.64 (KO)). This was in line with an increased cell number per area counted (oxidative: 109±16 (control); 112±19 (KO) vs glycolytic: 86±10 (control); 82±6 (KO)). The density of capillaries was also analyzed and was found to be higher in oxidative muscle fibers compared to glycolytic fibers (oxidative: 182±19 (control); 190±30 (KO) vs glycolytic: 82±14 (control); 90±13 (KO)).

Now the question arose, whether these parameters change after ANGII treatment. Therefore they were also analyzed after 48 hours of ANGII treatment as seen in figure 4.8. The capillary density remained unchanged in oxidative and glycolytic fibers (oxidative: 206±30 (control); 202±24 (KO) vs glycolytic: 88±16 (control); 98±16 (KO)). The number of fibers per area counted was unchanged in oxidative fibers (111±29 (control); 115±29 (KO)) as well as their CSAs (1615.00±372.11 (control); 1458.00±337.05 (KO)).

In glycolytic muscles however, the fiber number was increased in KO animals after ANGII treatment compared to baseline (82±8 baseline; 97±7 2d ANGII; p=0.0094), which was supported by decreased cell size in these fibers (2132μm^2±338 basal; 1917μm^2±172 2d ANGII; p=0.11).

To summarize the histological findings, it could be demonstrated that SM22p38MAPKα KO mice did not show any differences under baseline conditions. Whereas oxidative fibers stayed unaffected after ANGII treatment, the glycolytic fibers seemed to become smaller, as indicated by higher cell number per area counted, probably the first sign of glycolytic fiber-specific atrophy. Additionally the histological characterization of heart failure bearing SM22p38MAPKα KO mice revealed morphologically differently appearing type 2a and 2d/x fibers, which was neither caused by lipid droplets accumulation nor infiltrating immune cells.

4.3 Microarray Transcript Expression Analysis of Heart and *M. plantaris*

The histological findings and the body weight loss in SM22p38MAPKα KO mice provided enough evidence to have a closer look on transcript expression of heart and skeletal muscles. For most reliable results the choice of an appropriate muscle is of great importance. Both, the morphologically differently appearing fibers as well as the increased number of glycolytic fibers per area pointed towards an effect in glycolytic muscles, which are rich in type 2 fibers. Therefore *M. plantaris* was chosen for microarray transcript expression analysis, as it is a well defined muscle, mainly composed of type 2 fibers, which are homogeneously distributed throughout the muscle.

M. plantaris was harvested and messenger RNA (mRNA) was isolated from SM22p38 MAPKα control and KO animals as described in section 3.6.1.

The transcript expression profile of SM22p38MAPKα control and KO hearts and skeletal muscles (*M. plantaris*) (n=4) – untreated and after 48 hours of ANGII treatment – was assessed using Agilent 8x60K Mouse Array by Dr. René Deenen from the BMFZ (*Biologisch-Medizinisches Forschungszentrum*), Düsseldorf. This high-throughput method allows the detection of 60,000 different transcripts on a single chip.

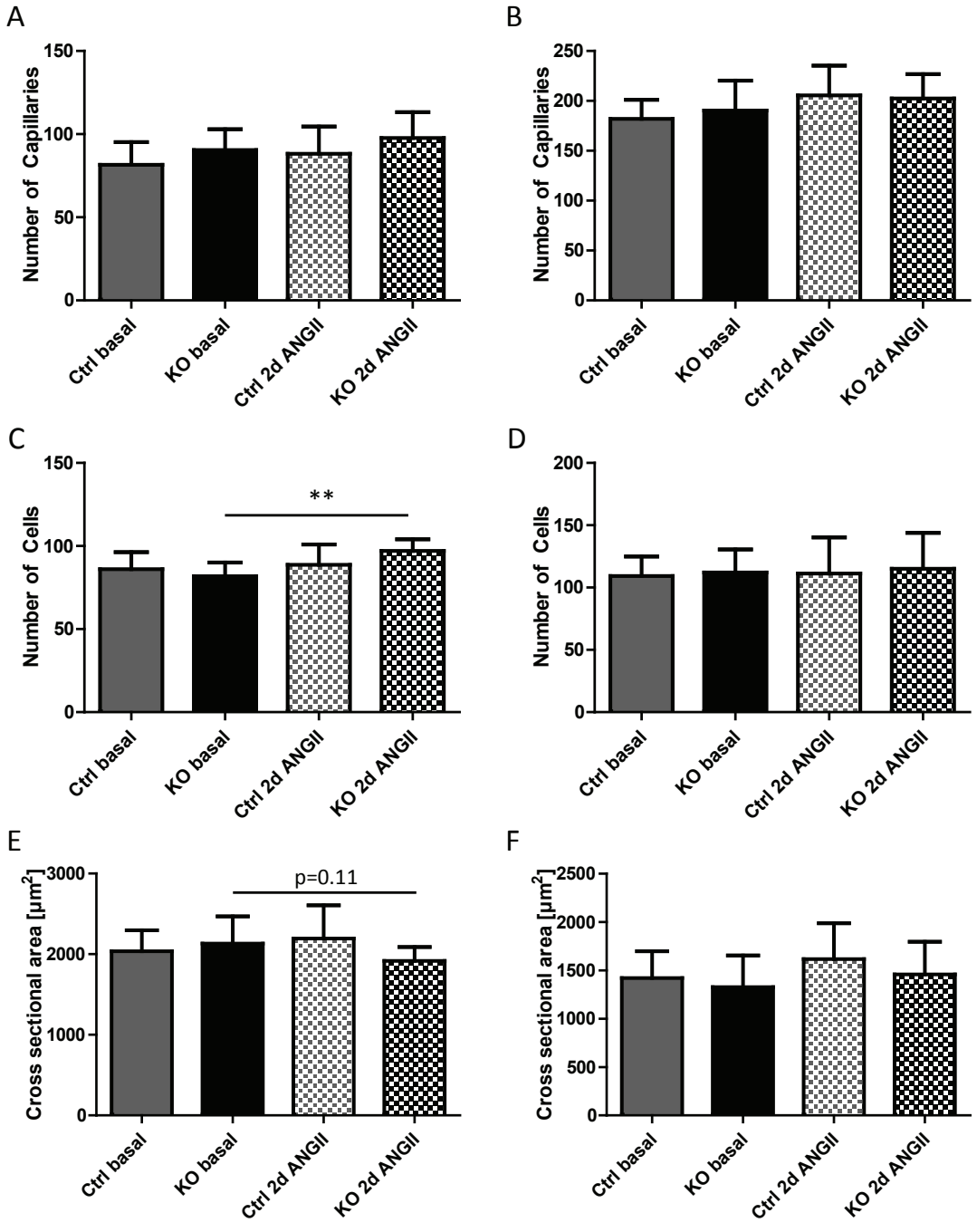

Figure 4.8: Skeletal Muscle Fiber Number, Size and Capillary Density in Control and KO Mice

The number of capillaries (A, B), number of cells (C, D) and their cross sectional area (CSA) (E, F) of SM22p38MAPKα control (grey) and KO (black) animals were analyzed under baseline (full bars) condition and after 2d of ANGII treatment (squared bars). Additionally they were categorized into mainly glycolytic (A, C, E) or oxidative (B, D, F) muscle fibers, respectively. Two 400x500μm areas of mainly glycolytic or oxidative muscle fibers, respectively, of 4-6 animals per group (control basal, KO basal, control 2d ANGII, KO 2d ANGII) were analyzed. Data represent mean±SD, ** $p<0.01$.

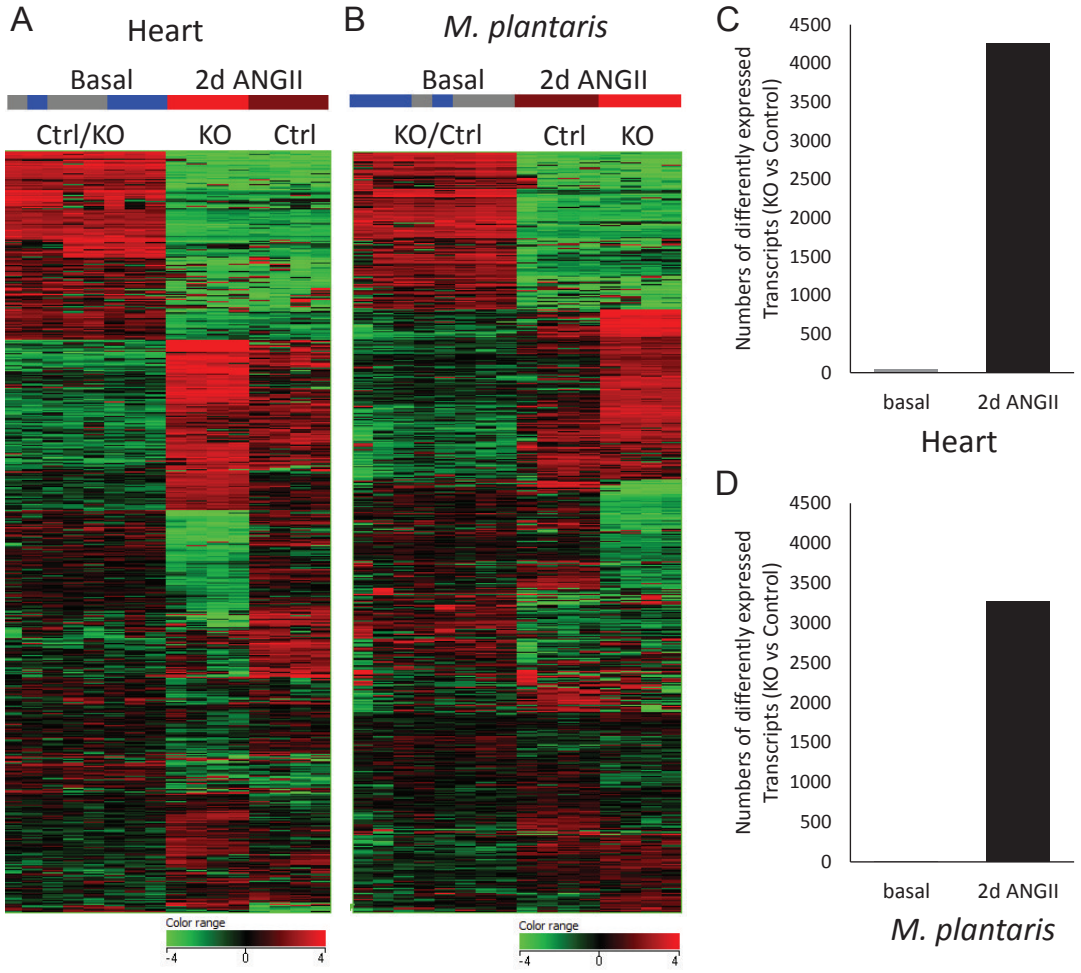

Figure 4.9: Microarray transcript expression analyses of the heart and *M. plantaris* before and after 2 days of ANGII treatment
Heatmap of heart (A) and *M. plantaris* (B) of Agilent 8x60K Mouse Array showing the transcript expression profile of four SM22p38MAPKα control and KO mice at baseline conditions and after two days of ANGII treatment, respectively. ANGII treatment induced major transcript expression alterations in SM22p38MAPKα control and KO hearts and plantaris muscle. Moreover, comparison of transcript expression in controls and KOs after ANGII revealed major differences in transcript expression in heart (C) and *M. plantaris* (D). 4,268 (hearts) and 3,267 (*M. plantaris*) transcripts were $\geq$2-fold differentially expressed ($p<0.01$) after ANGII treatment.

More than 33,000 transcripts could be detected in both tissues, of which 7,759 (control), 13,122 (KO) were significantly altered after ANGII treatment in *M. plantaris*. In hearts 8,626 (control) and 18,104 (KO) transcripts were significantly altered after ANGII treatment.

When ANGII treated KOs were compared to ANGII treated controls 3,267 transcripts were more than 2-fold changed in *M. plantaris*, and 4,268 altered transcripts were found in ANGII treated hearts, with a corrected p-value cut-off of 0.01 (figure 4.9).

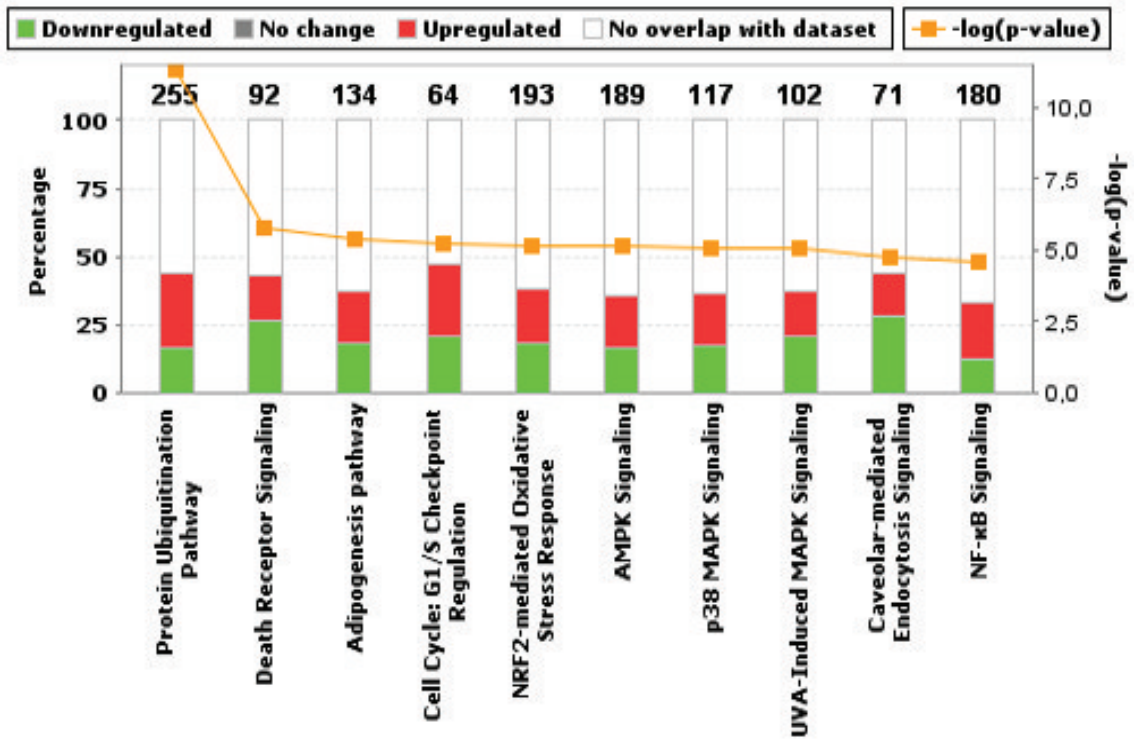

Figure 4.10: Top 10 Canonical Pathways of *M. plantaris* identified by IPA Software
The 10 highest affected canonical pathways of *M. plantaris* of SM22p38MAPKα KO mice after induction of heart failure as analyzed by IPA software.

4.3.1 Transcript Analysis using Ingenuity Pathway Analysis (IPA) Software

To identify a possible wasting related transcript expression profile of *M. plantaris*, systematic analysis of SM22p38MAPKα KO mice compared to controls after 48 hours of ANGII treatment was performed using the Ingenuity Pathway Analysis (IPA) software (also see section 3.7.1). This analysis identified 261 affected canonical pathways (log(p-value)>2), revealing the protein ubiquitination pathway to be highest affected (log(p-value)=11.374), as also shown in figure 4.10.

The induction of the protein ubiquitination pathway is a hallmark of muscle wasting, as well as autophagy, which is also highly associated with muscle wasting. Autophagy was also found to be affected using IPA software, revealing 21 out of 60 molecules associated with autophagy to be deregulated (17 up-, 4 down-regulated, log(p-value)=2.134), as shown in figure 4.11.

Also other highly affected canonical pathways (as listed in figure 4.10), such as NF-κB signaling, or p38 MAPK signaling are associated with skeletal muscle wasting.

Furthermore the altered transcripts detected by microarray could be associated to diseases and biological functions, where they got sorted by the so-called "activation z-score", with enables to predict the activation state of a regulator (<0: inhibited, >0: activated). In practice, z-scores greater than 2 or smaller than -2 can be considered significant.

The IPA analysis revealed 32 regulators to decrease specific functions and 9 regulators

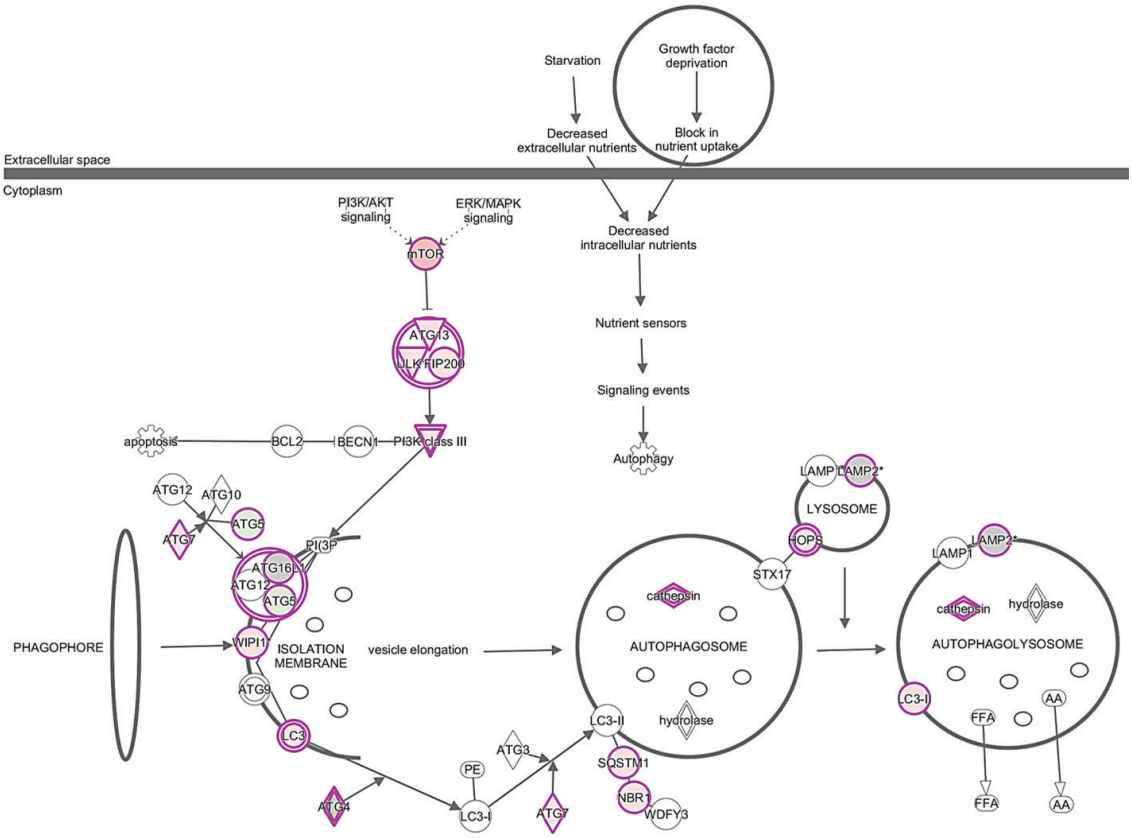

Figure 4.11: Impact of Heart Failure on Autophagy Canonical Pathway of *M. plantaris*
Deregulated transcripts found in *M. plantaris* of SM22p38MAPKα KO mice, which were associated with the autophagy canonical pathway after induction of heart failure as analyzed by IPA software. Detected proteins are framed in pink; the boxes are filled in red or green, which represent up- (red) or down- (green) regulation of proteins. The intensities of red and green indicate the expression differences (pale - moderate, intense - strong up-/downregulation) between control and KO animals. log(p-value)=2.134

to activate specific functions, as listed in supplemental figure 9.3. Decreased functions were mainly associated with impaired cellular functions, such as cellular movement, development, and function, but were also involved in deregulated skeletal and muscular development and function. These findings pointed towards impaired cell metabolism, as found in skeletal muscle wasting, which was accompanied by increased skeletal muscle cell death/necroses.

Interestingly functions involved in infectious diseases were also found to be highly induced according to activation z-score analysis (see supplemental figure 9.3). As cytokines play an important role in the heart failure induced muscle wasting (Gullestad et al. 2012), it was hypothesized that cytokine induction is caused by cardiac dysfunction of SM22p38MAPKα KO mice. Additionally the Il-6 canonical pathway was also found to be significantly affected (log(p-value)=2.296), as demonstrated in figure 4.12.

In table 4.1 the fold-change of transcript expression of several atrogenes (which are genes specifically associated with skeletal muscle wasting - Lecker et al. 2004), including proteasomal degradation related genes (*Trim63* (*Murf1*), *Fbxo32* (*Atrogin1*), *Foxo1* and *Foxo3*) and key autophagy markers (*Bnip3*, *Gabarapl1* and *Catepsin L* (*Ctsl*)) of *M. plantaris* after induction of heart failure are listed. Additionally, the fold-change of transcript expression of cytokines

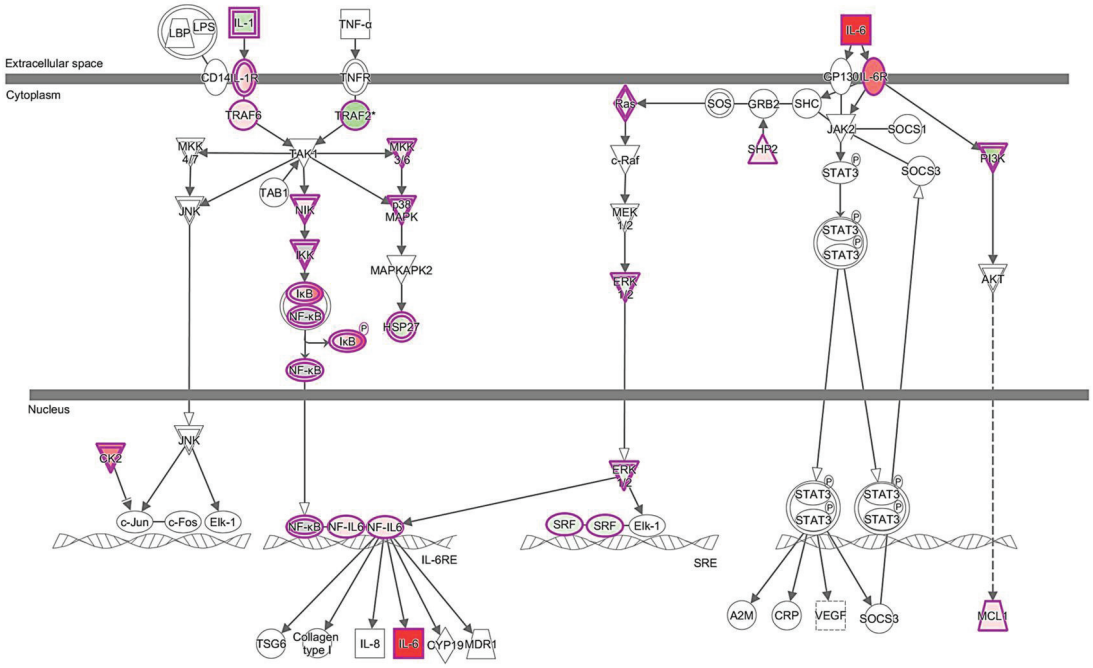

Figure 4.12: Impact of Heart Failure on Il-6 Canonical Pathway in *M. plantaris* Deregulated transcripts found in *M. plantaris* of SM22p38MAPKα KO mice, which were associated with the Il-6 canonical pathway after induction of heart failure as analyzed by IPA software. Detected proteins are framed in pink; the boxes are filled in red or green, which represent up- (red) or down- (green) regulation of proteins. The intensities of red and green indicate the expression differences (pale - moderate, intense - strong up-/downregulation) between control and KO animals. log(p-value)=2.296

and cytokine receptors in *M. plantaris* of SM22p38MAPKα KO mice were listed in table 4.2.

In addition to ANGII induced transcript deregulations, the analysis of microarray analysis revealed that 4,268 (hearts) and 3,267 (*M. plantaris*) transcripts were $\geq$2-fold differentially expressed ($p<0.01$) in ANGII treated SM22p38MAPKα KO mice when compared to ANGII treated controls. Within those the transcript expression of atrophy-related and inflammation associated programs was found to be induced in *M. plantaris* of SM22p38MAPKα KOs, suggesting that the deregulation of atrophy associated transcripts was due to the failing heart in these animals. Therefore it was speculated, whether the alterations were caused by increased cytokine expression in the heart. A plethora of cytokines and chemokines was found to be highly upregulated in SM22p38MAPKα KO hearts (supplemental figure 9.2). Interestingly several of those were increased in both organs, including *Il-6*, *Il-6ra* and *Il-1r2* (table 4.2), others such as *Il-1b* was only upregulated in the heart of SM22p38MAPKα KO mice, whereas the corresponding receptor (*Il-1r2*) was increased in both - *M. plantaris* and heart (table 4.2) .

Besides cytokines, which seem to play an important role in the heart failure-induced muscle wasting, the growth and differentiation factor *Myostatin* (*Mstn*), a factor known to inhibit myogenesis, is also suggested to induce skeletal muscle wasting, when released from the failing heart (Breitbart et al. 2011). At least at this early time point *Mstn* was only found to be upregulated in *M. plantaris* but not in the heart (see table 4.2).

Table 4.1: Expression of Atrogenes and Autophagy-related Transcripts in *M. plantaris*: The upregulation (indicated as fold-change) of transcripts involved in skeletal muscle wasting (atrogenes and autophagy-related genes) from ANGII treated SM22p38MAPKα skeletal muscle (*M. plantaris*) compared to ANGII treated controls detected by microarray transcript expression analysis.

Transcript Name	**upregulation [fold-change]**
ATROGENES	
Foxo3	61.6
Doc2b	59.4
Trim63	18.9
Il-1r2	11.8
Mt1l	10.2
Mt1b	10.0
Fbxo32	9.2
Cxcl13	7.5
Csnk2a2	7.5
Maff	6.9
Foxo1	5.5
Eif4g3	4.8
Tgif	4.3
Ranbp9	3.9
Eif4ebp1	3.8
AUTOPHAGY	**GENES**
Gabarapl1	5.1
Bnip3	4.7
Ctsl2	3.9

Table 4.2: Cytokine and Myostatin Transcript Expression of Heart and *M. plantaris*: The deregulation (indicated as fold-change) of cytokines and myostatin from ANGII treated SM22p38MAPKα KO hearts and *M. plantaris* compared to ANGII treated controls detected by microarray transcript expression analysis

Transcript Name	**Heart [fold-change]**	***M. plantaris* [fold-change]**
Mstn	$\leftrightarrow$	3x $\uparrow$
Il-6	33x $\uparrow$	20x $\uparrow$
Cxcl5	78x $\uparrow$	$\leftrightarrow$
Il-1r2	49x $\uparrow$	9x $\uparrow$
Cxcl1	20x $\uparrow$	$\leftrightarrow$
Ccl2	19x $\uparrow$	12x $\downarrow$
Cxcr2	11x $\uparrow$	$\leftrightarrow$
Il-1b	9x $\uparrow$	$\leftrightarrow$
Il-6ra	2x $\uparrow$	12x $\uparrow$

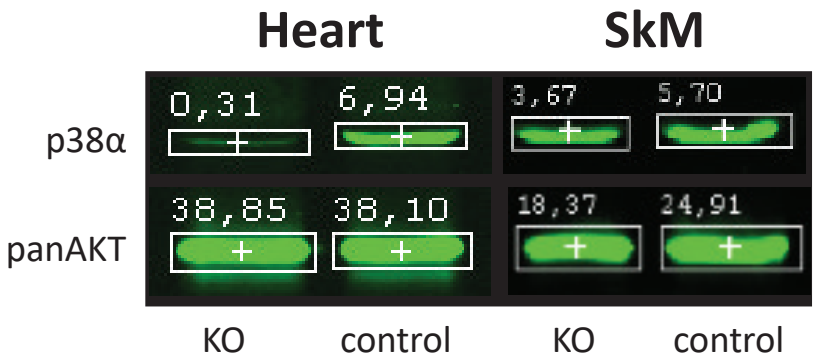

Figure 4.13: Validation of p38MAPKα Knock-out (KO) in Heart but not Skeletal Muscle (SkM)
KO of p38MAPKα in hearts but not skeletal muscles of iCMp38MAPKα KO mice compared to controls by western blot analysis. PanAKT used as loading control.

The microarray transcript expression analysis clearly demonstrated an induction of muscle wasting associated gene profile in *M. plantaris* with the induction of pro-inflammatory cytokines in the heart as well as in *M. plantaris*, which were not triggered by ANGII but most likely by the failing heart.

4.4 Inducible Cardiomyocyte specific p38 KO Mouse Model

The SM22p38MAPKα model is a robust model to induce heart failure within 2 days using Angiotensin II. This cardiac remodeling induces alteration in skeletal muscles, not only on a morphological, but also on a transcript expression level.

However there are some constraints of this model, as the p38MAPKα is not only inactivated in cardiomyocytes, but also in vascular smooth muscle cells, which might also contribute to the development of the severe cardiac phenotype. Additionally, p38MAPKα is constitutively inactivated in these animals. This might cause early developmental adaptions, which probably lead to a higher susceptibility to increased environmental stress, which ultimately could trigger heart failure. This assumption was further supported by the observation of female SM22p38MAPKα KO mice, which developed heart failure during pregnancy. This is in contrast to the majority of adult patients suffering from heart failure/cachexia, who develop the disease independent of genetic predispositions.

To overcome these disadvantages, an inducible cardiomyocyte-specific p38MAPKα KO mouse was generated (see section 3.1.2), thereafter referred to as iCMp38MAPKα mice. The KO was induced in 6-8 week old mice using tamoxifen (500μg/d i.p. injections for 10 days). After a 4 week recovery period p38MAPKα protein levels were analyzed in heart and skeletal muscle (SkM) by western blotting. As shown in figure 4.13 the cardiac protein levels of p38MAPKα dropped to approximately 5% of the control level, whereas the p38MAPKα protein levels remain unaltered in skeletal muscles. As the KO was fully established 4 weeks after induction, the cardiac characterization of iCMp38MAPKα mice under baseline conditions and after ANGII treatment could be performed (figure 4.14).

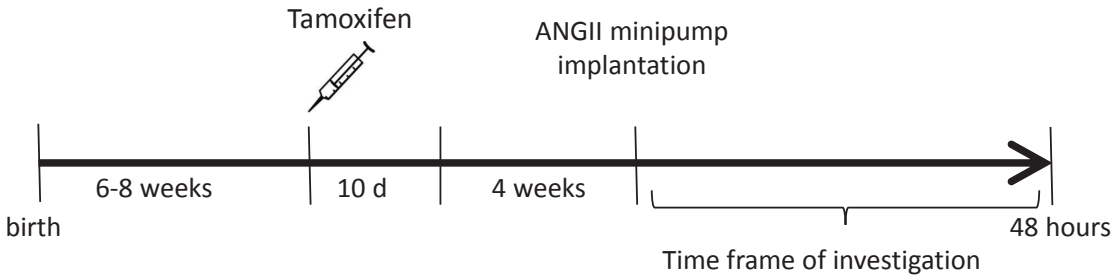

Figure 4.14: Heart Failure Induction in iCMp38MAPKα KO Mice
p38MAPKα KO was induced with 500μg 4OH-Tamoxifen, intraperitoneally (i.p.) injected for ten consecutive days 6-8 weeks after birth. After a recovery period of 4 weeks ANGII minipumps (1μg*kg^{-1}*min^{-1}) were implanted. Mice got sacrificed 12, 24 or 48 hours thereafter.

12 week old male mice were used for experiments. As control, p38MAPK$\alpha^{flox/flox}$ litter mates were used, without expressing the tamoxifen-inducible Cre-recombinase merCremer. Nonetheless the control mice were also injected with tamoxifen for 10 days to rule out any tamoxifen related effects.

Characterization of the cardiac phenotype was performed by echocardiographic analysis, which was done in cooperation with Dr. med. Katharina Bottermann. This analysis revealed that iCMp38MAPKα KO hearts developed a similar cardiac phenotype as SM22p38MAPKα KO mice. Under baseline conditions no significant differences in cardiac parameters were found in iCMp38MAPKα control and KO mice. After 48h of ANGII treatment impaired cardiac function with a dilative phenotype was observed as seen by reduced EF and increased end systolic and diastolic volumes (ESV, EDV). Histological investigations showed lipid droplet accumulation as well as neutrophil infiltration after 48h of ANGII treatment (see figure 4.15). The iCMp38MAPKα KO mice showed a similar phenotype as SM22p38MAPKα KO mice, hence it was concluded that inactivation of p38MAPKα in vascular smooth muscle cells, which occurred in the SM22p38MAPKα model, contributed only to a minor extent to the cardiac phenotype.

As the cardiac phenotype was found to be similar in both p38MAPKα KO models, the question arose, whether skeletal muscles were also affected in this model.

4.5 Transcript Expression Analysis using Quantitative Real Time PCR (qPCR)

To test whether iCMp38MAPKα KO mice also showed an altered transcript expression in skeletal muscles as found by microarray analysis in SM22p38MAPKα KO mice, the transcript expression of selected genes was investigated after 48 hours of treatment using SybrGreen based quantitative real time PCR (qPCR) as described in section 3.6.

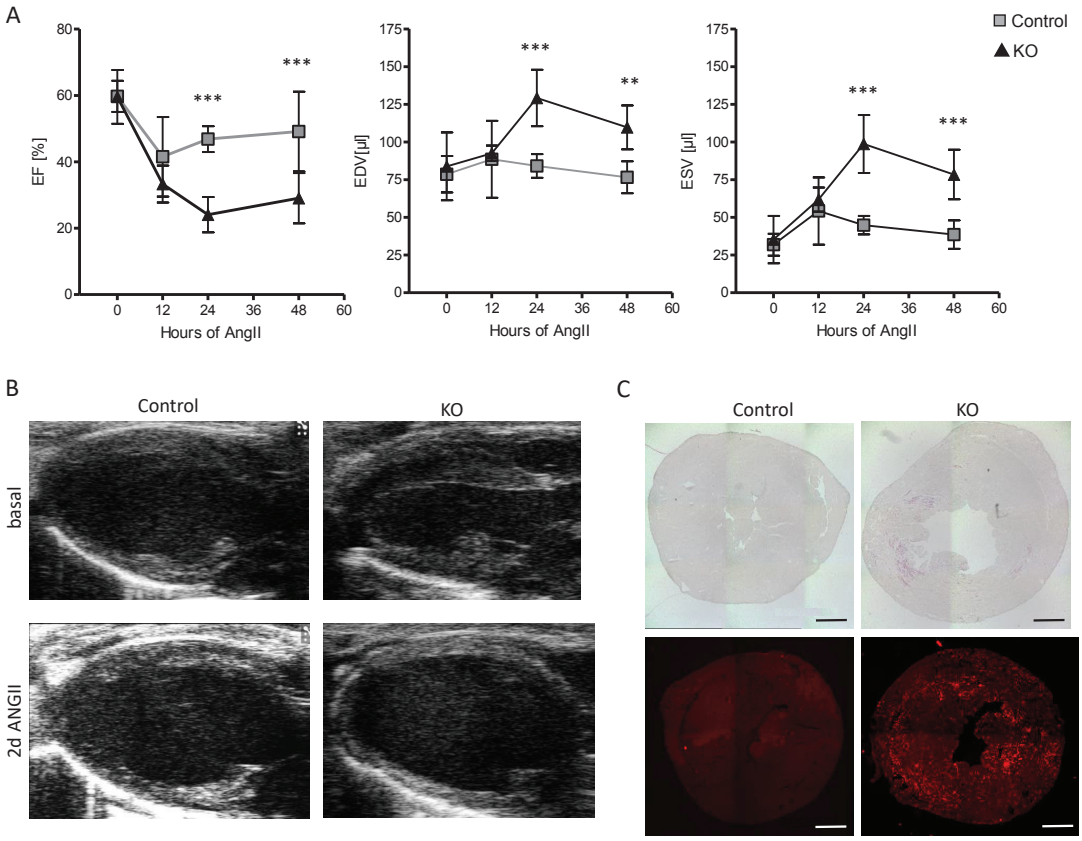

Figure 4.15: Characterization of the iCMp38MAPKα Model
The development of cardiac dysfunction the time course of A) ejection fraction (EF), end diastolic volume (EDV) and end systolic volume (ESV) of iCMp38MAPKα control (grey) and KO (black) hearts at baseline and after 12, 24 and 48 hours of ANGII treatment is shown. Data represent mean±SD; **: $p<0.01$, ***: $p<0.001$; n=4-6. B) High resolution ultrasound images (parasternal long axis, B-mode) of control and KO hearts under baseline conditions (upper panel) and after 48 hours of ANGII treatment (lower panel). C) Fat red staining (upper panel) and anti-Ly6G immunofluorescence staining (lower panel) of iCMp38MAPKα control and KO hearts after 48h of ANGII treatment.

4.5.1 Selection of Reference Genes

Another essential parameter of qPCR is an appropriate internal control. According to microarray data the transcript expression levels of classical reference or housekeeping genes such as *Hypoxanthine Phosphoribosyltransferase 1* (*Hprt1*) and *Lactate Dehydrogenase* (*Ldh*) were significantly deregulated after ANGII treatment (*Hprt1*: 1.9-fold up regulated; *Ldh*: 1.65-fold down regulated), making them impossible to use as internal controls. *Glyceraldehyde 3-phosphate Dehydrogenase* (*Gapdh*), another frequently used housekeeping gene, was not significantly changed according to microarray data, nevertheless its expression level is much higher than those of the genes of interest, making the analysis error-prone. To overcome this obstacle the microarray transcript expression results were screened for transcripts showing the least alteration of transcript expression within all genotypes (control and KO) and conditions (basal and after ANGII treatment). Three of those, *Ribosomal Protein S17* (*Rps17*), *Casein*

Expression difference KO vs. Ctrl in *M. plantaris* (fold-change)				
up/down-regulated		Reference *Csnk2b*	Reference *Gstz1*	Reference *Rps17*
Baseline	*Csnk2b*	-	1,37	1,39
	Gstz1	1,37	-	1,01
	Rps17	1,39	1,01	-
2d ANGII	*Csnk2b*	-	1,69	1,22
	Gstz1	1,69	-	2,06
	Rps17	1,22	2,06	-

Expression difference 2d ANGII vs. baseline in *M. plantaris* (fold-change)				
up/down-regulated		Reference *Csnk2b*	Reference *Gstz1*	Reference *Rps17*
Ctrl	*Csnk2b*	-	1,57	1,13
	Gstz1	1,57	-	1,40
	Rps17	1,13	1,40	-
KO	*Csnk2b*	-	1,47	1,01
	Gstz1	1,47	-	1,46
	Rps17	1,01	1,46	-

Figure 4.16: Analysis of Reference Genes in *M. plantaris*
Potential reference genes, *Csnk2b*, *Gstz1* and *Rps17*, were measured in against each other *M. plantaris* of SM22p38MAPKα KO and control mice under baseline conditions and after 2 days of ANGII treatment. Their fold-change was analyzed using qPCR. In yellow the comparison of *Csnk2b* and *Rps17* is highlighted.

Kinase 2 beta (*Csnk2b*) and *Glutathione S Transferase zeta 1* (*Gstz1*) were chosen to test for reliability and stability in *M. plantaris* of SM22p38MAPKα KO and control mice.

As depicted in figure 4.16, *Csnk2b*, *Gstz1* and *Rps17* were measured against each other. The transcript expression of *Rps17* and *Csnk2b* showed the highest stability when compared with each other (variation $<$1.4-fold) in qPCR analysis of p38MAPKα control and KO muscle samples under baseline condition as well as after 2 days of ANGII treatment. As the expression level of *Csnk2b* was closest to the expression levels of genes of interest, it was chosen as reference gene throughout all experiments. The same was done for heart, where *Nudc* (*Nuclear distribution C, dynein complex regulator)* was chosen as most reliable reference gene.

4.5.2 Calibrator Analysis

To be able to compare several qPCR plates with each other, it was necessary to include a calibrator on each plate. The calibrator consisted of cDNA gained from pooled RNA samples of different animals at different conditions. It is important, that the reverse transcription of the pooled RNA is done in one approach to guarantee the use of the same cDNA on every plate. Therefore, a rough estimate of how many plates will be made was important. 1ml of calibrator cDNA was prepared and portioned in 10μl aliquots, to avoid multiple freeze-thaw cycles. The calibrator was included on each plate and was measured for each transcript investigated on a plate. The data of the calibrator from several plates was collected and analyzed to test the reproducibility and comparability of qPCR runs. The analysis of 18 different qPCR runs including *Csnk2b* resulted in a maximal fluctuation of the C_T value of 3.8% between different runs (C_T=21.72$\pm$0.41; the mean cycle, where *Csnk2b* reached a specified threshold, n=18). These minor fluctuations were possibly caused by random errors such as pipetting mistakes, which cannot be fully avoided. Because of this high consistency between different qPCR runs, the fluctuation was considered as negligible and not included in calculations.

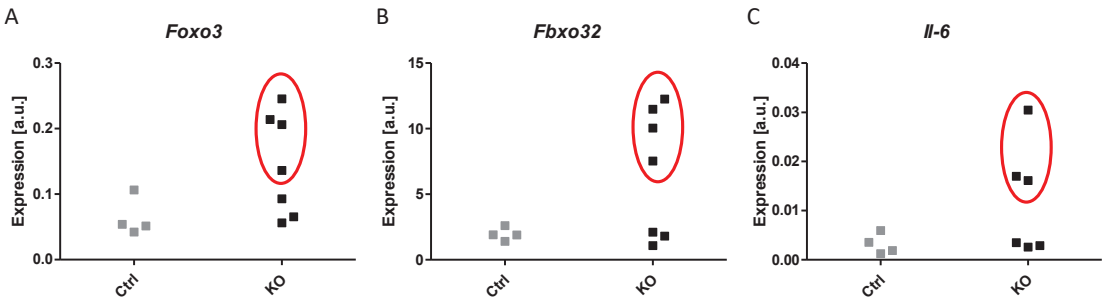

Figure 4.17: Expression Profile of *M. plantaris* after Heart Failure
The expression levels of *Foxo3* (A), *Fbxo32* (B) and *Il-6* (C) in *M. plantaris* of iCMp38MAPKα control and KO mice after 48 hours of ANGII treatment. In red those KO animals are highlighted, which show an induction of transcript expression (n=4-7).

4.5.3 Severity of Heart Failure correlates with Transcript Expression Alterations in Skeletal Muscle

Since induction of atrogenes is a hallmark of skeletal muscle wasting and cytokines are involved in heart failure induced muscle wasting the transcript expression of *Trim63 (Murf1), Fbxo32 (Atrogin1), Foxo1, Foxo3, Il-1b, Il-1r2, Il-6* and *Il-6ra* was first analyzed after 48 hours of ANGII treatment. The transcript expression levels varied in iCMp38MAPKα KO animals as exemplary shown by *Foxo3*, *Fbxo32* and *Il-6* in figure 4.17. Whereas in some *M. plantaris* of iCMp38MAPKα KOs a clear upregulation of the transcript was observed, other KOs were apparently not affected when compared to ANGII treated controls.

Interestingly those animals, which showed the induction of transcripts in skeletal muscles, also showed the morphological alterations of native tissue sections (see figure 4.3). Additionally, although all mice displayed an impaired cardiac function after 2d of ANGII treatment, the severity was different in these two KO groups (Controls: EF=49.12±12.03; KO: no effect: EF=35.01±1.81, effect: EF=21.08±0.53). Hence the severity of cardiac dysfunction seems to play an important role in the induction of an atrophy related gene expression program.

As the aim of this project was to unravel the heart-skeletal muscle communication, only those KO mice were chosen for further analysis, which showed a severe cardiac impairment that ultimately effected transcript expression in skeletal muscles.

4.5.4 Time Course of Transcript Expression

The transcript expression analysis of *M. plantaris* by qPCR of selected iCMp38MAPKα KO mice revealed a similar induction of atrogenes, cytokines and autophagy-related genes after 48 hours of ANGII treatment, as previously detected by microarray analysis of SM22p38MAPKα KO mice (table 4.3 48h ANGII).

To further elucidate the time course of heart-skeletal muscle cross talk leading to the induction of the wasting associated transcript expression program additional points in time were added. The transcript expression of 12 genes (*Trim63 (Murf1), Fbxo32 (Atrogin1), Foxo1, Foxo3, Il-1b, Il-1r2, Il-6 Il-6ra*, *Bnip3*, *Gabarapl1*, *Catepsin L* (*Ctsl*) and *Myostatin, (Mstn)*) of *M. plantaris* was investigated in the course of time in iCMp38MAPKα controls and KO mice

Table 4.3: Time Line of Transcript Expression Alterations in *M. plantaris*: The up- (↑) and down- (↓) regulation (indicated as fold-change) of atrogenes, cytokines and their receptors, autophagy related genes and *Myostatin* in *M. plantaris* of iCMp38MAPKα KO animals compared to controls, analyzed by qPCR before and after 12, 24 and 48 hours of ANGII treatment.

M. plantaris	**basal**	**12h ANGII**	**24h ANGII**	**48h ANGII**
Growth Factor				
Mstn	↔	↔	↔	2.7x ↑
Cytokines				
Il-1b	↔	↔	↔	↔
Il-6	↔	↔	2.9x ↓	7.7x ↑
Il-1r2	↔	↔	↔	2.0x ↑
Il-6ra	↔	↔	3.4x ↑	8.0x ↑
Atrogenes				
Foxo1	↔	↔	2.6 ↑	2.1x ↑
Foxo3	↔	↔	↔	3.3x ↑
Fbxo32	↔	↔	↔	5.3x ↑
Trim63	↔	↔	2.0↑	7.7x ↑
Autophagy Genes				
Bnip3	↔	↔	2.6 ↑	2.2x ↑
Ctsl	↔	↔	↔	↔
Gabarapl1	↔	↔	↔	2.7 ↑

Table 4.4: Time Line of Transcript Expression in Heart: The up-regulation (indicated as fold-change) of *Myostatin* and cytokines in hearts of iCMp38MAPKα KO animals compared to controls, analyzed by qPCR before and after 12, 24 and 48 hours of ANGII treatment.

Heart	**basal**	**12h ANGII**	**24h ANGII**	**48h ANGII**
Mstn	↔	↔	↔	↔
Il-1b	↔	↔	7x ↑	3x ↑
Il-6	↔	↔	11x ↑	2x ↑
Cxcl5	↔	↔	6x ↑	2x ↑
Ccl2	↔	↔	5x ↑	4x ↑

at baseline levels, as well as after 12, 24 and 48 hours of ANGII treatment (see table 4.3). For each given time point 4-6 animals (controls and KOs) were investigated. As it is very likely, that factors released from the heart (eg. cytokines) induce the atrophy related gene program, it was hypothesized that expression changes in *M. plantaris* occurred later than in the heart. To test this, transcript expression data for *M. plantaris* were compared to data for the heart.

All of the cytokines analyzed in the heart of iCMp38MAPKα KO mice peaked after 24 hours of ANGII treatment, whereas in *M. plantaris* the most prominent upregulation in cytokines and atrogenes was seen after 48 hours of treatment. This finding pointed towards an initial deregulation in KO hearts followed by the induction of wasting related genes in *M. plantaris*, which further supported the hypothesis of a heart-skeletal muscle cross talk.

In tables 4.3 and 4.4 solely the relative fold change of transcript expression (as calculated

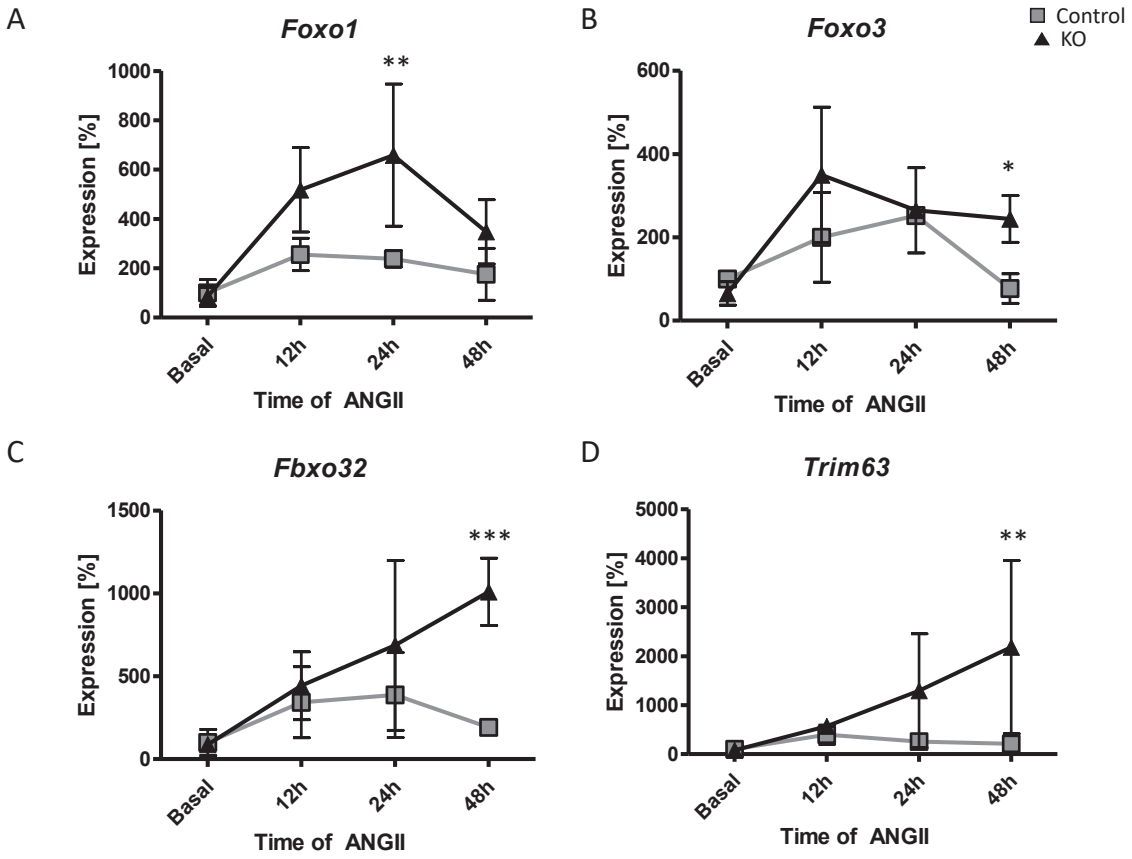

Figure 4.18: Transcript Expression Changes of Atrogenes in *M. plantaris* after ANGII Treatment
The transcript expression (assessed by qPCR) of atrogenes (*Trim63 (Murf1), Fbxo32 (Atrogin1), Foxo1, Foxo3*) of *M. plantaris* of iCMp38MAPKα controls (grey) was compared to iCMp38MAPKα KOs (black) at baseline conditions as well as after 12, 24 and 48 hours of ANGII treatment. Each value was normalized to the baseline transcript expression value of controls, which represents 100%. 4-6 animals were analyzed per group. Data represent mean$\pm$SD, * $p<0.05$, ** $p<0.01$, *** $p<0.001$.

by the comparative Ct method - see section 3.6.5) between KO and controls were summarized, without providing further information about expression levels or expression differences between individuals. Moreover, the fold-change does not provide any information about the direction of expression values in comparison to baseline values. A difference of 4-fold is compatible with a 4-fold upregulation of a transcript in eg KO, a 4-fold downregulation in controls or all combinations of up- and downregulation resulting in a 4-fold difference. For that reason transcript expression was also analyzed using the X_0 method (see section 3.6.5).

The modulation of atrogene expression is shown in figure 4.18, were an upregulation of *Foxo1* (2.0$\pm$0.7 $\uparrow$), *Foxo3* (3.2$\pm$0.7 $\uparrow$), *Fbxo32* (5.3$\pm$1.1 $\uparrow$) and *Trim63* (10.4$\pm$8.5 $\uparrow$) was found in iCMp38MAPKα KO *M. plantaris* after 48h of ANGII treatment. In controls, transcript expression levels appeared to increase to a lower extend, but the differences were not significant. Interestingly the expression of *Foxo1* peaked already after 24 hours of treatment in iCMp38MAPKα KOs (2.8$\pm$1.2 fold upregulated). This finding is in line with its known involvement in the initiation of *Trim63 (Murf1) and Fbxo32 (Atrogin1)* (also see section 1.3.1),

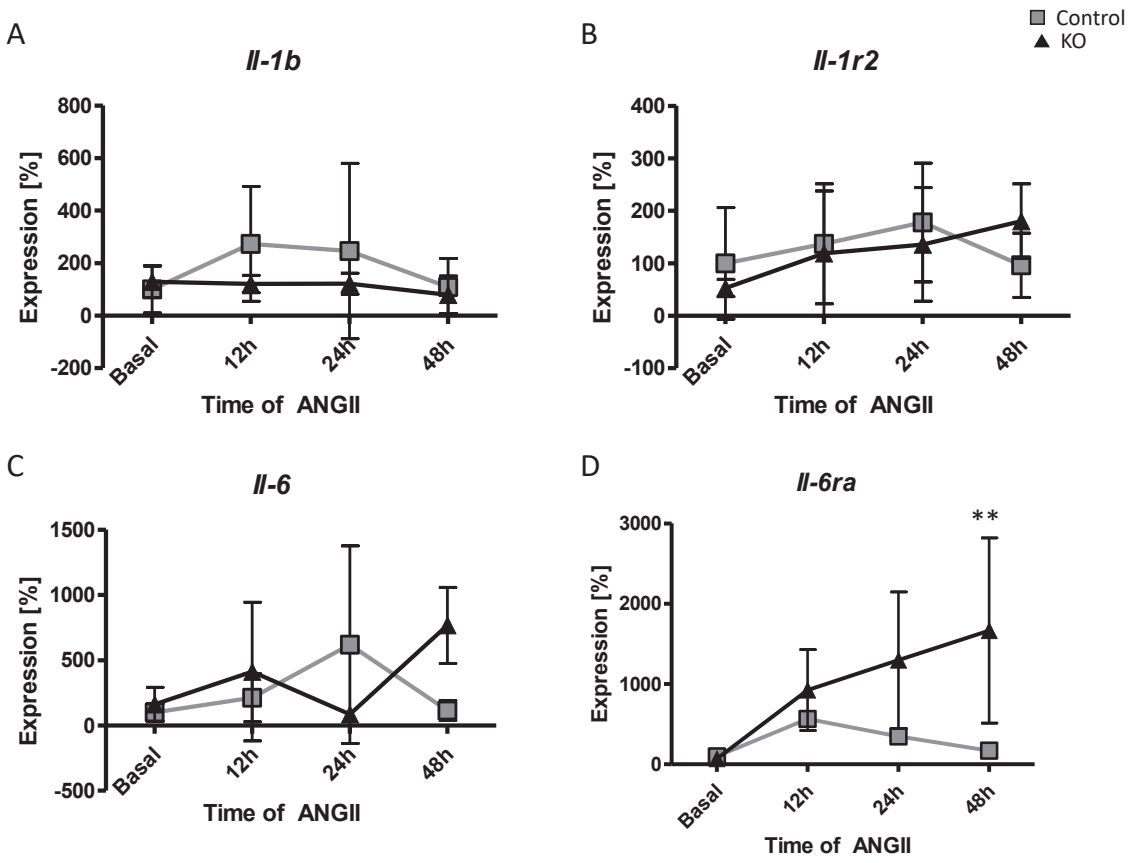

Figure 4.19: Transcript Expression Changes of Cytokines in *M. plantaris* after ANGII Treatment
The transcript expression (assessed by qPCR) of cytokines and their receptors (*Il-1b, Il-1r2, Il-6 Il-6ra*) of *M. plantaris* of iCMp38MAPKα controls (grey) was compared to iCMp38MAPKα KOs (black) at baseline conditions as well as after 12, 24 and 48 hours of ANGII treatment. Each value was normalized to the baseline transcript expression value of controls, which represents 100%. 4-6 animals were analyzed per group. Data represent mean±SD, ** $p<0.01$.

which show a retarded expression kinetics in comparison to *Foxo1*.

Besides atrogenes, induction of cytokines plays an important role in heart failure-induced muscle wasting, which was supported by transcript expression analysis as seen in figure 4.19. In control animals (depicted in grey) only minor, non significant, transient induction of transcripts was detectable, whereas the expression of *Il-1r2, Il-6, Il-6ra* increased over time and peaked after 48 hours of ANGII treatment in KO mice (depicted in black). Nonetheless due to high standard deviations, only the 9.8±6.8-fold upregulation of *Il-6ra* was found to be significant in iCMp38MAPKα KO *M. plantaris* after 48h of ANGII treatment compared to controls (*Il-1r2*: 1.9±0.7 ↑; *Il-6*: 6.7±2.6 ↑).

Figure 4.20 A-C shows transcript expression levels of autophagy related transcripts, were : *Gabarapl1* (3.3±1.2 ↑) and *Bnip3* (2.3±1.0 ↑) were found to be significantly upregulated in KO *M. plantaris* after 48h of ANGII treatment compared to controls but not *Ctsl* (1.6±0.6 ↑).

The expression of *Myostatin*, an inhibitor of myogenesis, (figure 4.20 D) is also significantly induced (2.8±1.0 fold up-regulated) in ANGII treated KO mice compared to ANGII treated

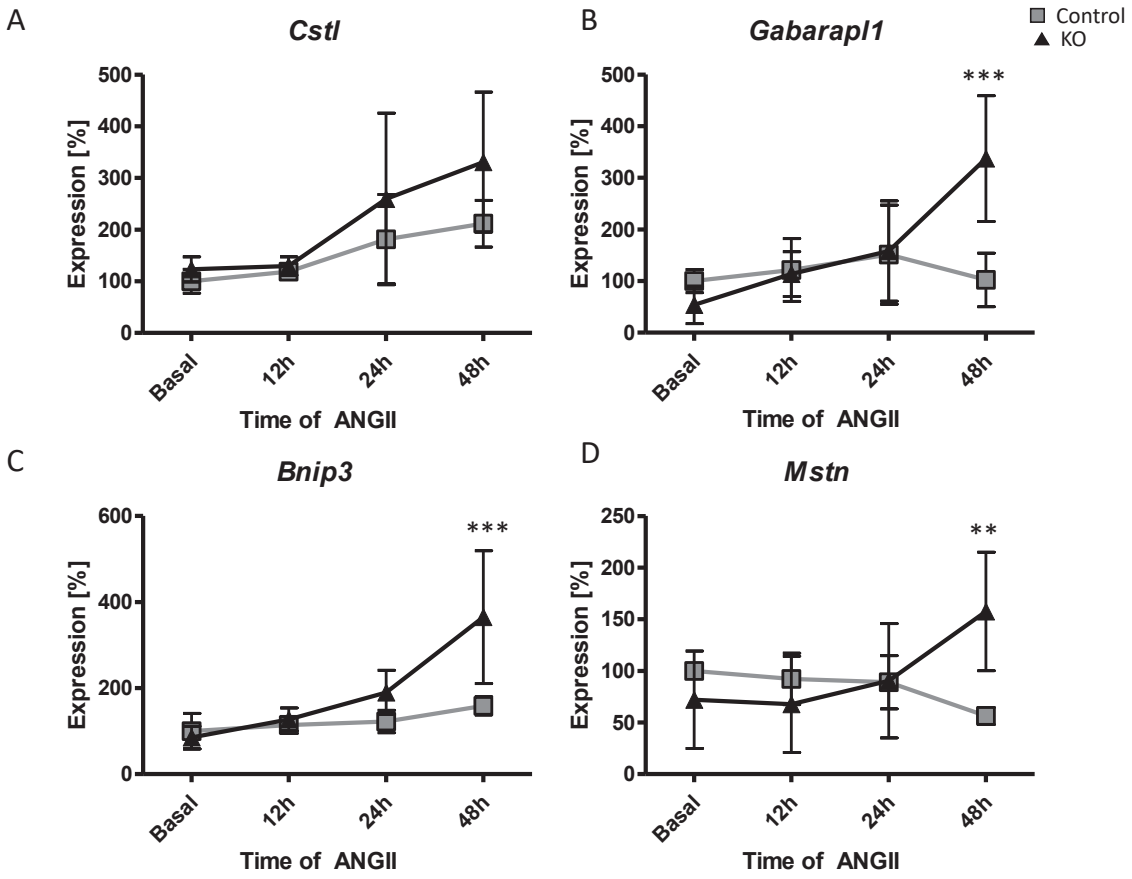

Figure 4.20: Transcript Expression Changes of Autophagy related Genes and Growth Factor Myostatin in *M. plantaris* after ANGII Treatment
The transcript expression (assessed by qPCR) of autophagy related genes (*Catepsin L* (*Ctsl*), *Gabarapl1*, *Bnip3*) (A-C) and *Myostatin (Mstn)* (D) of *M. plantaris* of iCMp38MAPKα controls (grey) was compared to iCMp38MAPKα KOs (black) at baseline conditions as well as after 12, 24 and 48 hours of ANGII treatment. Each value was normalized to the baseline transcript expression value of controls, which represents 100%. 4-6 animals were analyzed per group. Data represent mean±SD, * $p<0.05$, ** $p<0.01$, *** $p<0.001$.

controls after 48h.

In summary, the transcript expression alterations found in *M. plantaris* of iCMp38MAPKα mice were most likely a consequence of the failing heart in these mice. The remodeling process greatly induced the cytokine transcript expression in hearts, which peaked after 24 hours of ANGII treatment and was followed by massive alterations of transcript expression levels of atrogenes, cytokines and autophagy related genes in *M. plantaris* after additional 24 hours. These results strongly suggested that heart failure induced an atrophy related gene expression program in iCMp38MAPKα KO mice.

4.6 Comparison of Transcript Profile of *M. plantaris* and *M. soleus*

M. plantaris, which is mainly composed of type 2 fibers, was chosen for analysis, as both histological as well as transcriptional analyses revealed a big impact on glycolytic muscles.

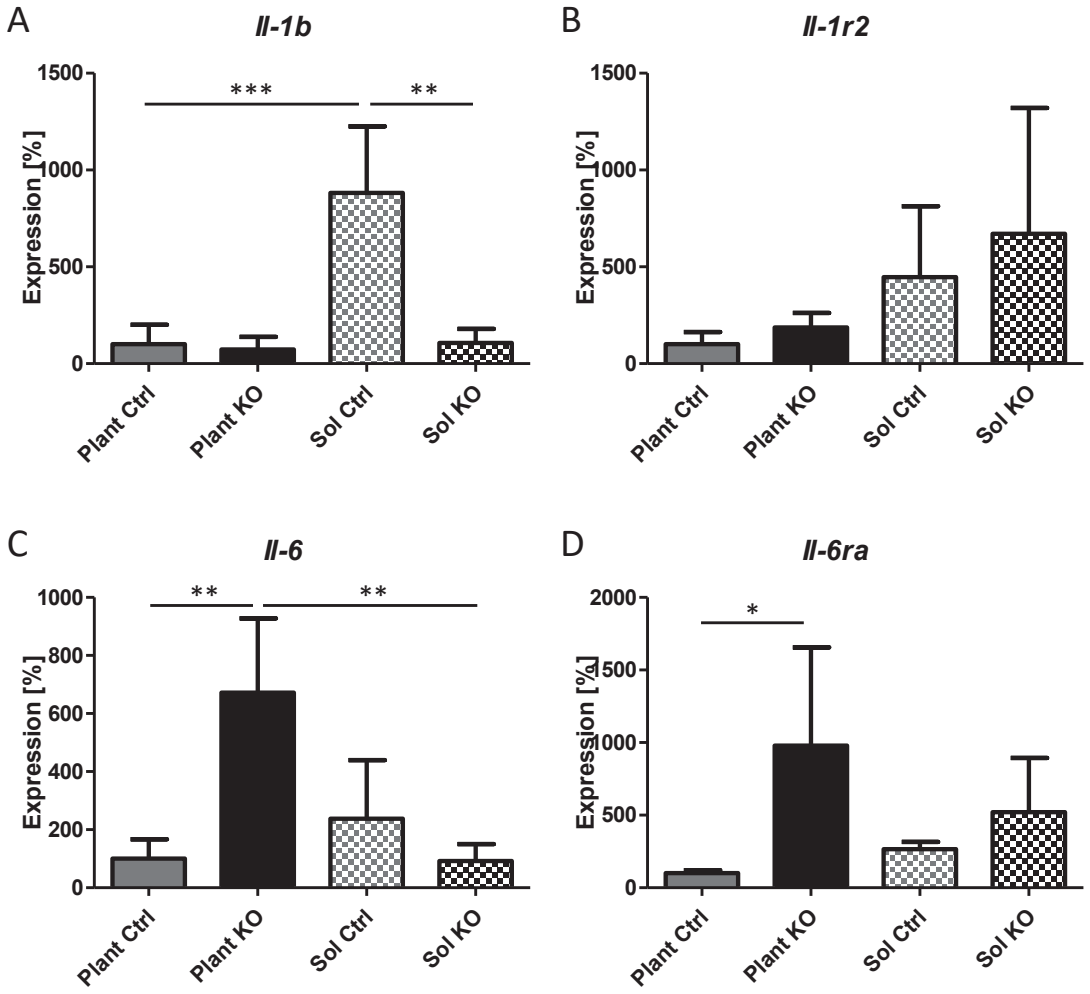

Figure 4.21: Comparison of Cytokine Transcript Expression Levels of *M. plantaris* and *M. soleus* after Induction of Heart Failure
Transcript expression of *M. plantaris* (full bars) and *M. soleus* (squared bars) of iCM p38MAPKα control (grey) and KO (black) animals was analyzed using qPCR after 48 hours of ANGII treatment. The values of *M. soleus* (Sol Ctrl and Sol KO) and the KO value of *M. plantaris* (Plant KO) of each gene were normalized to the control value of *M. plantaris* (Plant Ctrl) (which equals 100%). The transcript expression of cytokines and their receptors (*Il-1b, Il-1r2, Il-6 Il-6ra*) is depicted. 4 animals were analyzed per group. Data represent mean±SD, *p<0.05, ** p<0.01, *** p<0.001.

This rose the question, if oxidative muscles react in a different manner in heart failure. This question was addressed by transcript analysis in *M. soleus*. Unlike *M. plantaris*, which mainly consists of type 2 fibers, *M. soleus* is composed of oxidative muscle fibers (type 1 and 2a) (Allen et al. 2001), also see section 4.2.1. The transcript expression levels of the same 12 transcripts (*Trim63 (Murf1), Fbxo32 (Atrogin1), Foxo1, Foxo3, Il-1b, Il-1r2, Il-6 Il-6ra*, *Bnip3*, *Gabarapl1*, *Catepsin L* (*Ctsl*) and *Myostatin, (Mstn)*) were measured in *M. soleus* after 48 hours of treatment and were compared to *M. plantaris*. Interestingly the transcription profile of *M. soleus* differed significantly from *M. plantaris* as shown in figures 4.21, 4.22 and 4.23. None of the transcripts measured were significantly changed in *M. soleus*, except of *Il-1b*, which was

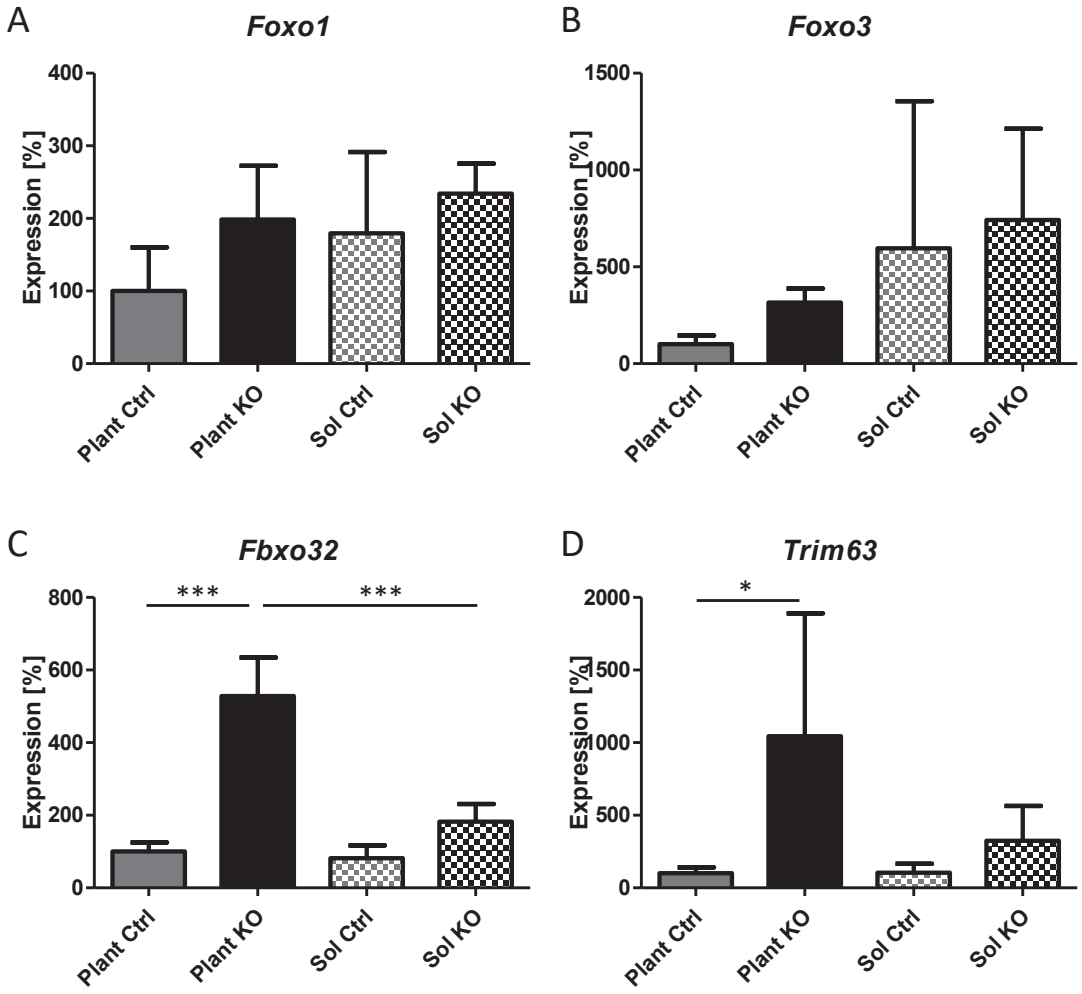

Figure 4.22: Comparison of Atrogene Transcript Expression Levels of *M. plantaris* and *M. soleus* after Induction of Heart Failure
Transcript expression of *M. plantaris* (full bars) and *M. soleus* (squared bars) of iCM p38MAPKα control (grey) and KO (black) animals was analyzed using qPCR after 48 hours of ANGII treatment. The values of *M. soleus* (Sol Ctrl and Sol KO) and the KO value of *M. plantaris* (Plant KO) of each gene were normalized to the control value of *M. plantaris* (Plant Ctrl) (which equals 100%). The transcript expression of atrogenes (*Trim63 (Murf1), Fbxo32 (Atrogin1), Foxo1, Foxo3*) is depicted. 4 animals were analyzed per group. Data represent mean$\pm$SD, *p$<$0.05, *** p$<$0.001.

massively down-regulated (8.2$\pm$5.5 fold) in iCMp38MAPKα KO compared to control. The induction of *Fbxo32 (Atrogin1)*, *Trim63 (Murf1)* (figures 4.22 C+D), *Il-6*, *Il-6ra* (figures 4.21 C+D), *Gabarapl1* and *Mstn* (fig 4.23 C+D), which was detectable in *M. plantaris*, was not seen in *M. soleus* at this early time point, leading to the conclusion that the atrophy related gene expression program has not been started yet in *M. soleus*, at least not to the same extent as seen in *M. plantaris*. This fiber type specific induction of atrogene transcripts further supported a fiber type specificity in heart failure-induced muscle wasting in iCMp38MAPKα KO mice.

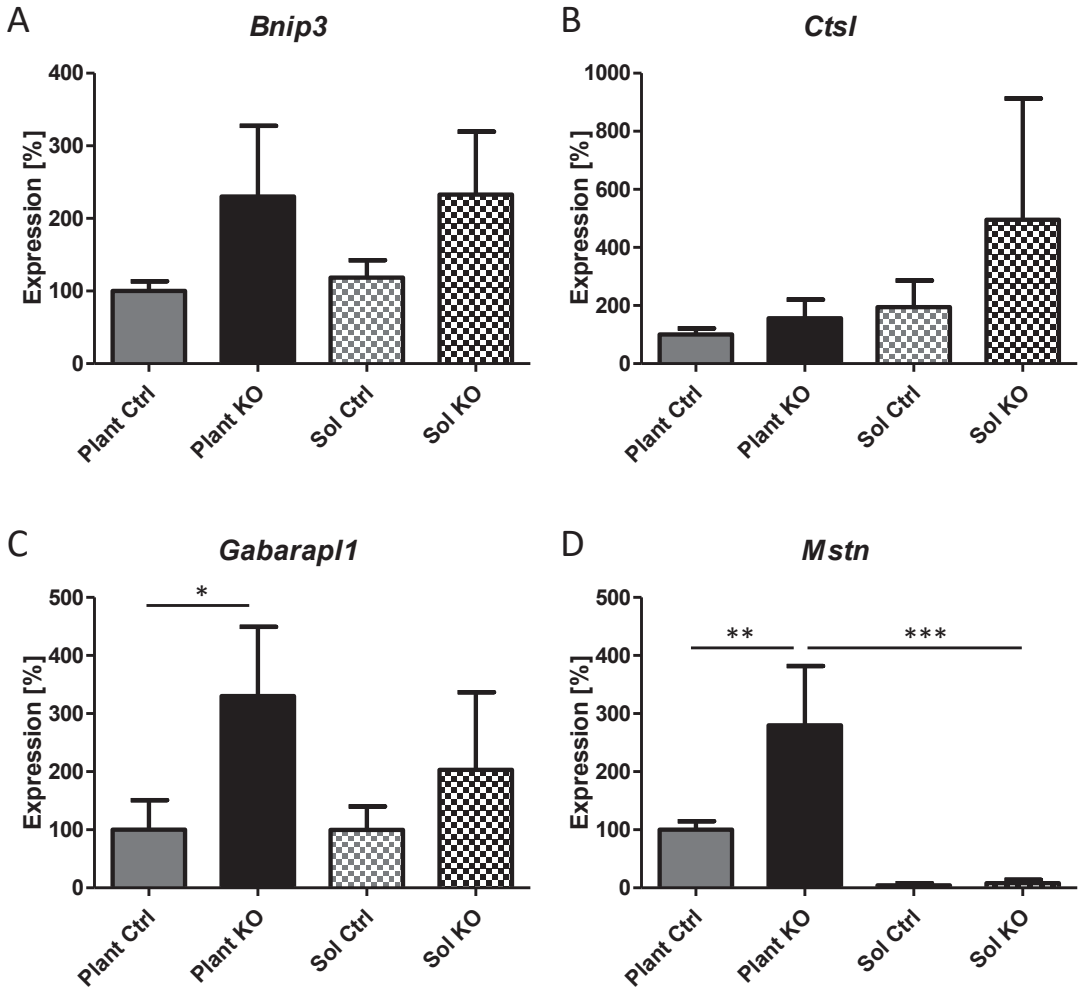

Figure 4.23: Comparison of Transcript Expression Levels of Autophagy Related Genes and Myostatin in *M. plantaris* and *M. soleus* after Induction of Heart Failure

Transcript expression of *M. plantaris* (full bars) and *M. soleus* (squared bars) of iCM p38MAPKα control (grey) and KO (black) animals was assessed using qPCR after 48 hours of ANGII treatment. The values of *M. soleus* (Sol Ctrl and Sol KO) and the KO value of *M. plantaris* (Plant KO) of each gene were normalized to the control value of *M. plantaris* (Plant Ctrl) (which equals 100%). The transcript expression of autophagy related genes (*Bnip3*, *Gabarapl1*, *Catepsin L* (*Ctsl*)) (I-K) and *Myostatin, (Mstn)* is depicted. 4 animals were analyzed per group. Data represent mean±SD, *p$<$0.05, ** p$<$0.01, *** p$<$0.001.

4.7 Muscle Weight Progression over Time

The muscle weights of *M. plantaris*, *M. soleus* and *M. gastrocnemius* of iCMp38MAPKα mice were measured at time of harvest (before, and after 12, 24 and 48 hours of ANGII treatment) and did not significantly decline within the first 48 hours of ANGII treatment in iCMp38MAPKα control and KO mice (figure 4.24). Analysis of bodyweight progression after ANGII treatment revealed that iCMp38MAPKα KO animals were more affected than controls after 48 hours of ANGII treatment as shown by a significant reduction of body mass (Control 95.39%±2.10; KO 86.27%±3.18; p$<$0,001) depicted in figure 4.25.

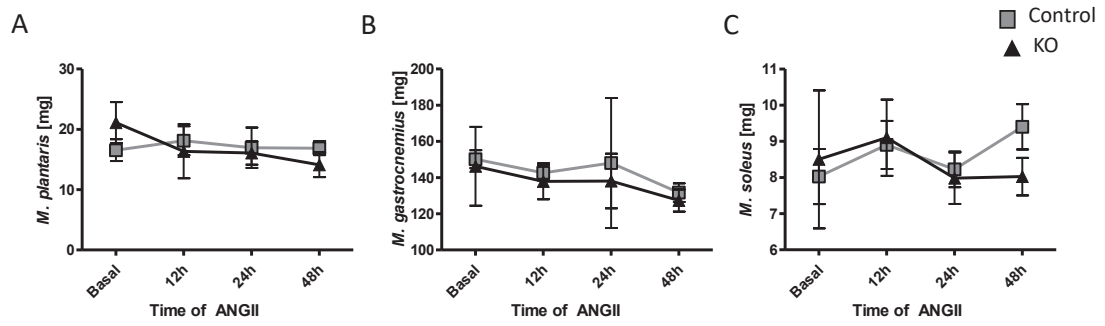

Figure 4.24: Progression of Skeletal Muscle Weight after Induction of Heart Failure
The muscle weight of *M. plantaris* (A), *M. gastrocnemius* (B) and *M. soleus* (C) before and after 12, 24 and 48 hours of ANGII treatment. 4-6 animals were analyzed per group.

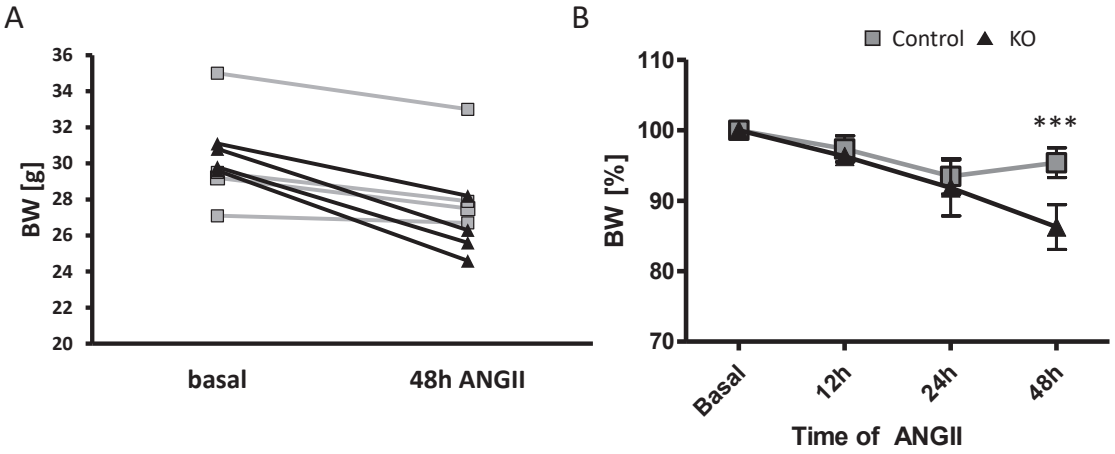

Figure 4.25: Progression of Body Weight after Induction of Heart Failure
Body weights of iCMp38MAPKα control (grey) and KO (black) mice were measured over time (before and after 12, 24 and 48 hours of ANGII). (A) The bodyweight progression of four control and KO animals, respectively, before and after 48 hours of ANGII treatment is depicted. (B) The loss of body weight is calculated by the ratio of initial body weight compared to body weight at time of harvest. 4-6 animals were analyzed per group. Data represent mean$\pm$SD, *** $p<0.001$.

4.8 Neutrophil Depletion

In the hearts of iCMp38MAPKα KO mice a massive infiltration of neutrophils was found after 48 hours of ANGII treatment (see figure 4.15 C). In line with this finding there was a significant up-regulation of cytokine transcripts in these hearts (see table 4.4 and supplemental figure 9.2). To test whether this infiltration was cause or consequence of cardiac remodeling in iCMp38MAPKα KO mice, neutrophils got depleted using Ly6G specific antibodies (AB) (see section 3.9). As a control group both control and KO mice were treated with isotype (IT) antibodies at the same concentration as Ly6G antibodies, to rule out non-specific effects.

To clarify the treatment of the four different groups, which were analyzed, they will be

named as listed below:

1. isotype antibody treated iCMp38MAPKα control group is referred to as **Ctrl+IT** (n=6)
2. isotype antibody treated iCMp38MAPKα KO group is referred to as **KO+IT** (n=6)
3. anti-Ly6G antibody treated iCMp38MAPKα control group is referred to as **Ctrl+AB** (n=8)
4. anti-Ly6G antibody treated iCMp38MAPKα KO group is referred to as **KO+AB** (n=8)

4.8.1 Injection of Antibodies and ANGII Pump Implantation

12-16 hours after intraperitoneal (anti-Ly6G or isotype) antibody injection (500μg), heart failure was induced by implanting ANGII minipumps (1.5μg/g/day) into iCMp38MAPKα control and KO mice. 48 hours later the mice were sacrificed and the depletion of neutrophils, solely found in anti-Ly6G treated mice, was confirmed by FACS analysis of the blood. This analysis was performed in cooperation with Dr. Grandoch and can be found in supplemental figure 9.4. *M. plantaris* and hearts of all four groups were harvested and analyzed.

4.8.2 Functional Analysis of the Heart

First, functional heart parameters were assessed using high resolution ultrasound, which revealed a significant improvement in KO+AB mice compared to KO+IT mice after ANGII treatment (Bottermann, Leitner et al, in preparation). This was indicated by improved ejection fraction (EF) (KO+IT: 19.52%±3.69; KO+AB: 39.27%±14.02), cardiac output (CO) (KO+IT: 13.02ml/min±4.21; KO+AB: 22.45ml/min±3.73), end diastolic volumes (EDV) (KO+IT: 122.76μl±31.18; KO+AB: 101.94μl±20.55) and end systolic volumes (ESV) (KO +IT: 98.68μl±24.34; KO+AB: 64.18μl±24.76) (see supplemental figure 9.5). As neutrophil depleted KO mice showed a significant improvement in cardiac function, its effect on transcript expression levels in heart and *M. plantaris* was analyzed.

4.8.3 Transcript Expression Analysis by qPCR

To test the influence of neutrophil depletion on *M. plantaris* the transcript expression of several cytokines (*Il-1r2, Il-6 and Il-6ra*), atrogenes (*Foxo1, Foxo3, Fbxo32 and Trim63*) and *Mstn* was measured in all four groups (6-8 animals per group). Additionally several cytokines (*Cxcl1, Cxcl5, Cxcr2, Il-1b and Il-6*) were measured in the hearts of these mice.

Heart

As seen in figure 4.26, qPCR analysis of the heart revealed that cytokines and their receptors were up-regulated in KO+IT mice when compared to Ctrl+IT mice after 48 hours of ANGII treatment (*Cxcl1*: 2.0±1.0; *Cxcl5*: 2.8±1.4; *Cxcr2*: 6.8±6.9; *Il-1b*: 1.9±1.1 and *Il-6*: 2.4±1.1).

This upregulation was nearly completely abolished in KO+AB mice when compared to Ctrl+AB mice, whereas the expression level was similar between Ctrl+IT and Ctrl+AB mice. Only the transcript expression level of *Il-6* of KO+AB mice was elevated as seen before.

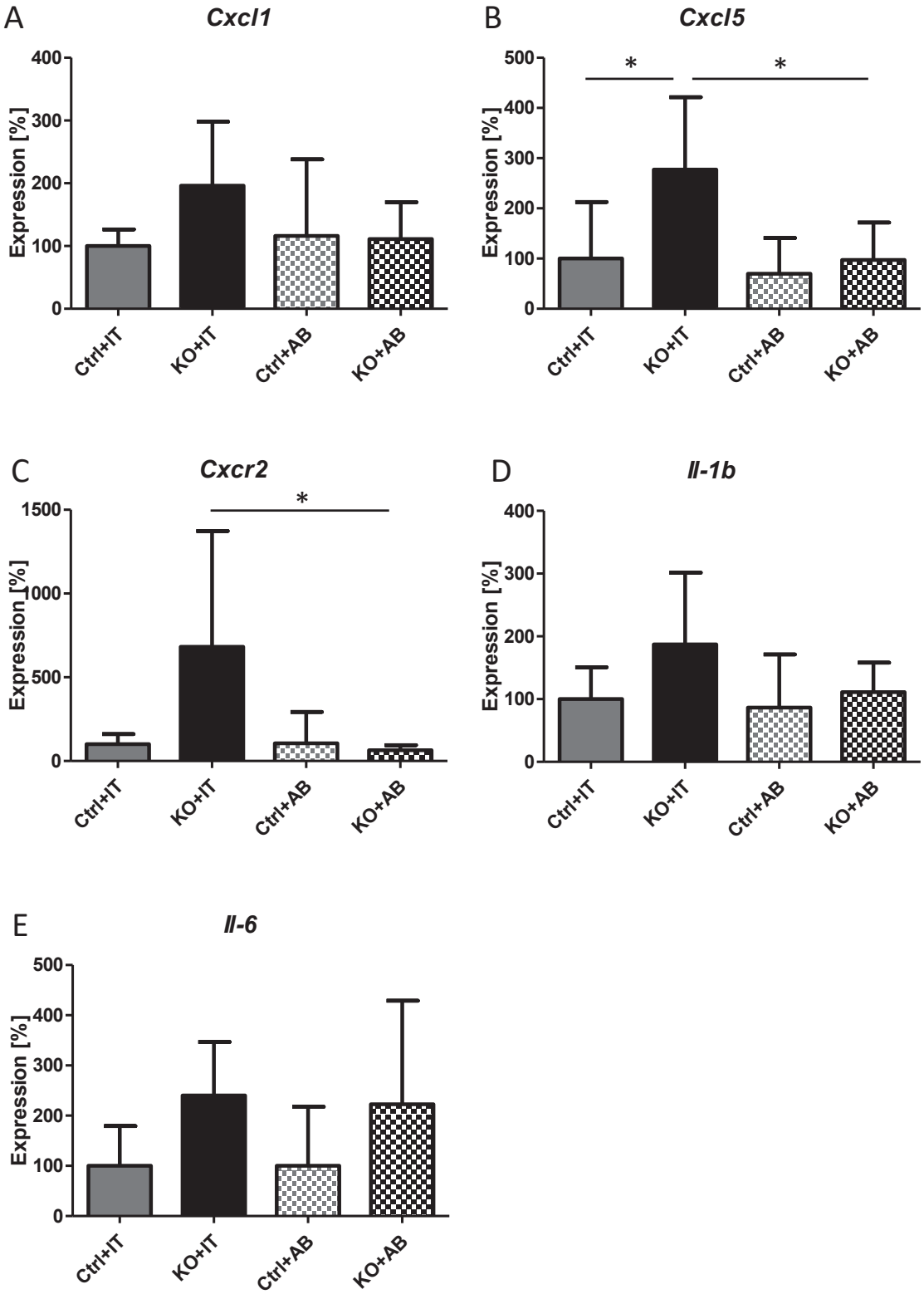

Figure 4.26: The Impact of Neutrophil Depletion on Transcript Expression in Heart after ANGII Treatment

Transcript expression of hearts of isotype (IT)-treated (full bars) and anti-Ly6G treated (squared bars) iCMp38MAPKα control (grey) and KO (black) animals was assed using qPCR after 48 hours of ANGII treatment. All animals were treated with 500μg of antibody (IT or anti-Ly6G), 12 hours before the implantation of ANGII minipumps. The values of anti-Ly6G treated controls (Ctrl+AB) and KOs (KO+AB) and IT-treated KOs (KO+IT) of each gene were normalized to the value of IT-treated controls (Ctrl+IT) (which represents 100%). In A-E the transcript expression of different cytokines and receptor (*Cxcl1, Cxcl5, Cxcr2, Il-1b and Il-6*) is depicted. 6-8 animals were analyzed per group. Data represent mean$\pm$SD, * $p<0.05$.

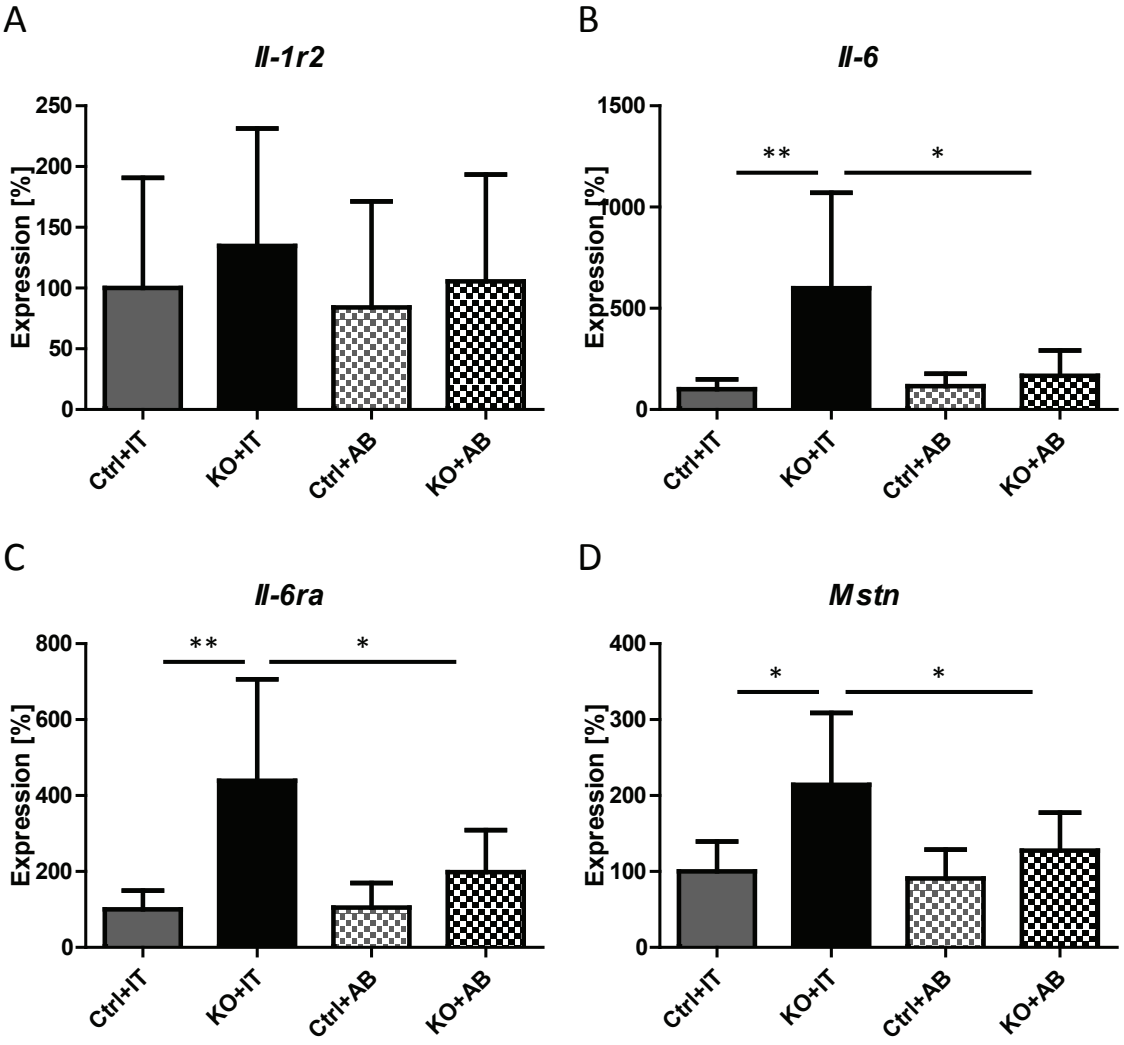

Figure 4.27: The Impact of Neutrophil Depletion on Transcript Expression of Cytokines and *Myostatin* in *M. plantaris* after ANGII Treatment
Transcript expression of *M. plantaris* of isotype (IT)-treated (full bars) and anti-Ly6G treated (squared bars) iCMp38MAPKα control (grey) and KO (black) animals was assessed using qPCR after 48 hours of ANGII treatment. The values of anti-Ly6G treated controls (Ctrl+AB) and KOs (KO+AB) and IT-treated KOs (KO+IT) of each gene were normalized to the value of IT-treated controls (Ctrl+IT) (which represents 100%). The transcript expression of cytokines, their receptors (*Il-1r2, Il-6, Il-6ra*) (A-C) and *Myostatin* (D) is depicted. 6-8 animals were analyzed per group. Data represent mean±SD, * $p<0.05$, ** $p<0.01$.

M. plantaris

As shown in figures 4.27 and 4.28, in *M. plantaris* the expression of *Il-6*, *Il-6ra*, *Myostatin*, *Fbxo32* and *Trim63* was significantly induced in ANGII treated KO+IT group compared to ANGII treated Ctrl+IT group by 6.5±4.7 (*Il-6*), 4.4±2.7 (*Il-6ra*), 2.1±0.4 (*Myostatin*), 4.4±1.4 (*Fbxo32*) and 10.8±6.5 (*Trim63*).

In contrast, in anti-Ly6G treated groups solely *Fbxo32 (Atrogin1)* expression remained significantly up-regulated (3.0±2.1) in KO+AB mice compared to Ctrl+AB mice after induction of heart failure.

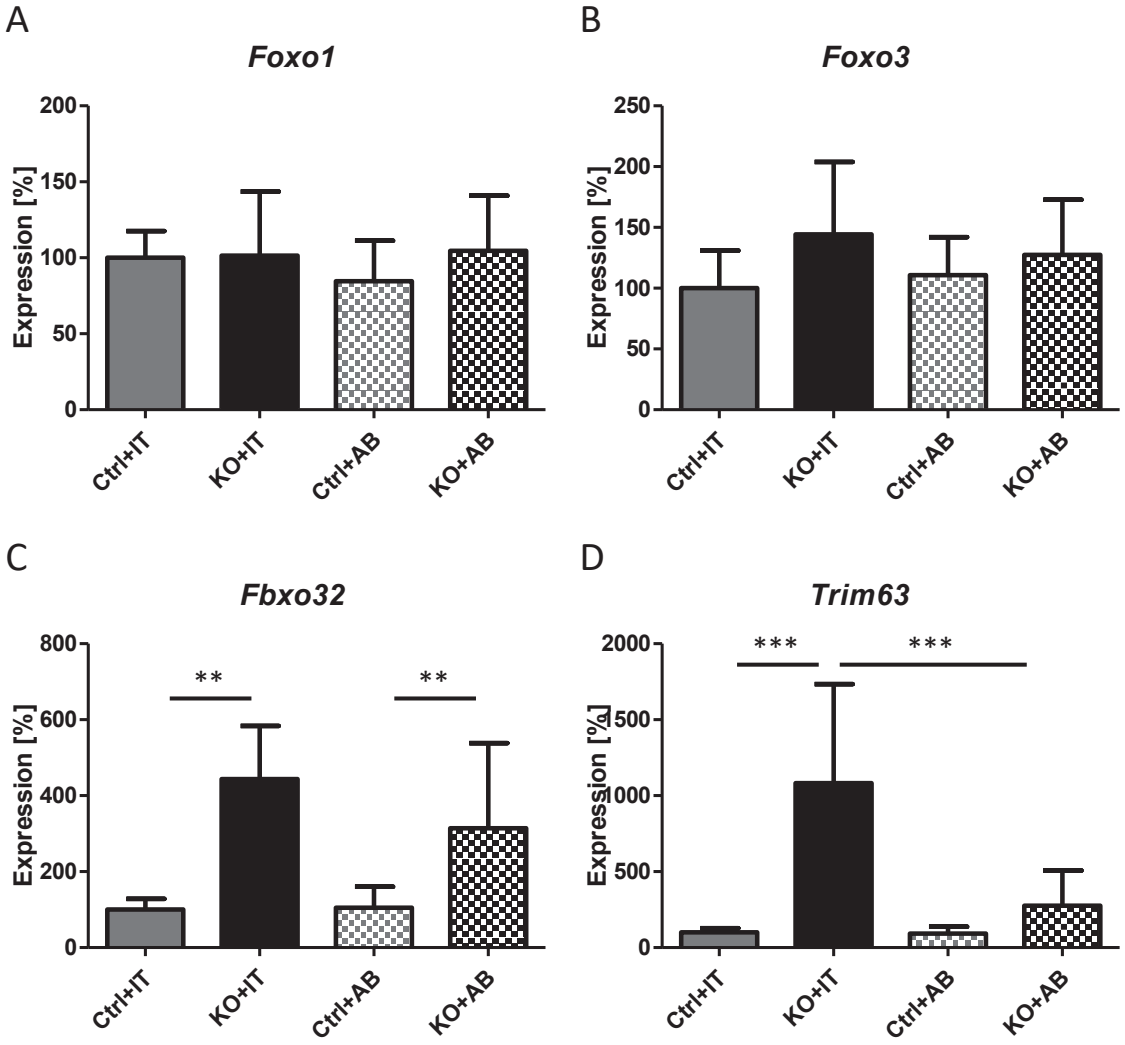

Figure 4.28: The Impact of Neutrophil Depletion on Transcript Expression of Atrogenes in *M. plantaris* after ANGII Treatment
Transcript expression of *M. plantaris* of isotype (IT)-treated (full bars) and anti-Ly6G treated (squared bars) iCMp38MAPKα control (grey) and KO (black) animals was assessed using qPCR after 48 hours of ANGII treatment. The values of anti-Ly6G treated controls (Ctrl+AB) and KOs (KO+AB) and IT-treated KOs (KO+IT) of each gene were normalized to the value of IT-treated controls (Ctrl+IT) (which represents 100%). The transcript expression of atrogenes (*Trim63 (Murf1), Fbxo32 (Atrogin1), Foxo1, Foxo3*) is depicted. 6-8 animals were analyzed per group. Data represent mean±SD, ** $p<0.01$, *** $p<0.001$.

4.8.4 Analysis of Body and Skeletal Muscle Weights

Additionally to the altered transcript expression profile, the muscles were also morphologically investigated after 48 hours of ANGII treatment. Only KO+IT mice exhibited the fiber type 2a and 2x specific alterations, as described in section 4.2, whereas this could not be detected in KO+AB mice after ANGII treatment.

Surprisingly, as demonstrated in figure 4.29, the body weight (depicted %) in both KO groups differed significantly from controls (Ctrl+IT: 94.12%±1.86 vs KO+IT: 86.12%±3.00 and Ctrl+AB: 94.76%±3.4 vs KO+AB: 87.71%±4.66).

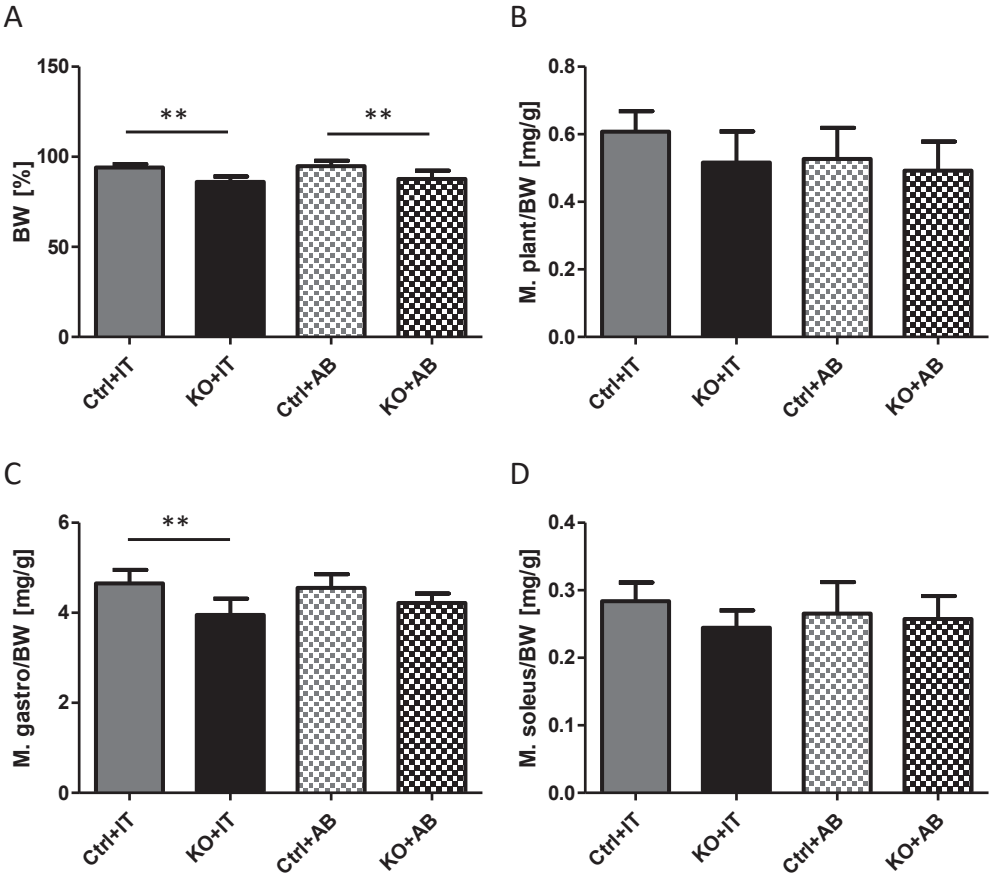

Figure 4.29: The Effect of Neutrophil Depletion on Body and Muscle Weights
Body weights of isotype (IT)-treated (full bars) and anti-Ly6G treated (squared bars) iCMp38MAPKα control (grey) and KO (black) animals were measured after 48 hours of ANGII treatment. The weight loss is calculated by the reduction of body weight after treatment (A). The muscle weight to basal body weight ratio of *M. plantaris* (B), *M. gastrocnemius* (C) and *M. soleus* (D) after treatment. 6-8 animals were analyzed per group. Data represent mean $\pm$SD, ** $p<0.01$.

To check whether this loss of body weight was due to reduced muscle mass, *M. plantaris*, *M. soleus* and *M. gastrocnemius* were analyzed as well. As all KO mice showed a significantly reduced body weight at time of harvest, which might conceal muscle weight loss, the muscle weight to initial body weight ratio was calculated to detect possible changes in muscle weights.

In *M. soleus* and *M. plantaris* this ratio was unaltered in both groups (KO compared to controls). Interestingly the *M. gastrocnemius* weight to initial body weight ratio was significantly reduced in KO+IT mice compared to Ctrl+IT mice after ANGII treatment, which was not found in KO+AB group compared to Ctrl+AB group after ANGII treatment, suggesting the body weight loss in neutrophil depleted KO+AB mice is more likely due to loss of fat mass than of muscle mass.

Summarizing the results of the neutrophil depletion experiment it is very likely that neu-

trophils infiltrating the heart at least contribute to the cardiac remodeling process in ANGII treated p38MAPKα KO mice. Once the neutrophils were depleted the transcript expression of cytokines in the heart was reduced and the cardiac function was partly preserved and as a consequence the atrophy-related transcript expression program was attenuated in plantaris muscle.

4.9 Analysis of Potency of Circulating Factors in Serum

The neutrophil depletion experiment as well as the amount of increased expressed cytokines after induction of heart failure supported the hypothesis of the involvement of inflammation in the onset of heart failure induced muscle wasting. It is very likely that the failing heart releases inflammatory factors into the blood, which might impact peripheral tissues.

To test whether serum levels of those factors were high enough to induce an atrophy related gene expression profile in a healthy mouse, serum of ANGII treated p38MAPKα control and KO mice was collected, pooled and injected into untreated wildtype mice.

4.9.1 Constitutive Cardiomyocyte-specific p38MAPKα Mouse Model

I performed these experiments during my research stay at Prof. Dr. Zhen Yan's Lab at the University of Virginia (UVA). In contrast to the tamoxifen-inducible iCMp38MAPKα used before, a constitutive cardiomyocyte specific p38MAPKα KO mouse model (cCMp38MAPKα) was used (see section 3.1.3).

To characterize the cCMp38MAPKα mouse model, ANGII minipumps were implanted into 12 week old male mice and heart function was assessed after two days of ANGII treatment using echocardiography. The analysis revealed a similar cardiac impairment within two days comparable to SM22p38MAPKα and iCMp38MAPKα KO mice. The ejection fraction (EF) of treated control mice was not significantly impaired, whereas the EF of treated KO mice significantly dropped after ANGII treatment (see figure 4.30).

The impact of heart failure on *M. plantaris* was shown by transcript expression analysis of *Il-6*, *Il-6ra*, *Fbxo32* and *Trim63* using qPCR.

The analysis revealed induction of these transcripts in ANGII treated cCMp38 MAPKα KO mice compared to ANGII treated controls, as demonstrated in other p38MAPKα KO models used before:

Transcript Name	**upregulation** [**fold-change**]
Il-6	4.4
Il-6ra	3.0
Fbxo32	2.2
Trim63	13.1

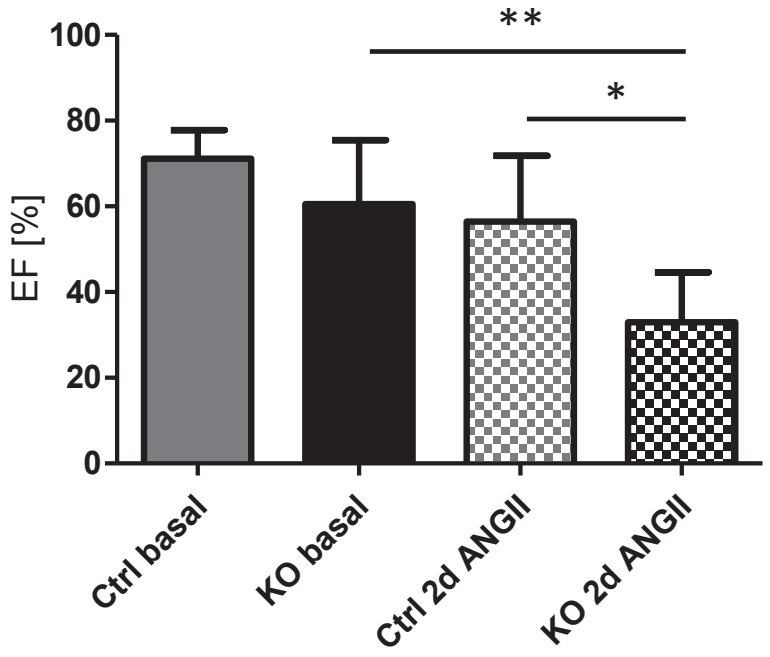

Figure 4.30: Ejection Fraction of cCMp38MAPKα Mice before and after ANGII Treatment
Ejection Fraction of cCMp38MAPKα control (grey) and KO (black) mice at baseline and after 2 days of ANGII treatment. 6-8 animals were analyzed per group. Data represent mean$\pm$SD, * $p<0.05$, ** $p<0.01$.

4.9.2 Analysis of Serum Injections

The experiment was performed according to the protocol of our collaboration partner Zhen Yan from the University of Virginia (UVA). His lab showed that intraperitoneal (i.p.) injections of 1ml serum, gained from extracellular superoxide dismutase (EcSOD) overexpressing mice, into wildtype animals significantly elevated the EcSOD levels in the serum of these injected mice (Yan et al, unpublished data), demonstrating that even large proteins such as EcSOD (MW:135 kDa) can be absorbed when injected intraperitoneally.

For serum injections, the blood of cCMp38MAPKα control and KO mice was collected after 48 hours of ANGII treatment. The induction of an atrophy related transcript expression program was validated via qPCR of *M. plantaris*. Thereafter the serum of cCMp38MAPKα control and positively tested KO mice was pooled, respectively. 1ml of serum was then injected i.p. into 3 month old wildtype male mice. Due to limited animal numbers (3-4 animals were needed to collect enough blood to obtain 1ml of serum), only two wildtype mice could be injected with either control or KO serum. Non-injected wildtype mice were used as negative controls.

Timeline analysis of transcript expression levels in heart and *M. plantaris* (see table 4.2) had shown that the highest induction of cytokines in the heart occurred after 24 of ANGII treatment. 24 hours later a high expression level of atrogenes in *M. plantaris* was found.

Therefore mice were sacrificed 24 hours after serum injection. As shown in figure 4.31, the few experiments performed revealed no difference in atrogene expression due to serum injection from ANGII treated control and cCMp38MAPKα KO mice.

As the serum experiments did not show any differences in wildtype animals, further testing would be needed to optimize the protocol, which is discussed in section 5.6. Nonetheless it could be demonstrated that the cardiac dysfunction and the transcript expression profile of *M. plantaris* of cCMp38MAPKα KO mice were comparable to the p38MAPKα KO models described before.

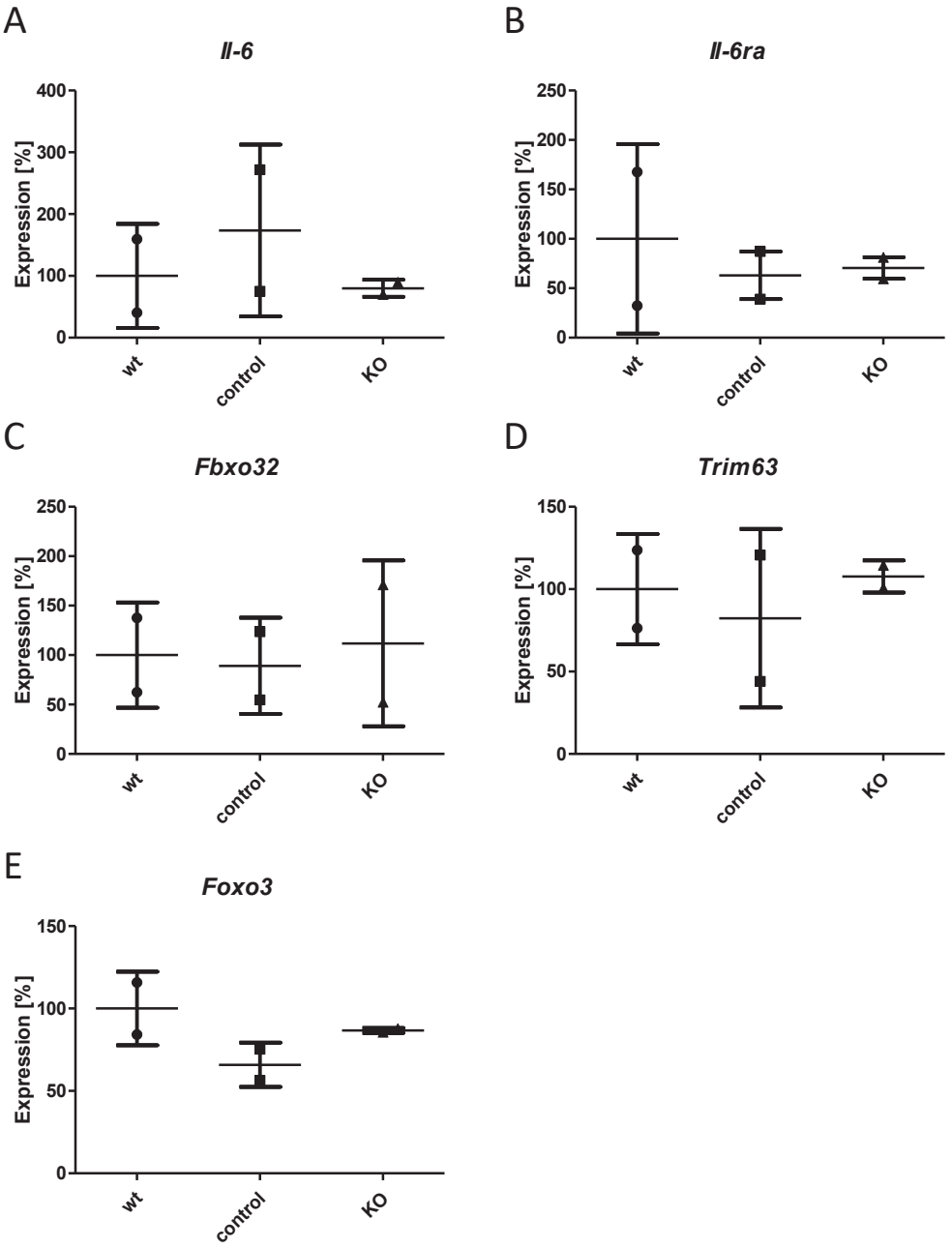

Figure 4.31: The Impact of ANGII treated cCMp38MAPKα Control or KO Serum Injections on *M. plantaris* of Wildtype Mice
1ml of ANGII treated cCMp38MAPKα control or KO Serum was injected i.p. into untreated wildtype mice. After 24 hours the transcript expression of *Il-6* (A), *Il-6ra* (B), *Fbxo32* (C), *Trim63* (D) and *Foxo3* (E) of *M. plantaris* was assessed in untreated wildtype mice (circles), wildtype mice treated with control serum (squares) and wildtype mice treated with KO serum (triangles). The transcript expression of serum treated animals was normalized to the expression of untreated wildtypes (equals 100%). 2 animals were analyzed per group.

5 Discussion

8-42% of patients suffering from chronic heart failure develop cardiac cachexia, which is accompanied by irreversible loss of muscle and fat mass. This end stage metabolic condition dramatically increases the 1-year mortality in these patients, but until now no efficient treatment could be developed (also described in section 1.1.1).

The strongest indication of emerging cachexia is loss of body mass due to skeletal muscle and adipose tissue degradation. Until now this early processes could be hardly investigated, as the onset of cardiac cachexia is hard to define in existing cardiac cachexia mouse models. It is of importance to know, that, especially in end stage heart failure, functional parameters of the failing organ can not predict cachexia (Anker et al. 1997, Anker et al. 2004).

To overcome these limitations the cardiac specific p38MAPKα KO mouse models, described in this work, offer a novel and unique possibility to investigate initiation steps of heart failure-induced muscle wasting, as heart failure can be precisely and reproducibly induced within 48 hours in adult p38MAPKα KO mice by ANGII minipump implantation.

This work provides strong evidence that heart failure induces substantial changes in skeletal muscle transcript expression. The resulting pattern is compatible with muscle wasting. This could be demonstrated at different levels, including histological as well as transcript expression analysis.

5.1 Transcript Expression Analysis of *M. plantaris*

5.1.1 Transcript Expression Analysis in SM22p38MAPKα Mice

Angiotensin II (ANGII) is not only known to induce pressure overload cardiac hypertrophy in rodents (Rosenkranz 2004, Matsumoto et al. 2013) but also induces muscle wasting by itself and antagonizes the anabolic action of growth factors, such as IGF-1 (Brink et al. 2001). ANGII induces the production of reactive oxygen species (ROS) in skeletal muscle (Semprun-Prieto et al. 2011, Sukhanov et al. 2011), which, besides their signaling functions, also induce oxidative damage of proteins and lipids. As ANGII was applied via osmotic minipumps, side effects in addition to the desired increase in blood pressure cannot be ruled out.

A systemic effect of ANGII on transcript expression was also detectable in this work by the microarray data from heart and skeletal muscle, which clearly showed transcript expression differences comparing SM22p38MAPKα control and KO animals before and after 48 hours of

ANGII treatment (see figure 4.9).

But in addition to ANGII induced transcript expression alterations, the SM22p38MAPKα KOs could still be discriminated from controls after ANGII treatment by an even higher amount of differentially expressed transcripts. The systematic analysis of transcript expression data of *M. plantaris* after ANGII treatment revealed a high induction of the protein ubiquitination pathway as well as the autophagy pathway, both highly involved in skeletal muscle atrophy (see section 4.3). These deregulation of transcripts includes key markers of both pathways, such as *Trim63* (*Murf1*), *Fbxo32* (*Atrogin1*), *Foxo1*, *Foxo3*, *Bnip3*, *Gabarapl1* and *Catepsin L*. All of them are found to be highly upregulated in ANGII treated *M. plantaris* of SM22p38MAPKα KO mice compared to ANGII treated controls.

An atrophy-related transcript expression program was solely found to be induced in *M. plantaris* of ANGII treated SM22p38MAPKα KOs when compared to ANGII treated controls, suggesting that the deregulation of atrophy associated transcripts was due to the failing heart in KO animals. This assumption was further supported by the microarray data analysis which showed a significant induction of inflammation associated pathways (such as the Il-6 pathway) in ANGII treated plantaris muscles of KO mice (see figure 4.12). Additionally a high number of cytokines was induced in hearts of KO animals (see supplemental figure 9.2), which pointed towards an involvement of cardiac released factors to trigger heart failure-induced muscle wasting.

5.1.2 Transcript Expression Analysis in iCMp38MAPKα Mice

In the SM22p38MAPKα model, p38MAPKα is not only constitutively inactivated in cardiomyocytes, but also in vascular smooth muscle cells, which might also contribute to the cardiac phenotype. As p38MAPKα is constitutively inactivated in these animals this might cause early developmental adaptions, which could lead to an altered susceptibility to increased environmental stress, which ultimately could trigger heart failure. This assumption was supported by the observation of some male SM22p38MAPKα KO mice, which already showed an impaired cardiac function before ANGII treatment. Additionally, female SM22p38MAPKα KO mice sometimes developed heart failure during pregnancy. This might be caused by the increased workload which naturally occurs during pregnancy and usually leads to a physiological hypertrophy in healthy mice. Because of this observation it is very likely that the HF is inducible by different stress conditions and not only in ANGII induced pressure overload.

To overcome developmental or vascular smooth muscle related issues an inducible cardiomyocyte-specific p38MAPKα KO mouse was generated (referred to as iCMp38MAPKα mice). In this model p38MAPKα was inactivated in adult cardiomyocytes using the tamoxifen-inducible Cre-recombinase merCremer (as described in sections 3.1.2 and 4.4). Besides its cardiomyocyte specificity, this model also more reliably mimics the situation in the majority of adult patients suffering from heart failure/cardiac cachexia, who develop the disease independent of genetic predispositions.

Although both models showed a similar cardiac phenotype, the severity of heart failure showed a higher variability in iCMp38MAPKα KO mice than in SM22p38MAPKα KOs. This difference was probably caused in part by the influence of vascular smooth muscle cells, where

p38MAPKα was also inactivated. Also developmental effects due to the constitutive knock out of p38MAPKα in the SM22p38MAPKα mouse model must be considered. Because heart failure severity varied in inducible iCMp38MAPKα KO mice, it was found that only those KO mice showed alterations in skeletal muscle transcript expression, which suffered from severe heart failure. Hence, only mice which developed severe heart failure were used for further transcript expression analysis by qPCR.

Besides the similar cardiac phenotype in both models, the transcript expression analysis of *M. plantaris* of iCMp38MAPKα control and KO mice also revealed a similar upregulation of atrophy and inflammation associated transcripts in iCMp38MAPKα KO mice as identified by microarray analysis in the SM22p38MAPKα model after 48 hours of ANGII treatment.

To further characterize a cardiac dependent deregulation of transcripts in skeletal muscle, a timeline analysis (before and after 12, 24 and 48 hours of ANGII treatment) of transcript expression was performed in iCMp38MAPKα control and KO mice. This analysis revealed an upregulation of most atrogenes (figure 4.18), autophagy related transcripts (figure 4.20) and cytokines (figure 4.19) after 48 hours of ANGII treatment in KO mice, whereas the transcript expression levels of controls remained unchanged within the first 48 hours, further supporting the hypothesis, that these alterations were induced by the failing heart and not by ANGII.

In the heart of iCMp38MAPKα KOs the upregulation of cytokines started already after 24 hours of ANGII treatment, followed by the transcript deregulation in *M. plantaris* 24 hours later, further pointing towards a heart - skeletal muscle cross talk.

5.2 Effects of Neutrophil Depletion on Heart Failure-induced Muscle Wasting

Inflammation plays an important role in heart failure-induced muscle wasting (Gullestad et al. 2012). A major involvement of inflammation in heart failure of iCMp38MAPKα KO mice was not only supported by the high induction of cytokines in the heart, but also by a massive neutrophil infiltration of KO hearts found after 48 hours of ANGII treatment (see figure 4.15 C). To examine the effect of infiltrating neutrophils, they were depleted using anti-Ly6G specific antibodies (AB) (see section 3.9). Control and KO mice, treated with isotype (IT) antibodies, were used as a control group to rule out non-specific effects.

The important finding of this experiment was, that neutrophil depletion substantially improved cardiac function in ANGII treated iCMp38MAPKα KO mice. This functional improvement led to important alterations also in *M. plantaris*.

First most of the cytokines and atrogenes upregulated in the iCMp38MAPKα KO mice with heart failure, returned to control levels. One could speculate, whether the reduced cytokine transcript levels found in *M. plantaris* were due to systemic depletion of neutrophils, which was very unlikely, as histological analysis of skeletal muscle did not reveal neutrophil infiltration after induction of heart failure (figure 4.6 B-F (anti-Ly6G)).

In hearts of both KO groups, only *Il-6* remained comparably upregulated and also *Fbxo32* stayed upregulated in *M. plantaris* in both KO groups (see figure 4.28). Thus most of the cytokines in the heart were elevated due to neutrophil infiltration either expressed by neu-

trophils or induced by it. *Il-6* might be expressed from cardiomyocytes, as its expression level remained comparably upregulated in hearts of both KO groups.

This finding demonstrated that *Il-6* by itself is not able to induce muscle atrophy as postulated by several groups, as the atrophy associated expression profile was no longer induced in neutrophil depleted KO mice. *Il-6* and its involvement in skeletal muscle wasting will be discussed below in section 5.3.1 in more detail.

Second, the body weight loss after 48 hours of ANGII treatment was significantly higher in both KO groups compared to control groups. Interestingly the analysis of the muscle weight to initial body weight ratio revealed a significant reduced ratio of *M. gastrocnemius* in non-depleted KO mice compared to non-depleted controls, which was not seen in the neutrophil depleted group.

This finding suggested that the reduced body weight in neutrophil depleted animals was rather due to loss of fat mass than muscle mass, in contrast to non-depleted KO mice, where the reduction of body weight was at least partly due to loss of muscle mass as well (see figure 4.29).

Additionally histological sections of skeletal muscles were made, which revealed, that the typical morphological alterations in skeletal muscles occurring in type 2 fibers of mice with only severe heart failure were not detectable after neutrophil depletion, whereas they were still found in non-depleted KOs after ANGII treatment.

Summarizing the findings of the neutrophil depletion experiment, it could be demonstrated that cardiac neutrophil infiltration is highly involved in the initial phase of cardiac remodeling in iCMp38MAPKα KO mice. By depleting infiltrating neutrophils not only cardiac remodeling was significantly improved, but consequently also skeletal muscle atrophy could be nearly completely rescued.

5.3 The Potential Roles of Myostatin or IL-6 as Biomarkers of Cardiac Cachexia

Until now it is not fully understood, how heart failure-induced muscle wasting is mediated. It is suggested that the failing heart releases specific factors which consequently induce skeletal muscle atrophy. In this context, both, Myostatin as well as IL-6, are suggested candidates of heart failure induced skeletal muscle wasting (Breitbart et al. 2011, Carson and Baltgalvis 2010).

5.3.1 IL-6

Interleukin-6 (IL-6) is commonly described as a pleiotropic cytokine, which is both produced by a variety of cell types, targets a variety of cell types, and has the capacity to induce several different intracellular signaling pathways. Circulating IL-6 levels are normally very low or undetectable. It can transiently increase 100-fold in the circulation following prolonged exercise, whereas in inflammatory conditions it remains dramatically increased, often related to the acute phase immune response to infection (Carson and Baltgalvis 2010). Elevated levels of circulating IL-6 are highly associated with skeletal muscle wasting (Haddad et al.

2005, Baltgalvis et al. 2009, White et al. 2012). Although overexpression of IL-6 was shown to accelerate cancer cachexia in genetically predisposed $Apc^{Min/-}$ mice (an established mouse model of colon cancer), overexpression of IL-6 was not sufficient to induce muscle wasting in wildtype animals (Puppa et al. 2012).

Results from this thesis also argue against a single role of Il-6 in early events leading to muscle wasting.

Il-6 was highly induced in hearts of both p38MAPKα KO models. The microarray data revealed a 33-fold upregulation of *Il-6* in SM22p38MAPKα KO mice, whereas a 7-fold induction of *Il-6* was found already after 24 hours of ANGII treatment in iCMp38MAPKα KO mice (see tables 4.2 and 4.4).

When mice were depleted from neutrophils transcript expression levels of *Il-6* were comparably elevated in control and neutrophil depleted KO mice, demonstrating that cardiac *Il-6* expression was not triggered by neutrophil depletion (figure 4.26 D). This was in contrast to other cytokines, which were significantly reduced after neutrophil depletion.

Nonetheless the atrophy related transcript expression program was almost completely extinguished. Thus Il-6, at least in the heart failure model used in this work, was not sufficient to trigger HF-induced muscle wasting.

5.3.2 Myostatin

Myostatin, also known as growth/differentiation factor 8, was the first identified myokine of the TGFβ superfamily. Inactivation of the *Myostatin* gene (knockout) results in extensive skeletal muscle hypertrophy in mice, cattle and humans (McPherron et al. 1997, McPherron and Lee 1997, Dschietzig 2014). Myostatin is one of the very prominent examples of a secreted growth factor suggested to be involved in the development of cardiac cachexia. It is generated predominantly in muscle and acts as a major suppressor of muscle growth. Interestingly, cardiomyocyte-specific deletion of the *Myostatin* gene in mice attenuates skeletal muscle wasting in response to pressure overload (Breitbart et al. 2011). This association was also demonstrated by others, which showed an induction of *Myostatin* on transcriptional levels in rodent models of chronic heart failure (CHF), which were also associated with elevated circulating levels of myostatin (Cook et al. 2002, Shyu et al. 2006, Lenk et al. 2009). Other groups, including Christensen et al did not find increased levels of circulating Myostatin in CHF patients (Christensen et al. 2013).

In this work no alteration of *Myostatin* transcript expression levels in the heart within the first 48 hours of ANGII treatment could be detected in neither of the p38MAPKα models (tables 4.2 and 4.4), suggesting that cardiac release of Myostatin was not involved in the modulation of atrogenes in plantaris muscles.

Nonetheless in skeletal muscle *Myostatin* was significantly upregulated after 48 hours of ANGII treatment (3-fold upregulated in SM22p38MAPKα KO mice and 2.7-fold upregulated in iCMp38MAPKα KO mice), indicating its early involvement in the induction of skeletal muscle atrophy. Thus, in the context of heart failure *Myostatin* induction in skeletal muscle might represent an additional parakrine mechanism for induction of a skeletal muscle wasting

program. Assuming an involvement of skeletal muscle *Myostatin*, the question rises, how *Myostatin* is induced. At least *Il-6* is an unlikely candidate to induce *Myostatin*, as it remained upregulated in neutrophil depleted mice whereas *Myostatin* was not induced in this mice.

It could be demonstrated that the induction of a SkM wasting-related program was not dependent on cardiac-expressed *Il-6* or *Myostatin* in these models, as transcript expression levels of both factors did not correlate with the induction of a wasting-related program. Therefore other humoral factors are likely involved. In this context the plethora of cytokines and chemokines upregulated in the failing heart (see supplemental figure 9.2), provide novel potential candidates, which might be causally involved in the upregulation of atrogenes either directly and/or via induction of *Myostatin*.

5.4 Fibertype-specific Susceptibility of Skeletal Muscle

A possible fibertype specificity in p38MAPKα KO models was demonstrated by histological analysis, which revealed an increased number of glycolytic fibers per defined area, which was in line with a reduction of fiber size in SM22p38MAPKα KO mice after ANGII treatment, whereas oxidative cells remained unaffected. Additionally the morphologically different appearing cells were found to be type 2a and 2d/x specific (see figure 4.5), also pointing towards a fiber-type specificity in this model.

In muscle wasting, induced by chronic disease, glycolytic fibers tend to be first affected in contrast to oxidative fibers (also reviewed by Wang and Pessin 2013). Nonetheless the fiber type susceptibility after heart failure is controversially discussed in literature, where Li et al found oxidative fibers to be more protected in wasting conditions (Li et al. 2007), whereas Drexler et al showed a shift from oxidative to glycolytic fibers of patients with chronic heart failure (Drexler et al. 1992).

This alleged discrepancy is likely explained by the different setting of these studies. In contrast to human patients, who suffered from chronic heart failure (CHF) over years, the CHF in mice is relatively rapidly induced (3-4 weeks). Hence the findings displayed in these studies reflect an early stage of muscle wasting (mice) whereas the human data reflect later stages of CHF, where both fibers types are likely affected. Additionally the human data was gained from single muscle biopsies, which do not provide any insight about whole muscle atrophy.

In the heart failure model used in this work only glycolytic muscles were found to be affected, pointing towards a susceptibility of type 2 fibers after heart failure, at least at the onset of muscle wasting.

The origin of the type 2a and 2d/x specific alterations remains to be elucidated, but the alterations could be used as an indicator for the severity of cardiac dysfunction, as these alterations were only found in mice, which suffered from severe heart failure (see section 4.5.3). Intriguingly this effect seemed to be a general mechanism in heart failure bearing mice, as it was found to be neither muscle specific (it was also detectable in *M. tibialis anterior* and *M. extensor digitorum longus*) nor model specific, as it was not only found in both p38MAPKα KO models (SM22p38MAPKα and iCMp38MAPKα) but also in another heart failure mouse model (cardiac specific AKT1/AKT2 double KO) as shown in supplemental figure 9.1.

Also on the molecular level fiber type-specificity in muscle atrophy was found. In contrast to glycolytic *M. plantaris*, oxidative *M. soleus* did not induce the transcript expression of cytokines (figure 4.21), atrogenes (figure 4.22), autophagy related genes and *Myostatin* (figure 4.23) The only exception found was an upregulation of *Il-1b* in *M. soleus*.

5.5 Body Weight Progression

Additionally to the transcriptional and histological alterations found in skeletal muscles of cardiac specific p38MAPKα KOs after induction of heart failure, these mice also showed a significant higher loss of body weight when compared to controls.

In SM22p38MAPKα KO mice the loss of body mass could already be seen 2 days after treatment and stayed below baseline body weight throughout 14 days, whereas controls recovered from a drop in body weight after 2 days within 7 days (see figure 4.1). A similar body weight progression was found in iCMp38MAPKα KO animals after 48 hours of ANGII treatment, where the loss of body mass was found to be more severe in KO mice compared to controls (see figure 4.25). However, single muscle weight analysis of *M. plantaris*, *M. soleus* and *M. gastrocnemius* did not reveal a significant reduction of muscle mass within the first after two days of ANGII treatment (see figure 4.24). This might be due to the early time point, where muscle degradation was about to start, but had not yet reached significant levels. Thus, the loss of fat mass might have accounted for the reduction of bodyweight at this early timepoint.

The body and muscle weight analysis of neutrophil depleted animals uncovered, that, although neutrophil depleted KO animals showed a similar loss of body weight than non-depleted KOs after ANGII treatment, skeletal muscle mass was not affected in neutrophil depleted KO mice, whereas a significant reduction of muscle mass could be demonstrated in non-depleted KO mice. This ongoing skeletal muscle degradation was further supported by an induction of an atrophy-related transcript expression profile, as well as the morphological alterations, which were only detectable in non-depleted KO mice.

5.6 Involvement of Circulating Factors in Heart Failure-induced Muscle Wasting

This work provides strong evidence that heart failure in p38MAPKα KO mice did not only induce extensive alterations of skeletal muscle transcript expression but also led to an increased loss of bodyweight. Inflammatory processes seemed to be highly involved in the initiation of this inter-organ communication, as seen by the high induction of cytokines on a transcriptional level in p38MAPKα KO hearts (see tables 4.2 and supplemental figure 9.2) as well as by the cardiac infiltration of neutrophils (see figure 4.15 C).

By inhibiting cardiac infiltration of neutrophils (as described above) the transcriptional alterations were nearly completely prevented in hearts and skeletal muscles of KO mice. This further supported a pivotal role of inflammatory processes in heart failure-induced muscle wasting in the iCMp38MAPKα model.

To test the effect of circulating factors on skeletal muscle, and whether these would be sufficient to induce muscle wasting, the parabiosis model was considered to be performed in the lab of Prof. Yan at the University of Virginia (UVA), where the parabiosis model is well established.

The principle of parabiosis is based on a shared blood circulation between two animals. This is achieved by stitching them together along their body sides (cf. conjoined twins). Briefly, a long incision of the skin is made from the front to the back limb (opposite sides of two animals). Then these two animals (which shall be same sex litter mates) are combined by fixing their elbows and knee joints together. Thereafter, the skin of these two animals is sutured alongside their bodies. This is sufficient to induce the establishment of microvasculature, which ultimately leads to a shared blood circulation within 10-14 days. A detailed (video-) protocol of this procedure can be found here: Kamran et al. 2013. Until now, there is only one publication using a rat parabiosis model to investigate cancer cachexia, where this model provided evidence for the humoral mediation of cancer-associated cachexia (Norton et al. 1985).

The activation of atrogenes in a control mouse (as litter mates are preferable, Cre- control mice could be used) after induction of heart failure in the conjoined cardiac specific p38MAPKα KO mouse would provide the ultimate proof of a transferable wasting-inducing factor.

For this aim a constitutive cardiomyocyte-specific p38MAPKα mouse model was generated at the Yan lab, which showed a similar phenotype as the other p38MAPKα KO models (see section 4.9.1), thereafter referred to as cCMp38MAPKα. Interestingly some KO animals already showed an impaired cardiac function before ANGII treatment, similar to the SM22p38MAPKα model, suggesting that the constitutive inactivation of p38MAPKα increases the susceptibility to stress in these mice as well. This was an interesting observation, as the more severe phenotype seen in constitutive SM22p38MAPKα KO mice compared to inducible iCMp38MAPKα KO mice seemed to be due to the constitutive inactivation of p38MAPKα in cardiomyocytes rather than vascular smooth muscle related issues.

As cCMp38MAPKα appeared to be more susceptible to stress, it had to be expected that a parabiotical combination of a control and a cCMp38MAPKα KO mouse would lead to a substantial stress situation which would result in heart failure of the cCMp38MAPKα KO mouse. Since it takes up to 14 days until the circulation of both parabiots is combined to allow a sufficient transfer of circulating factors, the advantage of a defined start of heart failure to induce expression changes in *M. plantaris* of the healthy mouse would be lost.

For those reasons it was decided to try a more direct approach first, as described in section 4.9. This was based on former experiments done in Yan lab, where they were able to show that intraperitoneal (i.p.) injections of 1ml serum, gained from extracellular superoxide dismutase (EcSOD) overexpressing mice, into wildtype animals significantly elevated the EcSOD levels in the serum of these injected mice. There it was demonstrated that even large proteins such as EcSOD (MW:135 kDa) could be absorbed if applied intraperitoneally (Yan et al, unpublished data).

Based on this protocol, serum of ANGII treated cCMp38MAPKα control and KO animals

were collected. *M. plantaris* of ANGII treated cCMp38MAPKα KO mice were screened for altered atrogene expression. Only serum of positively tested KO mice, as well as of ANGII treated controls was pooled and injected into wildtype animals, respectively. An untreated wildtype mouse was used as control. After 24 hours *M. plantaris* of injected mice were analyzed to detect possible transcript expression changes of atrophy related transcripts using qPCR. This timepoint was chosen, as the timeline analysis of iCMp38MAPKα control and KO animals revealed transcriptional alterations in *M. plantaris* just 24 hours after first transcriptional alterations were detected in heart of KO mice.

Despite applying an experimental protocol that was close to in vivo situation, *M. plantaris* of these mice did not reveal any differences in atrogene expression when compared to control serum treated wildtype mice (see figure 4.31). Probably circulating factors were not sufficient to induce muscle wasting in a healthy wildtype mouse, but this cannot be assuredly concluded from the few experiments. There were different uncertainties, why these experiments might not have worked and which require a systematic testing of the protocol:

- Wrong amount/concentration of serum injected
- Duration between injection of serum and harvest of *M. plantaris* was too short/long
- Circulating factors are not stable enough in serum (plasma probably better)
- Wrong way of application – whole serum was applied at once, multiple times could be better, to mimic continuous release of factors
- Wrong injection site – probably factors from the serum, which were applied intraperitoneally were not sufficiently absorbed
- Wildtype serum protected animals against muscle wasting

The potency of circulating factors could be first tested using an in-vitro assay (as suggested in section 6.2.1), to define concentration and duration of treatment of these factors, which would help to optimize the in-vivo approach, as these novel mouse models provide optimal prerequisites to investigate early triggers of heart failure-induced muscle wasting.

6 Outlook

The p38MAPKα KO models offer the unique possibility to investigate initial steps of heart failure-induced muscle wasting. This is a valuable advance to existing cachectic mouse models where the onset of muscle wasting was neither predictable nor inducible. For the p38MAPKα KO models it was demonstrated that first alterations of skeletal muscle, as notable by histological and transcriptional changes, were seen 48 hours after the induction of heart failure, providing a defined window in time, to investigate the onset of heart-skeletal muscle cross talk. This model offers a plethora of possibilities to unravel this poorly understood early phase of interorgan communication.

6.1 Protein Expression Analysis

Protein expression and activity analysis will provide more insights in the progression of muscle wasting. The extensive transcript expression alterations found in skeletal muscles of p38MAPKα KO mice strongly suggest the induction of wasting associated pathways including the ubiquitin-proteasome pathway as well as the autophagy pathways. An upregulation of proteosomal activity in muscles can be shown using western blot analysis to test for increased amounts of active E3 ligases in ANGII treated KO animals compared to ANGII treated controls (Sandri 2013). The proteosomal activity itself can be additionally measured using luminescence-based proteasomal activity assays, which are commercially available (Strucksberg et al. 2010).

6.2 Approaches to Investigate Mediators of Muscle Wasting

Circulating inflammatory factors, likely secreted from the failing heart, are highly suggested to at least contribute to heart-skeletal muscle cross talk. As direct injection of KO serum into wildtype mice did not work, other approaches can be considered, to test for their potency. Thereafter an optimized in-vivo approach of serum injections could be performed.

Analyzing circulating factors from the blood (either plasma or serum) of p38MAPKα KO mice would allow to conclude whether humoral factors are sufficient to induce muscle wasting. It would not provide any information of the origin of these factors, which might not come exclusively from the failing heart. To discriminate between factors exclusively released from the diseased organ and generally elevated circulating factors (probably released from

peripheral tissues), heart effluates could be collected and analyzed (e.g. isolated perfused heart assay (Langendorff)).

As the concentration of circulating/released cytokines/factors is rather low (1-100 pg/ml range for cytokines) a sensitive detection method has to be considered (Kleiner et al. 2013), such as Mass spectrometers, ELISA or Multiplex Analysis. Additionally, in vitro cell culture assays might help to reveal the potency of circulating factors:

6.2.1 In vitro Assay

As an indirect test for the abundance of wasting inducing factors, C2C12 cells (a murine myoblasts cell line) will be used. The myoblasts can be differentiated into myotubes, and be stimulated with plasma/serum/effluates of p38MAPKα KO mice and tested for activation of atrogenes. To analyze the induction of atrogenes, a reporter cell line is currently under construction, combining an atrogene promoter (e.g. Foxos, E3 ligases, which were highly induced in KO mice after induction of heart failure) with either a fluorescent (eg. GFP) or luciferase reporter gene. Alternatively the transcript expression levels can also be analyzed using qPCR. In vitro assays increase the feasibility to test for different concentrations and durations of treatment with minimal volumes required.

6.3 Perspectives to Further Characterize p38MAPKα Models

6.3.1 Non-chemical Induction of Heart Failure

As discussed in section 5.1 ANGII shows a great impact on transcript expression profile of hearts and skeletal muscles, and it is associated with skeletal muscle wasting. Although this work demonstrated, that ANGII itself did not induce skeletal muscle atrophy within the first two days, it possibly affects skeletal muscles if later time points are investigated.

If so, heart failure could be induced differently in p38MAPKα KO models. This would further strengthen the hypothesis, that heart failure is sufficient to induce muscle wasting in KO mice. Therefore heart failure should not be triggered chemically, but mechanically, either by using surgical interventions (such as transverse aortic constriction (TAC)) or other external stress stimuli (such as forced exercise training). As discussed in section 5.1.2, it seems that especially constitutive p38MAPKα KO mice are susceptible to stress as some mice already showed an impaired cardiac function before ANGII treatment and female KO mice sometimes developed heart failure during pregnancy as well.

6.3.2 Muscle Function

Muscle atrophy does not only affect muscle mass, but also muscle strength, which further contributes to the fatigue of patients. Muscle strength was not examined in this model, nonetheless it would be an interesting parameter. To simply preserve or restore muscle mass is not sufficient, if muscle function remains impaired. There would be different methods to investigate murine muscle strength, in vitro and in vivo (Romanick et al. 2013):

- Forelimb grip strength

- Four limb-hanging test
- Assessment of muscle contractility and force

The assessment of skeletal muscle function and not only skeletal muscle atrophy would provide more insights in pathways involved in the onset and the progression of muscle wasting.

6.3.3 Nutrition

A logical intervention of body weight loss seems to be increased nutrient supplementation. But the loss of muscle and fat mass seen in cachectic patients is not only due to reduced food intake (anorexia), as it could not be reversed by forced alimentation (Gullett et al. 2011). Nonetheless there is rising amount of studies, which investigate the positive influence of a specific diet, rich in omega-3 fatty acids, amino-acid loading/protein supplementation and vitamin D (Camperi et al. 2013, Campos-Ferraz et al. 2014, Giacosa and Rondanelli 2008) on cachectic patients. As reviewed by Konishi et al in 2016, there are several animal studies as well, which describe the benefits of optimized nutrition in cachexia (Konishi et al. 2016).

Wasting is considered as a metabolic event, which occurs additionally to the initial burden of a chronic disease. Especially in chronic heart failure the nutrient and oxygen supply of peripheral organs is impaired, due to the reduced cardiac function. Over time the overall resilience (strength, endurance, activity) gets drastically diminished (Alsafwah et al. 2007, Ashrafian et al. 2007). This leads to further degradation of skeletal muscle and fat mass and ultimately leaves the patient immobilized - a vicious circle is formed. This dramatic diagnosis has to be kept in mind, to prevent or at least to intervene as early as possible with the progression of muscle wasting.

To investigate whether the body weight loss in this model is rather due to restriction of nutrient, by reduced food intake, or caused by stress, due to the cardiac remodeling, pair-feeding should be considered. In such experiments, the pair-feed mouse gets the same amount of food, which was consumed by the other mouse within the last 24 hours (Ellacott et al. 2010). Thereby it is guaranteed, that both mice get the same amount of food provided.

6.3.4 Exercise

The beneficial effect associated with physical activity in health and disease is constantly increasing. Its positive impact on cachexia patients is described in many studies (Argilés et al. 2012, Gould et al. 2013, Coletti et al. 2015). Especially for patients with chronic heart failure or cardiac cachexia this seem to be contradictory as the limited heart functions seems to greatly interfere with physical activity. But cardiovascular disease is not the only limiting effects on the ability of cardiac output to increase during exercise, it is also determined by age, sex, and conditioning status (Piã et al. 2003).

It is important to define the meaning of "exercise" which ranges from moderate, regular physical training (10 minutes 3 times a week) to high-performance sportive activities (several hours a day).

Moderate training in chronic heart failure patients showed the greatest impact to restore/ sustain skeletal muscle of all interventions so far (Benito and Nattel 2009), as seen by improved

skeletal muscle metabolism (Adamopoulos et al. 1993), an anti-inflammatory effect (Gielen et al. 2003) and antioxidative effects (Linke et al. 2005).

This effect could not only be observed in human CHF patients but also in different rodent heart failure models, which all showed improved cardiac functions after several weeks of endurance training, either using treadmills or by swimming (Oliveira et al. 2009, Miyachi et al. 2009, Coletti et al. 2015).

As the cardiac specific p38MAPKα KO models seem to be very sensitive to stress, excessive training is very likely detrimental for these animals. Nonetheless the effect of physical activity could still be monitored, by including moderate endurance training. Depending on the question to be addressed, there are several different approaches to consider – mice could be pre-trained before induction of heart failure, to test whether the outcome is attenuated or even deteriorated. Another option would be to test for a training effect, after the induction of heart failure. As heart failure developed rather quickly in this mice, animals have to be adapted to exercise equipment for about a week before the induction of heart failure.

As endurance or aerobic training seem to have the most promising results so far, treadmill as well as running wheel training seem to be the best approaches for this model.

Cachexia is considered to be a metabolic disorder (Petruzzelli and Wagner 2016, Porporato 2016), hence it is important to keep all contributors in mind which ultimately lead to muscle wasting, starting from the initial organ to fail, creating a systemic condition, which impairs whole body function on more than just one level. Therefore to prevent/intervene with progression of this unfavorable condition, a multifaceted approach, including nutrition, moderate physical activity, anti-inflammatory treatment as well as best medical treatment of the primary disease might be the most promising strategy to fight muscle wasting.

7 Conclusion

The novel mouse models used in this work provide a fast, inducible and reliable induction of heart failure to investigate especially the onset of skeletal muscle wasting.

The glycolytic fiber-specific induction of skeletal muscle atrophy could be demonstrated on different levels:

- Morphologically - by histological differently appearing type 2a and type 2d/x fibers as well as the glycolytic fiber-specific increase of fibers per area counted, indicating decreasing fiber size.
- Transcriptionally - indicated by an increased transcript levels of several cytokines, autophagy related genes and atrogenes in glycolytic *M. plantaris*, but not in oxidative *M. soleus*.

Additionally a severe weight loss was associated with heart failure.

As these changes were only found in animals, which developed severe heart failure, a communication between the failing heart and skeletal muscle is highly presumable. The existence of a heart-skeletal muscle cross talk was further supported by the neutrophil depletion experiment. Cardiac infiltrating neutrophils got depleted, which led to a significant preservation of cardiac function, as well as a nearly complete rescue of the skeletal muscle atrophy.

It could also be demonstrated that the induction of a SkM wasting-related program was not dependent on cardiac-expressed *Il-6* or *Myostatin* in these models, as transcript expression levels of both factors did not correlate with the induction of a wasting-related program.

Hence these models not only contribute to better understand and characterize heart failure induced muscle wasting, but also are novel and valuable tools to investigate possible interventions targeting this disease.

Literature

Acharyya, Swarnali et al. (2005). "Dystrophin glycoprotein complex dysfunction: a regulatory link between muscular dystrophy and cancer cachexia". *Cancer Cell* 8.5, pp. 421–432.

Adamopoulos, Stamatis et al. (1993). "Physical training improves skeletal muscle metabolism in patients with chronic heart failure". *Journal of the American College of Cardiology* 21.5, pp. 1101–1106.

Agah, R. et al. (1997). "Gene recombination in postmitotic cells. Targeted expression of Cre recombinase provokes cardiac-restricted, site-specific rearrangement in adult ventricular muscle in vivo". *J. Clin. Invest.* 100.1, pp. 169–179.

Allen, D. L. et al. (2001). "Mutation of the IIB myosin heavy chain gene results in muscle fiber loss and compensatory hypertrophy". *Am. J. Physiol., Cell Physiol.* 280.3, pp. C637–645.

Alsafwah, Shadwan et al. (2007). "Congestive Heart Failure is a Systemic Illness: A Role for Minerals and Micronutrients". *Clin Med Res* 5.4, pp. 238–243.

Anker, S. D. et al. (1997). "Wasting as independent risk factor for mortality in chronic heart failure". *Lancet* 349.9058, pp. 1050–1053.

Anker, Stefan D., Wolfram Steinborn, and Sabine Strassburg (2004). "Cardiac cachexia". *Ann. Med.* 36.7, pp. 518–529.

Argilés, Josep M. et al. (2012). "Are there any benefits of exercise training in cancer cachexia?" *J Cachexia Sarcopenia Muscle* 3.2, pp. 73–76.

Ashrafian, Houman, Michael P. Frenneaux, and Lionel H. Opie (2007). "Metabolic Mechanisms in Heart Failure". *Circulation* 116.4, pp. 434–448.

Baltgalvis, Kristen A. et al. (2009). "Muscle wasting and interleukin-6-induced atrogin-I expression in the cachectic Apc (Min/+) mouse". *Pflugers Arch.* 457.5, pp. 989–1001.

Bao, Weike et al. (2007). "Effects of p38 MAPK Inhibitor on angiotensin II-dependent hypertension, organ damage, and superoxide anion production". *J. Cardiovasc. Pharmacol.* 49.6, pp. 362–368.

Barton, Elisabeth R. et al. (2002). "Muscle-specific expression of insulin-like growth factor I counters muscle decline in mdx mice". *J. Cell Biol.* 157.1, pp. 137–148.

Bastie, Claire C. et al. (2005). "FoxO1 stimulates fatty acid uptake and oxidation in muscle cells through CD36-dependent and -independent mechanisms". *J. Biol. Chem.* 280.14, pp. 14222–14229.

Baumgartner, R. N. et al. (1999). "Age-related changes in sex hormones affect the sex difference in serum leptin independently of changes in body fat". *Metab. Clin. Exp.* 48.3, pp. 378–384.

Behr, T. M. et al. (2001). "Hypertensive end-organ damage and premature mortality are p38 mitogen-activated protein kinase-dependent in a rat model of cardiac hypertrophy and dysfunction". *Circulation* 104.11, pp. 1292–1298.

Benito, Begoña and Stanley Nattel (2009). "Exercise training as a treatment for heart failure: potential mechanisms and clinical implications". *J Physiol* 587 (Pt 21), pp. 5011–5013.

Berndsen, Christopher E. and Cynthia Wolberger (2014). "New insights into ubiquitin E3 ligase mechanism". *Nat. Struct. Mol. Biol.* 21.4, pp. 301–307.

Bertaggia, Enrico, Luisa Coletto, and Marco Sandri (2012). "Posttranslational modifications control FoxO3 activity during denervation". *Am. J. Physiol., Cell Physiol.* 302.3, pp. C587–596.

Bhasin, Shalender et al. (2003). "The mechanisms of androgen effects on body composition: mesenchymal pluripotent cell as the target of androgen action". *J. Gerontol. A Biol. Sci. Med. Sci.* 58.12, pp. M1103–1110.

Blaauw, Bert, Stefano Schiaffino, and Carlo Reggiani (2011). "Mechanisms Modulating Skeletal Muscle Phenotype". *Comprehensive Physiology*. John Wiley & Sons, Inc.

Bodine, S. C. et al. (2001). "Identification of ubiquitin ligases required for skeletal muscle atrophy". *Science* 294.5547, pp. 1704–1708.

Borrione, A. C. et al. (1988). "Neonatal myosin heavy chains are not expressed in Ni-induced rat rhabdomyosarcoma". *Differentiation* 38.1, pp. 49–59.

Bowker-Kinley, M. M. et al. (1998). "Evidence for existence of tissue-specific regulation of the mammalian pyruvate dehydrogenase complex". *Biochem. J.* 329 (Pt 1), pp. 191–196.

Braz, Julian C. et al. (2003). "Targeted inhibition of p38 MAPK promotes hypertrophic cardiomyopathy through upregulation of calcineurin-NFAT signaling". *J. Clin. Invest.* 111.10, pp. 1475–1486.

Breitbart, Astrid et al. (2011). "Myostatin from the heart: local and systemic actions in cardiac failure and muscle wasting". *Am. J. Physiol. Heart Circ. Physiol.* 300.6, H1973–1982.

Brink, M. et al. (2001). "Angiotensin II induces skeletal muscle wasting through enhanced protein degradation and down-regulates autocrine insulin-like growth factor I". *Endocrinology* 142.4, pp. 1489–1496.

Camperi, A. et al. (2013). "Role of vitamin D in the pathogenesis of muscle wasting in cancer cachexia". *Nutrition, Metabolism and Cardiovascular Diseases* 23, S51.

Campos-Ferraz, PatrÃcia Lopes de et al. (2014). "An overview of amines as nutritional supplements to counteract cancer cachexia". *J Cachexia Sarcopenia Muscle* 5.2, pp. 105–110.

Caregaro, L. et al. (2001). "Insulin-like growth factor 1 (IGF-1), a nutritional marker in patients with eating disorders". *Clin Nutr* 20.3, pp. 251–257.

Carson, James A. and Kristen A. Baltgalvis (2010). "Interleukin 6 as a key regulator of muscle mass during cachexia". *Exerc Sport Sci Rev* 38.4, pp. 168–176.

Chargé, Sophie B. P. and Michael A. Rudnicki (2004). "Cellular and molecular regulation of muscle regeneration". *Physiol. Rev.* 84.1, pp. 209–238.

Christensen, Heidi Marie et al. (2013). "Prevalence of cachexia in chronic heart failure and characteristics of body composition and metabolic status". *Endocrine* 43.3, pp. 626–634.

Ciciliot, Stefano and Stefano Schiaffino (2010). "Regeneration of mammalian skeletal muscle. Basic mechanisms and clinical implications". *Curr. Pharm. Des.* 16.8, pp. 906–914.

Ciciliot, Stefano et al. (2013). "Muscle type and fiber type specificity in muscle wasting". *Int. J. Biochem. Cell Biol.* 45.10, pp. 2191–2199.

Clarke, Brian A. et al. (2007). "The E3 Ligase MuRF1 degrades myosin heavy chain protein in dexamethasone-treated skeletal muscle". *Cell Metab.* 6.5, pp. 376–385.

Cohen, Shenhav et al. (2009). "During muscle atrophy, thick, but not thin, filament components are degraded by MuRF1-dependent ubiquitylation". *J. Cell Biol.* 185.6, pp. 1083–1095.

Cohen, Shenhav et al. (2012). "Ubiquitylation by Trim32 causes coupled loss of desmin, Z-bands, and thin filaments in muscle atrophy". *J. Cell Biol.* 198.4, pp. 575–589.

Coletti, Dario et al. (2015). "Spontaneous Physical Activity Downregulates Pax7 in Cancer Cachexia". *Stem Cells International* 2016, e6729268.

Cook, Stuart A. et al. (2002). "Transcriptional effects of chronic Akt activation in the heart". *J. Biol. Chem.* 277.25, pp. 22528–22533.

Cooper, Geoffrey M. (2000). "Actin, Myosin, and Cell Movement". *The Cell: A Molecular Approach. 2nd edition.*

Crowley, Steven D. et al. (2006). "Angiotensin II causes hypertension and cardiac hypertrophy through its receptors in the kidney". *PNAS* 103.47, pp. 17985–17990.

Csibi, Alfredo et al. (2010). "The translation regulatory subunit eIF3f controls the kinase-dependent mTOR signaling required for muscle differentiation and hypertrophy in mouse". *PLoS ONE* 5.2, e8994.

D'Agostino, P. et al. (1999). "Sex hormones modulate inflammatory mediators produced by macrophages". *Ann. N. Y. Acad. Sci.* 876, pp. 426–429.

Daitoku, Hiroaki et al. (2004). "Silent information regulator 2 potentiates Foxo1-mediated transcription through its deacetylase activity". *Proc. Natl. Acad. Sci.* 101.27, pp. 10042–10047.

Daitoku, Hiroaki, Jun-ichi Sakamaki, and Akiyoshi Fukamizu (2011). "Regulation of FoxO transcription factors by acetylation and protein-protein interactions". *Biochimica et Biophysica Acta* 1813.11, pp. 1954–1960.

DeBoer, Mark Daniel (2009). "Animal models of anorexia and cachexia". *Expert Opin Drug Discov* 4.11, pp. 1145–1155.

Deval, C et al. (2001). "Identification of cathepsin L as a differentially expressed message associated with skeletal muscle wasting." *Biochem J* 360 (Pt 1), pp. 143–150.

Dimitriadis, G. et al. (1997). "Effects of glucocorticoid excess on the sensitivity of glucose transport and metabolism to insulin in rat skeletal muscle". *Biochem. J.* 321 (Pt 3), pp. 707–712.

Drexler, H. et al. (1992). "Alterations of skeletal muscle in chronic heart failure". *Circulation* 85.5, pp. 1751–1759.

Dschietzig, Thomas Bernd (2014). "Myostatin - From the Mighty Mouse to cardiovascular disease and cachexia". *Clin. Chim. Acta* 433, pp. 216–224.

Ellacott, Kate L.J. et al. (2010). "Assessment of feeding behavior in laboratory mice". *Cell Metab* 12.1, pp. 10–17.

Emde, B. et al. (2014). "Wheat Germ Agglutinin Staining as a Suitable Method for Detection and Quantification of Fibrosis in Cardiac Tissue after Myocardial Infarction". *Eur J Histochem* 58.4.

Evans, William J. et al. (2008). "Cachexia: a new definition". *Clin Nutr* 27.6, pp. 793–799.

Furuno, K., M. N. Goodman, and A. L. Goldberg (1990). "Role of different proteolytic systems in the degradation of muscle proteins during denervation atrophy". *J. Biol. Chem.* 265.15, pp. 8550–8557.

Geng, Tuoyu et al. (2011). "PGC-1α Promotes Nitric Oxide Antioxidant Defenses and Inhibits FOXO Signaling Against Cardiac Cachexia in Mice". *Am J Pathol* 178.4, pp. 1738–1748.

Giacosa, Attilio and Mariangela Rondanelli (2008). "Fish oil and treatment of cancer cachexia". *Genes Nutr* 3.1, pp. 25–28.

Gielen, Stephan et al. (2003). "Anti-inflammatory effects of exercise training in the skeletal muscle of patients with chronic heart failure". *Journal of the American College of Cardiology* 42.5, pp. 861–868.

Glick, Danielle, Sandra Barth, and Kay F. Macleod (2010). "Autophagy: cellular and molecular mechanisms". *J Pathol* 221.1, pp. 3–12.

Gould, Douglas W. et al. (2013). "Cancer cachexia prevention via physical exercise: molecular mechanisms". *J Cachexia Sarcopenia Muscle* 4.2, pp. 111–124.

Grandoch, Maria et al. (2015). "Deficiency in lymphotoxin β receptor protects from atherosclerosis in apoE-deficient mice". *Circ. Res.* 116.8, e57–68.

Gullestad, Lars et al. (2012). "Inflammatory cytokines in heart failure: mediators and markers". *Cardiology* 122.1, pp. 23–35.

Gullett, Norleena P. et al. (2011). "Nutritional Interventions for Cancer-induced Cachexia". *Curr Probl Cancer* 35.2, pp. 58–90.

Guttridge, D. C. et al. (2000). "NF-kappaB-induced loss of MyoD messenger RNA: possible role in muscle decay and cachexia". *Science* 289.5488, pp. 2363–2366.

Haddad, F. et al. (2005). "IL-6-induced skeletal muscle atrophy". *J. Appl. Physiol.* 98.3, pp. 911–917.

Haehling, Stephan von and Stefan D. Anker (2010). "Cachexia as a major underestimated and unmet medical need: facts and numbers". *J Cachexia Sarcopenia Muscle* 1.1, pp. 1–5.

Halling, Jens F. et al. (2016). "PGC-1α promotes exercise-induced autophagy in mouse skeletal muscle". *Physiol Rep* 4.3.

Hanna, Rita A. et al. (2012). "Microtubule-associated Protein 1 Light Chain 3 (LC3) Interacts with Bnip3 Protein to Selectively Remove Endoplasmic Reticulum and Mitochondria via Autophagy". *J Biol Chem* 287.23, pp. 19094–19104.

Hatta, M., F. Liu, and L. A. Cirillo (2009). "Acetylation curtails nucleosome binding, not stable nucleosome remodeling, by FoxO1". *Biochem. Biophys. Res. Commun.* 379.4, pp. 1005–1008.

Hosaka, Taisuke et al. (2004). "Disruption of forkhead transcription factor (FOXO) family members in mice reveals their functional diversification". *Proc. Natl. Acad. Sci. U.S.A.* 101.9, pp. 2975–2980.

Hu, Ping et al. (2008). "Codependent activators direct myoblast-specific MyoD transcription". *Dev. Cell* 15.4, pp. 534–546.

Ju, Jeong-Sun et al. (2016). "Autophagy plays a role in skeletal muscle mitochondrial biogenesis in an endurance exercise-trained condition". *J Physiol Sci.*

Kaiser, Robert A. et al. (2004). "Targeted inhibition of p38 mitogen-activated protein kinase antagonizes cardiac injury and cell death following ischemia-reperfusion in vivo". *J. Biol. Chem.* 279.15, pp. 15524–15530.

Kamran, Paniz et al. (2013). "Parabiosis in mice: a detailed protocol". *J Vis Exp* 80.

Kedar, Vishram et al. (2004). "Muscle-specific RING finger 1 is a bona fide ubiquitin ligase that degrades cardiac troponin I". *Proc. Natl. Acad. Sci. U.S.A.* 101.52, pp. 18135–18140.

Kitamura, Yukari Ido et al. (2005). "FoxO1 protects against pancreatic beta cell failure through NeuroD and MafA induction". *Cell Metab.* 2.3, pp. 153–163.

Kleiner, Giulio et al. (2013). "Cytokine Levels in the Serum of Healthy Subjects". *Mediators of Inflammation* 2013, e434010.

Konishi, Masaaki et al. (2016). "Nutrition in cachexia: from bench to bedside". *J Cachexia Sarcopenia Muscle* 7.2, pp. 107–109.

Lecker, Stewart H. et al. (2004). "Multiple types of skeletal muscle atrophy involve a common program of changes in gene expression". *FASEB J.* 18.1, pp. 39–51.

Leitner, Lucia M. et al. (2017). "Reactive Oxygen Species/Nitric Oxide Mediated Inter-Organ Communication in Skeletal Muscle Wasting Diseases". *Antioxid. Redox Signal.*

Lenk, Karsten et al. (2009). "Impact of exercise training on myostatin expression in the myocardium and skeletal muscle in a chronic heart failure model". *Eur. J. Heart Fail.* 11.4, pp. 342–348.

Lepore, John J. et al. (2005). "High-efficiency somatic mutagenesis in smooth muscle cells and cardiac myocytes in SM22alpha-Cre transgenic mice". *Genesis* 41.4, pp. 179–184.

Li, Ping et al. (2007). "Oxidative phenotype protects myofibers from pathological insults induced by chronic heart failure in mice". *Am. J. Pathol.* 170.2, pp. 599–608.

Lin, Jiandie et al. (2002). "Transcriptional co-activator PGC-1 alpha drives the formation of slow-twitch muscle fibres". *Nature* 418.6899, pp. 797–801.

Linke, Axel et al. (2005). "Antioxidative Effects of Exercise Training in Patients With Chronic Heart Failure". *Circulation* 111.14, pp. 1763–1770.

Liu, Yun-He et al. (2005). "Inhibition of p38 mitogen-activated protein kinase protects the heart against cardiac remodeling in mice with heart failure resulting from myocardial infarction". *J. Card. Fail.* 11.1, pp. 74–81.

Livak, K. J. and T. D. Schmittgen (2001). "Analysis of relative gene expression data using real-time quantitative PCR and the 2(-Delta Delta C(T)) Method". *Methods* 25.4, pp. 402–408.

Lojda, Zdenek, Reinhart Gossrau, and Theodor Schiebler (1976). *Enzymhistochemische Methoden*. Springer-Verlag Berlin.

Lokireddy, Sudarsanareddy et al. (2012). "Identification of atrogin-1-targeted proteins during the myostatin-induced skeletal muscle wasting". *Am. J. Physiol., Cell Physiol.* 303.5, pp. C512–529.

Mammucari, Cristina et al. (2007). "FoxO3 controls autophagy in skeletal muscle in vivo". *Cell Metab.* 6.6, pp. 458–471.

Masiero, Eva and Marco Sandri (2010). "Autophagy inhibition induces atrophy and myopathy in adult skeletal muscles". *Autophagy* 6.2, pp. 307–309.

Masiero, Eva et al. (2009). "Autophagy is required to maintain muscle mass". *Cell Metab.* 10.6, pp. 507–515.

Matsumoto, Emi et al. (2013). "Angiotensin II-induced cardiac hypertrophy and fibrosis are promoted in mice lacking Fgf16". *Genes Cells* 18.7, pp. 544–553.

Matsuzaki, Hitomi et al. (2005). "Acetylation of Foxo1 alters its DNA-binding ability and sensitivity to phosphorylation". *Proc. Natl. Acad. Sci. U.S.A.* 102.32, pp. 11278–11283.

McPherron, A. C. and S. J. Lee (1997). "Double muscling in cattle due to mutations in the myostatin gene". *Proc. Natl. Acad. Sci.* 94.23, pp. 12457–12461.

McPherron, A. C., A. M. Lawler, and S. J. Lee (1997). "Regulation of skeletal muscle mass in mice by a new TGF-beta superfamily member". *Nature* 387.6628, pp. 83–90.

Mehl, Kristen A. et al. (2005). "Myofiber degeneration/regeneration is induced in the cachectic ApcMin/+ mouse". *J. Appl. Physiol.* 99.6, pp. 2379–2387.

Mendell, J. R. and W. K. Engel (1971). "The fine structure of type II muscle fiber atrophy". *Neurology* 21.4, pp. 358–365.

Milan, Giulia et al. (2015). "Regulation of autophagy and the ubiquitin-proteasome system by the FoxO transcriptional network during muscle atrophy". *Nat Commun* 6, p. 6670.

Miyachi, Masaaki et al. (2009). "Exercise training alters left ventricular geometry and attenuates heart failure in dahl salt-sensitive hypertensive rats". *Hypertension* 53.4, pp. 701–707.

Mizushima, Noboru et al. (2004). "In vivo analysis of autophagy in response to nutrient starvation using transgenic mice expressing a fluorescent autophagosome marker". *Mol. Biol. Cell* 15.3, pp. 1101–1111.

Molinari, Francesca et al. (2016). "Animal models of cardiac cachexia". *Int. J. Cardiol.* 219, pp. 105–110.

Monier, S., A. Le Cam, and Y. Le Marchand-Brustel (1983). "Insulin and insulin-like growth factor I. Effects on protein synthesis in isolated muscles from lean and goldthioglucose-obese mice". *Diabetes* 32.5, pp. 392–397.

Morley, John E., David R. Thomas, and Margaret-Mary G. Wilson (2006). "Cachexia: pathophysiology and clinical relevance". *Am. J. Clin. Nutr.* 83.4, pp. 735–743.

Nakae, Jun et al. (2002). "Regulation of insulin action and pancreatic beta-cell function by mutated alleles of the gene encoding forkhead transcription factor Foxo1". *Nat. Genet.* 32.2, pp. 245–253.

Nakayama, Hiroyuki, Kazuhiko Nishida, and Kinya Otsu (2016). "Macromolecular Degradation Systems and Cardiovascular Aging". *Circ. Res.* 118.10, pp. 1577–1592.

Narendra, Derek P. and Richard J. Youle (2011). "Targeting mitochondrial dysfunction: role for PINK1 and Parkin in mitochondrial quality control". *Antioxid. Redox Signal.* 14.10, pp. 1929–1938.

Nascimbeni, Anna Chiara et al. (2012). "Impaired autophagy contributes to muscle atrophy in glycogen storage disease type II patients". *Autophagy* 8.11, pp. 1697–1700.

Ni, Yan G. et al. (2006). "Foxo transcription factors blunt cardiac hypertrophy by inhibiting calcineurin signaling". *Circulation* 114.11, pp. 1159–1168.

Nichenko, Anna S. et al. (2016). "Mitochondrial maintenance via autophagy contributes to functional skeletal muscle regeneration and remodeling". *Am. J. Physiol., Cell Physiol.* 311.2, pp. C190–200.

Nishida, Kazuhiko et al. (2004). "p38alpha mitogen-activated protein kinase plays a critical role in cardiomyocyte survival but not in cardiac hypertrophic growth in response to pressure overload". *Mol. Cell. Biol.* 24.24, pp. 10611–10620.

Norton, Jeffrey A. et al. (1985). "Parabiotic Transfer of Cancer Anorexia/Cachexia in Male Rats". *Cancer Res* 45.11, pp. 5547–5552.

Okutsu, Mitsuharu et al. (2014). "Extracellular Superoxide Dismutase Ameliorates Skeletal Muscle Abnormalities, Cachexia and Exercise Intolerance in Mice with Congestive Heart Failure". *Circ Heart Fail* 7.3, pp. 519–530.

Oliveira, R. S. F. et al. (2009). "Cardiac anti-remodelling effect of aerobic training is associated with a reduction in the calcineurin/NFAT signalling pathway in heart failure mice". *J. Physiol. (Lond.)* 587 (Pt 15), pp. 3899–3910.

Otsu, Kinya et al. (2003). "Disruption of a single copy of the p38alpha MAP kinase gene leads to cardioprotection against ischemia-reperfusion". *Biochem. Biophys. Res. Commun.* 302.1, pp. 56–60.

Paul, Pradyut K. et al. (2010). "Targeted ablation of TRAF6 inhibits skeletal muscle wasting in mice". *J. Cell Biol.* 191.7, pp. 1395–1411.

Pende, A. et al. (1990). "Neuroendocrine effects of interferon alpha 2-a in healthy human subjects". *J. Biol. Regul. Homeost. Agents* 4.2, pp. 67–72.

Petruzzelli, Michele and Erwin F. Wagner (2016). "Mechanisms of metabolic dysfunction in cancer-associated cachexia". *Genes Dev.* 30.5, pp. 489–501.

Piã, Ileana L. et al. (2003). "Exercise and Heart Failure". *Circulation* 107.8, pp. 1210–1225.

Piepoli, Massimo F. and Antonio Crisafulli (2014). "Pathophysiology of human heart failure: importance of skeletal muscle myopathy and reflexes". *Exp. Physiol.* 99.4, pp. 609–615.

Polge, Cécile et al. (2011). "Muscle actin is polyubiquitinylated in vitro and in vivo and targeted for breakdown by the E3 ligase MuRF1". *FASEB J.* 25.11, pp. 3790–3802.

Porporato, P. E. (2016). "Understanding cachexia as a cancer metabolism syndrome". *Oncogenesis* 5.2, e200.

Puppa, Melissa J. et al. (2012). "The effect of exercise on IL-6-induced cachexia in the Apc (Min/+) mouse". *J Cachexia Sarcopenia Muscle* 3.2, pp. 117–137.

Raben, Nina et al. (2008). "Suppression of autophagy in skeletal muscle uncovers the accumulation of ubiquitinated proteins and their potential role in muscle damage in Pompe disease". *Hum. Mol. Genet.* 17.24, pp. 3897–3908.

Rached, Marie-Therese et al. (2010). "FoxO1 expression in osteoblasts regulates glucose homeostasis through regulation of osteocalcin in mice". *J. Clin. Invest.* 120.1, pp. 357–368.

Rathbone, Christopher R., Frank W. Booth, and Simon J. Lees (2008). "FoxO3a preferentially induces p27Kip1 expression while impairing muscle precursor cell-cycle progression". *Muscle Nerve* 37.1, pp. 84–89.

Rauramaa, R., P. Kuusela, and E. Hietanen (1980). "Adipose, muscle and lung tissue lipoprotein lipase activities in young streptozotocin treated rats". *Horm. Metab. Res.* 12.11, pp. 591–595.

Ren, Jie et al. (2005). "Role of p38alpha MAPK in cardiac apoptosis and remodeling after myocardial infarction". *J. Mol. Cell. Cardiol.* 38.4, pp. 617–623.

Romanick, Mark, LaDora V. Thompson, and Holly M. Brown-Borg (2013). "Murine models of atrophy, cachexia, and sarcopenia in skeletal muscle". *Biochimica et Biophysica Acta (BBA) - Molecular Basis of Disease*. Animal models of disease 1832.9, pp. 1410–1420.

Rosenkranz, Stephan (2004). "TGF-beta1 and angiotensin networking in cardiac remodeling". *Cardiovasc. Res.* 63.3, pp. 423–432.

Roth, Stephen M. and Sean Walsh (2004). "Myostatin: a therapeutic target for skeletal muscle wasting". *Curr Opin Clin Nutr Metab Care* 7.3, pp. 259–263.

Rydén, Mikael et al. (2004). "Targets for TNF-alpha-induced lipolysis in human adipocytes". *Biochem. Biophys. Res. Commun.* 318.1, pp. 168–175.

Sanchez, Anthony M. J., Robin B. Candau, and Henri Bernardi (2014). "FoxO transcription factors: their roles in the maintenance of skeletal muscle homeostasis". *Cell. Mol. Life Sci.* 71.9, pp. 1657–1671.

Sandri, Marco (2013). "Protein breakdown in muscle wasting: Role of autophagy-lysosome and ubiquitin-proteasome". *Int J Biochem Cell Biol* 45.10, pp. 2121–2129.

Sandri, Marco et al. (2004). "Foxo transcription factors induce the atrophy-related ubiquitin ligase atrogin-1 and cause skeletal muscle atrophy". *Cell* 117.3, pp. 399–412.

Sandri, Marco et al. (2006). "PGC-1alpha protects skeletal muscle from atrophy by suppressing FoxO3 action and atrophy-specific gene transcription". *Proc. Natl. Acad. Sci. U.S.A.* 103.44, pp. 16260–16265.

Schiaffino, S. et al. (1989). "Three myosin heavy chain isoforms in type 2 skeletal muscle fibres". *J. Muscle Res. Cell. Motil.* 10.3, pp. 197–205.

Schiaffino, Stefano and Carlo Reggiani (2011). "Fiber types in mammalian skeletal muscles". *Physiol. Rev.* 91.4, pp. 1447–1531.

Schiaffino, Stefano et al. (2013). "Mechanisms regulating skeletal muscle growth and atrophy". *FEBS J.* 280.17, pp. 4294–4314.

Schmoll, D. et al. (2000). "Regulation of glucose-6-phosphatase gene expression by protein kinase Balpha and the forkhead transcription factor FKHR. Evidence for insulin response unit-dependent and -independent effects of insulin on promoter activity". *J. Biol. Chem.* 275.46, pp. 36324–36333.

Schroeder, Andreas et al. (2006). "The RIN: an RNA integrity number for assigning integrity values to RNA measurements". *BMC Mol Biol* 7, p. 3.

See, Fiona et al. (2004). "p38 mitogen-activated protein kinase inhibition improves cardiac function and attenuates left ventricular remodeling following myocardial infarction in the rat". *J. Am. Coll. Cardiol.* 44.8, pp. 1679–1689.

Semprun-Prieto, Laura C. et al. (2011). "Angiotensin II induced catabolic effect and muscle atrophy are redox dependent". *Biochem. Biophys. Res. Commun.* 409.2, pp. 217–221.

Shintani, F. et al. (1995). "Role of interleukin-1 in stress responses. A putative neurotransmitter". *Mol. Neurobiol.* 10.1, pp. 47–71.

Shringarpure, Reshma et al. (2003). "Ubiquitin conjugation is not required for the degradation of oxidized proteins by proteasome". *J. Biol. Chem.* 278.1, pp. 311–318.

Shyu, K. G. et al. (2006). "Myostatin expression in ventricular myocardium in a rat model of volume-overload heart failure". *Eur. J. Clin. Invest.* 36.10, pp. 713–719.

Sohal, D. S. et al. (2001). "Temporally regulated and tissue-specific gene manipulations in the adult and embryonic heart using a tamoxifen-inducible Cre protein". *Circ. Res.* 89.1, pp. 20–25.

Stitt, Trevor N. et al. (2004). "The IGF-1/PI3K/Akt pathway prevents expression of muscle atrophy-induced ubiquitin ligases by inhibiting FOXO transcription factors". *Mol. Cell* 14.3, pp. 395–403.

Strucksberg, Karl-Heinz et al. (2010). "Proteasomal activity in skeletal muscle: a matter of assay design, muscle type, and age". *Anal. Biochem.* 399.2, pp. 225–229.

Sukhanov, Sergiy et al. (2011). "Angiotensin II, Oxidative Stress and Skeletal Muscle Wasting". *Am J Med Sci* 342.2, pp. 143–147.

Thomsen, Rune et al. (2010). "Analysis of qPCR data by converting exponentially related Ct values into linearly related X0 values". *J Bioinform Comput Biol* 8.5, pp. 885–900.

Tiao, G. et al. (1997). "Intracellular regulation of protein degradation during sepsis is different in fast- and slow-twitch muscle". *Am. J. Physiol.* 272.3, R849–856.

Tintignac, Lionel A. et al. (2005). "Degradation of MyoD mediated by the SCF (MAFbx) ubiquitin ligase". *J. Biol. Chem.* 280.4, pp. 2847–2856.

Ventura, Juan José et al. (2007). "p38α MAP kinase is essential in lung stem and progenitor cell proliferation and differentiation". *Nat Genet* 39.6, pp. 750–758.

Verrou, C. et al. (1999). "Comparison of the tamoxifen regulated chimeric Cre recombinases MerCreMer and CreMer". *Biol. Chem.* 380.12, pp. 1435–1438.

Wang, Yichen and Jeffrey E. Pessin (2013). "Mechanisms for fiber-type specificity of skeletal muscle atrophy". *Curr Opin Clin Nutr Metab Care* 16.3, pp. 243–250.

White, James P. et al. (2012). "IL-6 regulation on skeletal muscle mitochondrial remodeling during cancer cachexia in the Apc Min/+ mouse". *Skeletal Muscle* 2, p. 14.

Wing, S. S. and A. L. Goldberg (1993). "Glucocorticoids activate the ATP-ubiquitin-dependent proteolytic system in skeletal muscle during fasting". *Am. J. Physiol.* 264.4, E668–676.

Zammit, Peter S., Terence A. Partridge, and Zipora Yablonka-Reuveni (2006). "The skeletal muscle satellite cell: the stem cell that came in from the cold". *J. Histochem. Cytochem.* 54.11, pp. 1177–1191.

Zhang, Jifeng et al. (2006). "Generation of an adult smooth muscle cell-targeted Cre recombinase mouse model". *Arterioscler. Thromb. Vasc. Biol.* 26.3, e23–24.

Zhang, Shaosong et al. (2003). "Role of 14-3-3-mediated p38 mitogen-activated protein kinase inhibition in cardiac myocyte survival". *Circ. Res.* 93.11, pp. 1026–1028.

8 List of Abbreviations

A	
AMCA	Aminomethylcoumarin
ANGII	Angiotensin II
B	
BCA	Bicinchoninic acid
Bnip3	*BCL2 Interacting Protein 3*
BSA	Bovine serum albumin
bpm	beats per minute
C	
CO	Cardiac output
cDNA	Complementary deoxyribonucleic acid
Cre	Causes recombination
CSA	Cross sectional area
Csnk2b	Casein kinase 2 beta
CT	Threshold cycle
ctrl	Control
Ctsl	*Cathepsin L*
Cxcl5	*C-X-C Motif Chemokine Ligand 5*
Cxcr2	*C-X-C Motif Chemokine Receptor 2*
D	
d	day
Da	Dalton
ddH_2O	Double deionized water
DMEM	Dulbecco Modified Eagle Medium
DMSO	Dimethylsulfoxid
DNA	Deoxyribonucleic acid
dNTP	Deoxyribonucleic acid triphosphate
DTT	Dithiothreitol
E	
EcSOD	Extracellular superoxide dismutase
EDTA	Ethylendiamintetraacetate
EF	Ejection fraction

EDV	End diastolic volume
e.g.	*Exempli gratia*
ESV	End systolic volume
F	
FACS	Fluorescence-activated cell scanning
FBS	Fetal bovine serum
Fbxo32	*F-Box Protein 32 [Atrogin1]*
FITC	Fluorescein isothiocyanate
Foxo1/3	*Forkhead Box O1/3*
G	
g	Gram
Gabarapl1	*GABA Type A Receptor Associated Protein Like 1*
Gapdh	*Glyceraldehyde 3-phosphate Dehydrogenase*
Gstz1	*Glutathione S Transferase zeta 1*
H	
h	hour(s)
Hprt1	*Hypoxanthine Phosphoribosyltransferase 1*
I	
Il-1b	*Interleukin 1 beta*
Il-1r2	*Interleukin 1 receptor 2*
Il-6	*Interleukin 6*
Il-6ra	*Interleukin receptor A*
i.p.	Intraperitoneal
J	
K	
k-	Kilo-
KO	Knock out
L	
l	Liter
Ldh	*Lactate Dehydrogenase*
loxP	Locus of crossing over
LV	Left ventricle, left ventricular
LVAW	Left ventricular anterior wall
LVPW	Left ventricular posterior wall
M	
M	Molar
m	Milli-
M. xxx	Muscle xxx
μ	Micro-
MM	Mastermix
mer	Mutagenized estrogenreceptor
mRNA	Messenger RNA

Mstn	*Myostatin*
Murf1	*Muscle-Specific RING Finger Protein 1*
MW	Molecular weight
MyHC	Myosin heavy chain
N	
n	nano-
Nudc	*Nuclear distribution C, dynein complex regulator*
O	
P	
PAGE	Polyacrylamidgelelectrophoreses
PBS (PBST)	Phosphate bufferd saline (with 0.1 % Tween)
PCR	Polymerase chain reaction
Q	
qPCR	Quantitative real-time PCR
R	
RNA	Ribonucleic acid
rpm	Rounds per minute
Rps17	*Ribosomal Protein S17*
S	
SDH	Succinate dehydrogenase
SDS	Sodium dodecyl sulphate
SkM	Skeletal muscle
T	
TAE	Tris-acetate-EDTA
TBS (TBST)	Tris bufferd saline (with 0.1 % Tween)
TEMED	Tetramethylethylendiamin
TE-buffer	Tris EDTA buffer
TF	Transcription factor
Trim63	*Tripartite Motif Containing 63 [Murf1]*
Tris	Tris(hydroxymethyl)-aminomethan
U	
U	Unit
V	
W	
WGA	Wheat Germ Agglutinin
X	
Y	
Z	
z.B.	*Zum Beispiel*

9 Supplements

9.1 Heart Failure-induced Fibertype-specific Morphological Alterations

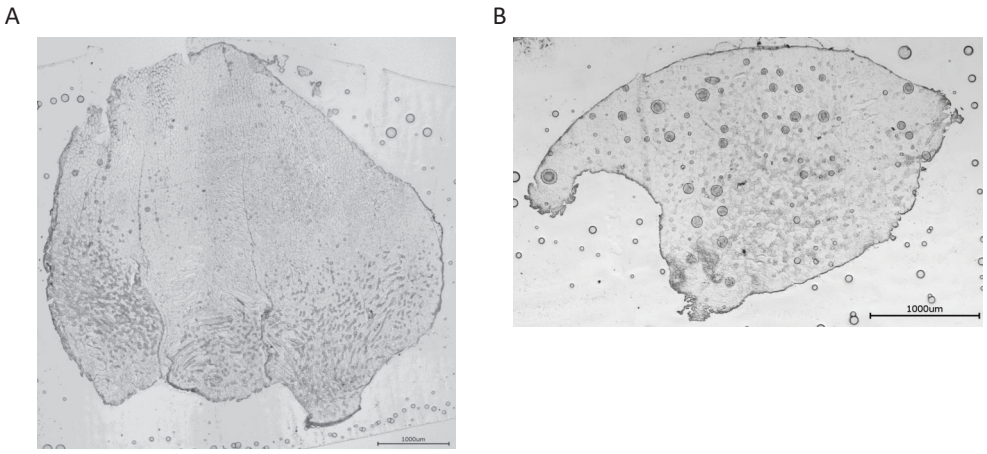

Figure 9.1: Morphological Alterations in Skeletal Muscles after Heart Failure
Heart failure induced morphological alterations in A) *M. gastrocnemius*, *M. plantaris* and *M. soleus* of cardiac-specific AKT1/2 KO (heart failure) mice and in B) *M. tibialis anterior* and *M. extensor digitorum longus* of iCMp38MAPKα KO mice. Scale bars = 1000μm.

9.2 Microarray Analysis

Synthesis of cDNA and subsequent fluorescent labeling of cRNA was performed according to the manufacturers' protocol (One-Color Microarray-Based Gene Expression Analysis / Low Input Quick Amp Labeling; Agilent Technologies). Briefly, 100ng of total RNA was transcribed into cDNA, followed by in vitro transcription and incorporation of Cy3-CTP into nascent cRNA. After fragmentation labeled cRNA was hybridized to Agilent SurePrint G3 Mouse GE 8x60K Microarrays for 17 h at 65°C and scanned as described in the manufacturers' protocol. Signal intensities on 20 bit tiff images were calculated by Feature Extraction software (FE, Vers. 11.0.1.1; Agilent Technologies). Data analyses were conducted with GeneSpring GX software (Vers. 12.5; Agilent Technologies). Probe signal intensities were quantile normalized

across all samples to reduce inter-array variability. Input data pre-processing was concluded by baseline transformation to the median of all samples. To improve signal-to-noise ratio, a given transcript had to be expressed above background (i.e. called 'detected' by FE) in all four replicates in any one of two, or both conditions to be further analyzed in pairwise comparisons. Differential gene expression was statistically determined by moderated T-tests (Benjamin-Hochberg FDR corrected, p(corr) < 0.05 and p(corr) < 0.01, respectively).

9.2.1 List of Cytokines and Chemokines after Induction of Heart Failure

ProbeName	p (Corr)	Regulation ko/wt	FC (abs) ko/wt	GeneSymbol	Description	Go	GenbankAccession	EnsemblID	EntrezGeneID	RefSeqAccess	UniGeneID
A_51_P47007	1,55E-05	up	70,05	Il1r2	Mus musculus	GO:0004910|	NM_010555	ENSMUST000	16178	NM_010555	Mm.1349
A_51_P11446	3,88E-04	up	36,26	Ccl17	Mus musculus	GO:0008009|	NM_011332	ENSMUST000	20295	NM_011332	Mm.41988
A_55_P19977	2,11E-04	up	33,07	Il6	Mus musculus	GO:0005515|	NM_031168	ENSMUST000	16193	NM_031168	Mm.1019
A_51_P28673	1,78E-04	up	20,58	Ccl2	Mus musculus	GO:0005515|	NM_011333	ENSMUST000	20296	NM_011333	Mm.290320
A_51_P34828	2,94E-05	up	16,44	Il17ra	Mus musculus	GO:1900017|	NM_008359	ENSMUST000	16172	NM_008359	Mm.4481
A_51_P21278	2,14E-04	up	12,50	Il1b	Mus musculus	GO:0032755|	NM_008361	ENSMUST000	16176	NM_008361	Mm.222830
A_51_P47445	9,57E-04	up	8,00	Socs3	Mus musculus	GO:0005515|	NM_007707	ENSMUST000	12702	NM_007707	Mm.3468
A_51_P43665	0,00121374	up	7,35	Ccl7	Mus musculus	GO:0008009|	NM_013654	ENSMUST000	20306	NM_013654	Mm.341574
A_51_P26778	5,16E-04	up	6,45	Il11	Mus musculus	GO:0046888|	NM_008350	ENSMUST000	16156	NM_008350	Mm.35814
A_51_P14071	0,00244981	up	6,11	Ccl3	Mus musculus	GO:0005515|	NM_011337	ENSMUST000	20302	NM_011337	Mm.1282
A_55_P20232	2,16E-04	up	5,88	Il20rb	Mus musculus	GO:0032703|	NM_001033543	ENSMUST000	213208	NM_0010335	Mm.242896
A_51_P24145	7,38E-05	up	5,21	Lilrb4	Mus musculus	GO:0016020|	NM_013532	ENSMUST000	14728	NM_013532	Mm.34408
A_66_P10461	3,11E-05	up	5,09	Ccl25	chemokine (C	GO:0031735|	AK043043	ENSMUST000	20300		Mm.7275
A_55_P19845	7,49E-04	up	5,07	Ccl12	Mus musculus	GO:0008009|	NM_011331	ENSMUST000	20293	NM_011331	Mm.867
A_55_P20177	7,93E-04	up	4,32	Il4ra	Mus musculus	GO:0005515|	NM_001008700	ENSMUST000	16190	NM_0010087	Mm.233802
A_55_P20795	0,00745865	up	4,29	Lilra6	Mus musculus	GO:0008150|	NM_011090	ENSMUST000	18726	NM_011090	Mm.440989
A_55_P19574	4,38E-04	up	3,83	Lilrb4	Mus musculus	GO:0016020|	NM_013532	ENSMUST000	14728	NM_013532	Mm.34408
A_55_P20876	8,05E-04	up	3,67	Il4i1	Mus musculus	GO:0001716|	NM_010215	ENSMUST000	14204	NM_010215	Mm.2565
A_55_P20353	5,06E-04	up	3,55	Nfil3	Mus musculus	GO:0005515|	NM_017373	ENSMUST000	18030	NM_017373	Mm.136604
A_51_P46095	0,00696599	up	3,53	Ccl6	Mus musculus	GO:0008009|	NM_009139	ENSMUST000	20305	NM_009139	Mm.137
A_51_P27150	1,16E-04	up	2,65	Il1r1	Mus musculus	GO:0005515|	NM_008362	ENSMUST000	16177	NM_008362	Mm.896
A_52_P10267	5,56E-04	up	2,46	Ecscr	Mus musculus	GO:0016020|	NM_001033141	ENSMUST000	68545	NM_0010331	Mm.329362
A_52_P22207	4,70E-04	up	2,01	Ackr2	Mus musculus	GO:0005515|	NM_021609	ENSMUST000	59289	NM_021609	Mm.258105
A_55_P20587	3,29E-04	up	2,00	Hilpda	Mus musculus	GO:0005811|	NM_023516	ENSMUST000	69573	NM_023516	Mm.45161
A_55_P20079	0,00389304	down	41,01	Cx3cr1	Mus musculus	GO:0043005|	NM_009987	ENSMUST000	13051	NM_009987	Mm.44065
A_55_P20543	0,00382711	down	24,34	Cx3cr1	Mus musculus	GO:0043005|	NM_009987		13051	NM_009987	Mm.44065
A_52_P99810	8,69E-04	down	9,08	Cx3cr1	Mus musculus	GO:0043005|	NM_009987	ENSMUST000	13051	NM_009987	Mm.44065
A_55_P20502	0,00522034	down	6,14	Ackr4	Mus musculus	GO:0007165|	AY072938		252837		Mm.269254
A_51_P46166	0,00132688	down	5,92	Cxcl9	Mus musculus	GO:0008009|	NM_008599	ENSMUST000	17329	NM_008599	Mm.766
A_51_P46470	0,00770386	down	4,72	Ccl8	Mus musculus	GO:0008009|	NM_021443	ENSMUST000	20307	NM_021443	Mm.42029
A_51_P18496	7,63E-05	down	3,82	Rilpl1	Mus musculus	GO:0005622|	NM_021430	ENSMUST000	75695	NM_021430	Mm.41180
A_52_P15461	3,01E-04	down	3,73	Il15	Mus musculus	GO:0008284|	NM_008357	ENSMUST000	16168	NM_008357	Mm.4392
A_55_P19807	0,00905052	down	3,56	Il2ra	Mus musculus	GO:0002437|	NM_008367	ENSMUST000	16184	NM_008367	Mm.915
A_51_P37270	0,00102354	down	3,49	Il16	Mus musculus	GO:0005515|	NM_010551	ENSMUST000	16170	NM_010551	Mm.10137
A_55_P21456	4,70E-04	down	3,02	Rilpl1	Mus musculus	GO:0005622|	NM_021430	ENSMUST000	75695	NM_021430	Mm.41180
A_52_P57738	5,50E-04	down	2,93	Il18bp	Mus musculus	GO:0042088|	NM_010531	ENSMUST000	16068	NM_010531	Mm.422756
A_55_P21811	1,05E-04	down	2,79	Il10rb	Mus musculus	GO:0005515|	NM_008349	ENSMUST000	16155	NM_008349	Mm.4154
A_55_P21303	2,76E-04	down	2,70	Rilp	Mus musculus	GO:0005739|	NM_001029938	ENSMUST000	280408	NM_0010299	Mm.41416
A_51_P23154	0,00788821	down	2,64	Mill2	Mus musculus	GO:0005515|	NM_153761	ENSMUST000	243864	NM_153761	Mm.233503
A_55_P19861	0,00724935	down	2,51	Ppil1	Mus musculus	GO:0008380|	NM_026845	ENSMUST000	68816	NM_026845	Mm.328928
A_55_P20687	8,86E-05	down	2,48	Ccl27a	Mus musculus	GO:0005515|	NM_001048179	ENSMUST000	20301	NM_0010481	Mm.335946
A_55_P20687	1,23E-04	down	2,47	Ccl27a	Mus musculus	GO:0005515|	NM_011336	ENSMUST000	20301	NM_011336	Mm.425176
A_55_P20994	0,00373349	down	2,28	Neil1	Mus musculus	GO:0003906|	NM_028347	ENSMUST000	72774	NM_028347	Mm.35749
A_55_P20107	6,33E-04	down	2,03	Il11ra1	Mus musculus	GO:0038154|	NM_001172054	ENSMUST000	16157	NM_0011720	Mm.193451

Figure 9.2: Deregulation of Cytokines and Chemokines after Heart Failure
Altered cytokine and chemokine expression levels in SM22p38MAPKα KO hearts compared to control hearts after 48 hours of ANGII treatment analyzed by microarray.

9.2.2 IPA Z-score Analysis

Altered transcripts detected by microarray were associated to diseases and biological functions and got sorted by the so-called "activation z-score", with enables to predict the activation state of a regulator (<0: inhibited, >0: activated). In practice, z-scores greater than 2 or smaller than -2 can be considered significant. The IPA analysis of of SM22p38MAPKα KO mice compared to SM22p38MAPKα controls 48 hours after ANGII treatment revealed 32 regulators to decrease specific functions and 9 regulators to activate specific functions, as listed in supplemental figure 9.3.

Categories	Diseases or Functions Annotation	p-Value	Predicted Activation State	Activation z-score	# Molecules
Cellular Movement	migration of cells	8,73E-09	Decreased	-3,806	610
Cellular Movement	cell movement	3,48E-10	Decreased	-3,158	694
Cellular Movement	migration of tumor cell lines	1,22E-06	Decreased	-2,984	248
Cellular Development	differentiation of cells	1,24E-16	Decreased	-2,904	766
Cellular Movement	cell movement of connective tissue cells	1,07E-06	Decreased	-2,771	85
Cellular Movement	migration of connective tissue cells	3,82E-07	Decreased	-2,746	70
Cancer, Organismal Injury and Abnormalities	benign neoplasia	1,67E-08	Decreased	-2,745	325
Cancer, Organismal Injury and Abnormalities, Renal and Urological Disease	urinary tract tumor	2,87E-09	Decreased	-2,626	456
Cellular Assembly and Organization	organization of organelle	1,85E-10	Decreased	-2,625	207
Developmental Disorder, Gastrointestinal Disease, Hepatic System Disease, Organismal Injury and Abnormalities	hypoplasia of liver	3,72E-05	Decreased	-2,610	20
Cellular Assembly and Organization, Cellular Function and Maintenance	organization of filaments	1,28E-05	Decreased	-2,601	72
Cancer, Organismal Injury and Abnormalities, Renal and Urological Disease	urinary tract cancer	6,08E-10	Decreased	-2,584	445
Cell-To-Cell Signaling and Interaction	attachment of cells	5,96E-05	Decreased	-2,544	48
Embryonic Development, Organ Development, Development, Skeletal and Muscular System Development and Function, Tissue Development	formation of muscle	1,48E-07	Decreased	-2,472	139
Cellular Movement	cell movement of tumor cell lines	3,56E-08	Decreased	-2,465	307
Cell Morphology, Cellular Assembly and Organization, Cellular Function and Maintenance	formation of cellular protrusions	1,38E-06	Decreased	-2,432	281
Cellular Movement, Connective Tissue Development and Function	cell movement of fibroblast cell lines	2,54E-08	Decreased	-2,373	79
Cardiovascular System Development and Function, Organismal Development	vasculogenesis	3,81E-10	Decreased	-2,301	267
Organismal Development	size of body	2,23E-06	Decreased	-2,289	277
Cancer, Organismal Injury and Abnormalities, Renal and Urological Disease	renal cancer	3,89E-09	Decreased	-2,267	361
Cancer, Organismal Injury and Abnormalities	urogenital cancer	5,91E-09	Decreased	-2,179	1467
Embryonic Development, Organismal Development	development of body trunk	9,12E-08	Decreased	-2,172	395
Cancer, Organismal Injury and Abnormalities, Renal and Urological Disease	Renal Cancer and Tumors	1,77E-09	Decreased	-2,165	370
Post-Translational Modification	phosphorylation of protein	6,93E-14	Decreased	-2,156	256
Lipid Metabolism, Molecular Transport, Small Molecule Biochemistry	concentration of lipid	4,64E-07	Decreased	-2,140	267
Neurological Disease, Skeletal and Muscular Disorders	neuromuscular disease	2,16E-05	Decreased	-2,122	286
Cardiovascular System Development and Function, Organismal Development	angiogenesis	2,71E-08	Decreased	-2,093	311
Cellular Development, Hematological System Development and Function	differentiation of blood cells	6,18E-08	Decreased	-2,091	286
Cell Death and Survival	neuronal cell death	5,88E-06	Decreased	-2,065	221
Cellular Assembly and Organization, Cellular Function and Maintenance	microtubule dynamics	2,40E-07	Decreased	-2,058	371
Cardiovascular System Development and Function	development of vasculature	1,56E-10	Decreased	-2,043	363
Cancer, Organismal Injury and Abnormalities	neoplasia of epithelial tissue	1,53E-49	Decreased	-2,015	3105
Cell Death and Survival, Skeletal and Muscular Disorders	cell death of muscle cells	5,12E-05	Increased	2,002	109
Infectious Diseases	infection by HIV-1	3,03E-07	Increased	2,143	206
Cell Death and Survival, Skeletal and Muscular Disorders	necrosis of muscle	1,40E-05	Increased	2,362	114
Cell Death and Survival	cell death of muscle	1,05E-05	Increased	2,362	115
Infectious Diseases	infection by RNA virus	4,12E-11	Increased	2,875	310
Infectious Diseases	infection of cells	1,46E-09	Increased	2,887	272
Infectious Diseases	infection of tumor cell lines	3,47E-05	Increased	3,029	161
Infectious Diseases	replication of virus	2,01E-06	Increased	3,726	181
Infectious Diseases	Viral Infection	5,96E-12	Increased	3,972	538

Figure 9.3: Analysis of Activation Z-scores of *M. plantaris* of SM22p38MAPKα KO Mice after Induction of Heart Failure

9.3 Neutrophil Depletion - Supplemental Figures

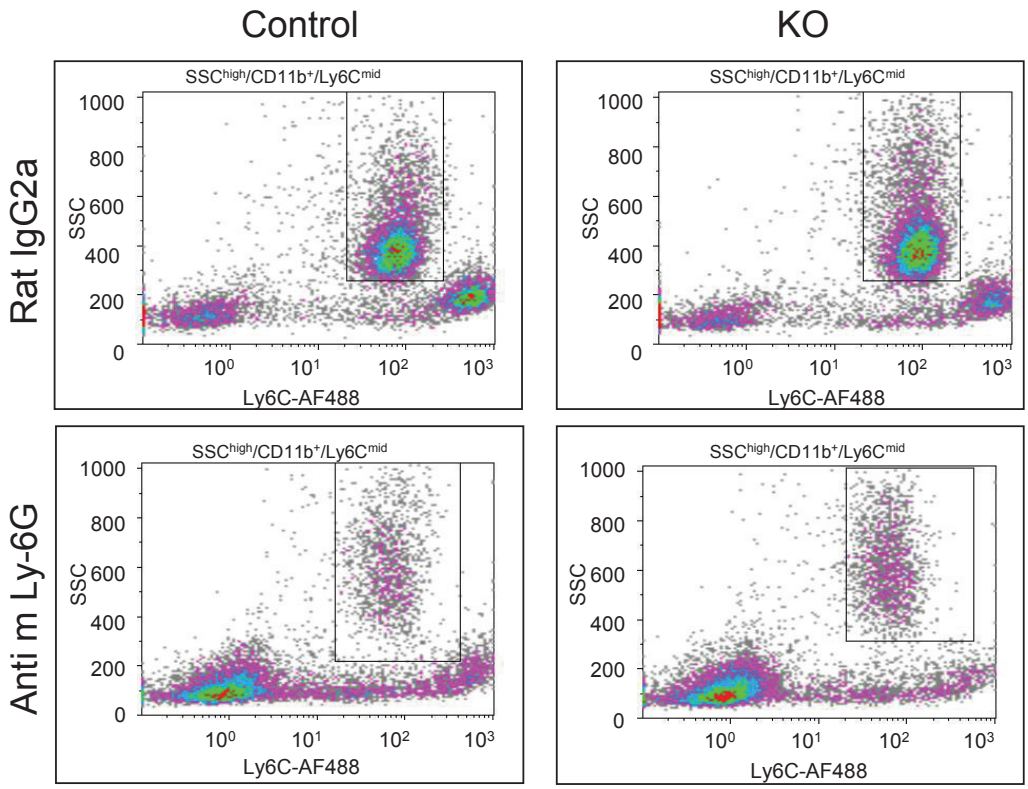

Figure 9.4: FACS Analysis of Neutrophil Depletion
FACS analyses of neutrophils in the blood of isotype (Rat IgG2A)-treated animals (upper panel) and anti-Ly6G-treated animals (lower panel) after 48 hours of ANGII treatment.

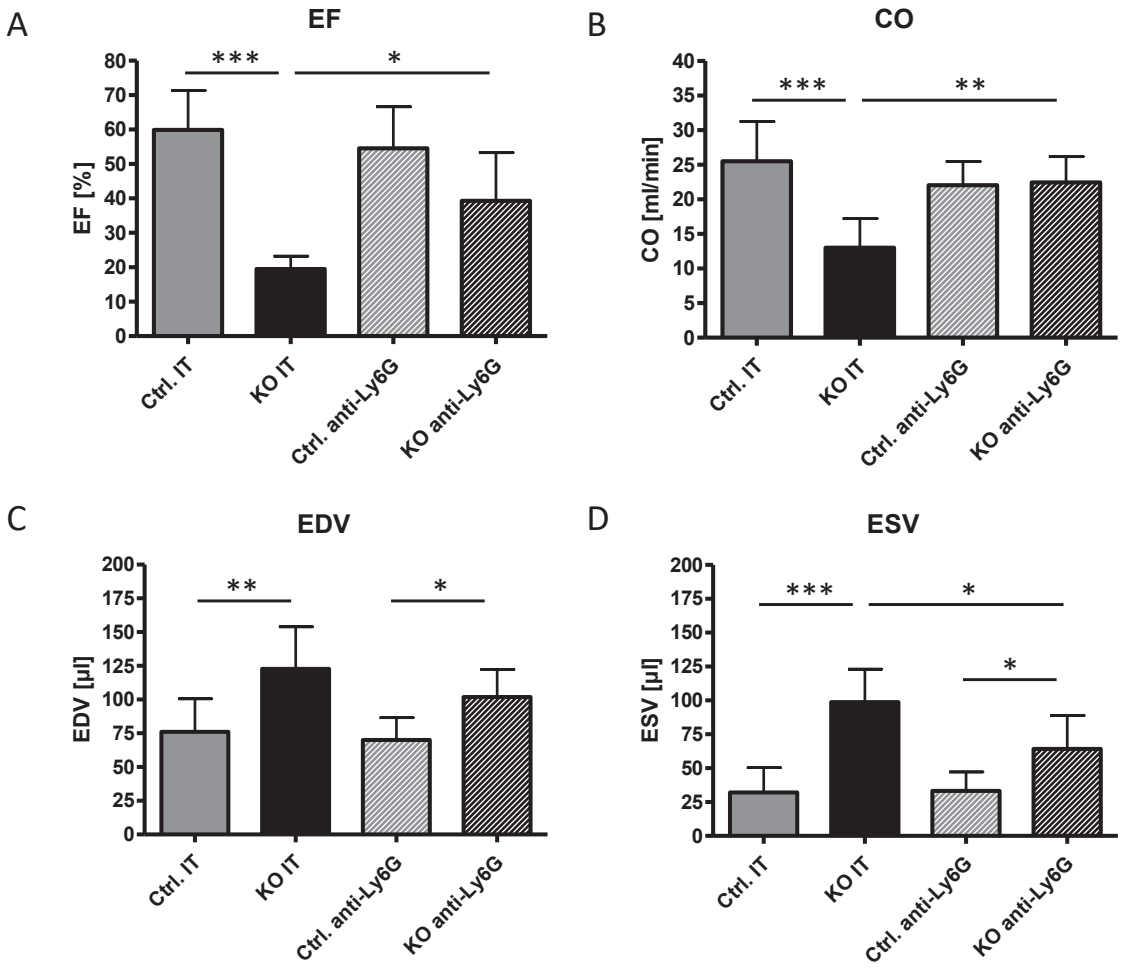

Figure 9.5: Assessment of Cardiac Function after Neutrophil Depletion
The A) Ejection fraction (EF), B) cardiac output (CO), C) end diastolic volume (EDV) and D) end diastolic volume (ESV) of isotype (IT) treated (full bars) and anti-Ly6G treated (striated bars) controls (grey bars) and KOs (black bars) after 48 hours of ANGII treatment was assessed by high resolution ultrasound. 6-8 animals were analyzed per group. Data represent mean ±SD, * $p<0.05$, ** $p<0.01$, *** $p<0.001$.

10 Statutory Declaration

Statutory declaration

I declare under oath that I have compiled my dissertation independently and without any undue assistance by third parties under consideration of the "Principles for the Safeguarding of Good Scientific Practice at Heinrich Heine University Düsseldorf". Furthermore, I assure that I did not submit this dissertation, either in full or in part, to any other faculty and did not absolve any promotion trials before.

Düsseldorf,

Lucia Maria Leitner

Eidesstattliche Erklärung

Ich versichere an Eides Statt, dass die Dissertation von mir selbstständig und ohne unzulässige fremde Hilfe unter Beachtung der "Grundsätze zur Sicherung guter wissenschaftlicher Praxis an der Heinrich-Heine Universität Düsseldorf" erstellt worden ist. Darüber hinaus versichere ich, dass ich die Dissertation weder in der hier vorgelegten noch in einer ähnlichen Form bei einem anderen Institut eingereicht habe und bisher keine Promotionsversuche unternommen habe.

Düsseldorf, den

Lucia Maria Leitner

11 Danksagung

Axel,
Danke, dass Du mir immer mit Rat und Tat zur Seite gestanden bist, mir die Möglichkeiten gegeben hast, mich weiterzuentwickeln - im Labor und außerhalb auf den zahlreichen Kongressen, die ich besuchen durfte. Danke, dass ich Teil Deines Teams sein durfte!
Käthi,
Danke für die unzähligen Stunden, die wir gemeinsam verbracht haben - für Deine Unterstützung und Deine Freundschaft.
Miri und Jana,
Danke, dass Ihr die besten Doktoranden wart, die man sich nur wünschen kann.
Rianne, Vici, Jacqueline, Lisa und alle Mitglieder des Instituts für Herzkreislaufphysiologie,
Danke für Euren Zusammenhalt und Eure Unterstützung. Ohne Euch wäre ich viel öfter verzweifelt.
Nicky, Nenja und Susi,
Danke, dass Ihr mich auf diesem Weg begleitet habt und so viel mit mir geteilt habt.
IRTG - allen voran Sandra,
Danke, dass ich Teil dieses aufregenden Programms sein durfte. Es ist nur durch Euch zu so etwas Besonderem geworden und begleitet uns hoffentlich noch lange!
Prof. Dr. Ulrich Rüther,
Danke für die Zeit, die Du Dir für die Projektbesprechungen und die Zweitbegutachtung genommen hast.

Aus tiefstem Herzen DANKE ich
Mama und **Papa**,
Jakob, **Judith** und **Lena**,
Mario,
und all meinen lieben **Freunden**.

Ich bin euch unendlich dankbar für Eure Unterstützung, Eure Liebe und Euer Verständnis. Danke, dass Ihr immer für mich da seid! Ich bin nichts ohne Euch!